THERMODYNAMIC ORIGINS OF SELECTIVITY IN THE INTERACTIONS OF N-TIMP VARIANTS AND MMP CATALYTIC DOMAINS

by

Haiyin Zou

A Dissertation Submitted to the Faculty of

The Charles E. Schmidt College of Science

In Partial Fulfillment of the Requirements for the Degree of

Doctor of Philosophy

Florida Atlantic University

Boca Raton, FL

May 2016

THERMODYNAMIC ORIGINS OF SELECTIVITY IN THE

INTERACTIONS OF N-TIMP VARIANTS AND MMP CATALYTIC DOMAINS

by

Haiyin Zou

This dissertation was prepared under the direction of the candidate's dissertation advisor, Dr. Keith Brew, Department of Biomedical Science, and has been approved by the members of her supervisory committee. It was submitted to the faculty of the Charles E. Schmidt College of Science and was accepted in partial fulfillment of the requirements for the degree of Doctor of Philosophy.

SUPERVISORY COMITTTEE:

Keith Brew, Ph.D.
Dissertation Advisor

Michael Lu, Ph.D.

Michelle Lizotte-Waniewski, Ph.D.

Rodney K. Murphey, Ph.D.
Chair, Department of Biological Sciences

Ewa Wojcikiewicz, Ph.D.

Janet Blanks, Ph.D.
Interim Dean, Charles E. Schmidt College of Science

Tanja Angela Godenschwege, Ph.D.

Deborah L. Floyd, Ed.D.
Dean, Graduate College

05/31/2016
Date

ACKNOWLEDGEMENTS

I would like to express my deep appreciation and gratitude to my advisor, Dr. Keith Brew, for the patient guidance and mentorship he provided to me throughout my Ph.D. study. Dr. Keith Brew's intellectual heft is matched only by his shining generous heart, endless passion to science and down-to-earth humility. He encouraged me to not only grow as an experimentalist and a biochemist but also as an independent thinker. I am not sure many graduate students are given such an opportunity to develop their own individuality and self-sufficiency, and I feel truly fortunate to have had the opportunity to work with him. His great wisdom has always inspired me and will inspire me in the future.

I would like to thank my committee members, Dr. Lu, Dr. Michelle Lizotte-Waniewski, Dr. EwaWojcikiewicz and Dr. Godenschwege, for the friendly guidance and thought-provoking suggestions that each of them offered to me over the years. I would like to thank Dr. Lu, for his constant help for my research and his kind encouragement for my career. With his suggestions I puzzled over many of the same problems in my experiments. I would like to thank Dr. Michelle Lizotte-Waniewski, for the warm atmosphere she brought to our lab and all the wise suggestions she gave to me not only for my research but also for my personal life over these years. Many thanks to Brittany Alise Stinson and Tim Logue. From the sleepless research nights to relaxed happy hours they were with me. It would have been a lonely lab without them and they are definitely one of the significant parts of this journey. My heartfelt gratitude goes to my family and

friends being beside me through the good times and the bad. Thanks them for the love they gave me, which is more precious than anything to me in this world.

ABSTRACT

Name: Haiyin Zou

Title: Thermodynamic Origins of Selectivity in the Interactions of N- TIMP Variants and Metalloproteinases Catalytic Domains

Institution: Florida Atlantic University

Dissertation Advisor: Dr. Keith Brew

Degree: Doctor of Philosophy

Year: 2016

Matrix metalloproteinases (MMPs) constitute the major class of enzymes capable of degrading all protein components of extracellular matrix (ECM) and have important roles in normal physiologic processes of maintaining tissue integrity and remodeling. However, excess MMP activities are associated with many diseases including rheumatoid arthritis and osteoarthritis, cardiomyopathy, and macular degeneration. The activity of MMPs is regulated by their endogenous protein inhibitors, the tissue inhibitors of metalloproteinases (TIMPs) which are avid broad-spectrum inhibitors of numerous human matrixins (MMPs and ADAMs). Uncontrolled matrix degradation occurs when the balance between TIMPs and MMPs is disrupted, resulting in serious diseases such as cancer, arthritis and chronic tissue ulcers. Thus, the engineering of TIMPs to produce highly selective and efficacious inhibitors of individual MMPs may be utilized for future treatment of diseases. Such engineering requires detailed analysis for the structural and biophysical information of MMP-TIMP interaction.

Changes in the dynamics of proteins and solvent that accompany their associations with different binding partners, influence the specificity of binding through entropic effects. From the current studies it appears that the interactions of the inhibitory domains of TIMPs-1 and -2 (N-TIMPs) with MT1-MMP are driven by entropy increases that are partitioned between solvent and conformational entropy (ΔS_{solv} and ΔS_{conf}), and a large conformational entropy penalty is responsible for the weak inhibition of MT1-MMP by NT1.We investigated how mutations that modify N-TIMP selectivity affect the thermodynamics of interactions with MMP1, MMP3 and MT1-MMP. The weak inhibition of MT1-MMP by N-TIMP-1 is enhanced by mutation of threonine 98, on the edge of the binding ridge, to leucine. This mutation increases the large ΔS_{conf} cost for binding to MT1-MMP but this is offset by a greater increase in $\Delta S_{solv.}$ In contrast, this mutation enhances binding to MMP3 by increasing ΔS_{conf} for the interaction. ΔS_{solv} and ΔS_{conf} show mutual compensation for all interactions, with characteristic ranges for each MMP. Distinct electrostatic and dynamic features of MMPs are key factors in their selective inhibition.

THERMODYNAMIC ORIGINS OF SELECTIVITY IN THE

INTERACTIONS OF N-TIMP VARIANTS AND MMP CATALYTIC DOMAINS

TABLES

FIGURES

NOMENCLATURE

ADAM	A Distintegrin and a Metalloproteinase
ADAMTS	A Distintegrin and a Metalloproteinase
CD/cd	Catalytic Domain
ECM	Extracellular Matrix
HPX	A Hemopexin domain
ITC	Isothermal Titration Calorimetry
K_i	Inhibition Constant
MMP	Matrix Metalloproteinase
MMPI	Matrix Metalloproteinase Inhibitors
MT-MMP	Membrane Type-MMP
OB-fold	Oligonucleotide-Binding fold
TACE	Tumor Necrosis Factor-alpha Converting Enzyme
TIMP	Tissue Inhibitor of metalloproteinase
VDW	Van der Waals interactions

I.INTRODUCTION

1. Matrix Metalloproteinase (MMPs)

1.1 Extracellular Matrix

The extracellular matrix (ECM) is a connective tissue that represents the environment of cells and undergoes remodeling during development and morphogenesis. It is composed of glycosaminoglycans, polysaccharides and fibrous proteins. Through variations in its composition, the ECM serves many different cellular functions, the most common being: 1) mechanical support of cells and tissues by providing strength and elasticity; 2) effects on cell adhesion, cell-to-cell communication, cellular development, and differentiation by interacting with cell-surface receptors and controlling the availability of many cellular growth factors. Changes in ECM structure play essential roles in processes like growth, tissue remodeling and fibrosis.

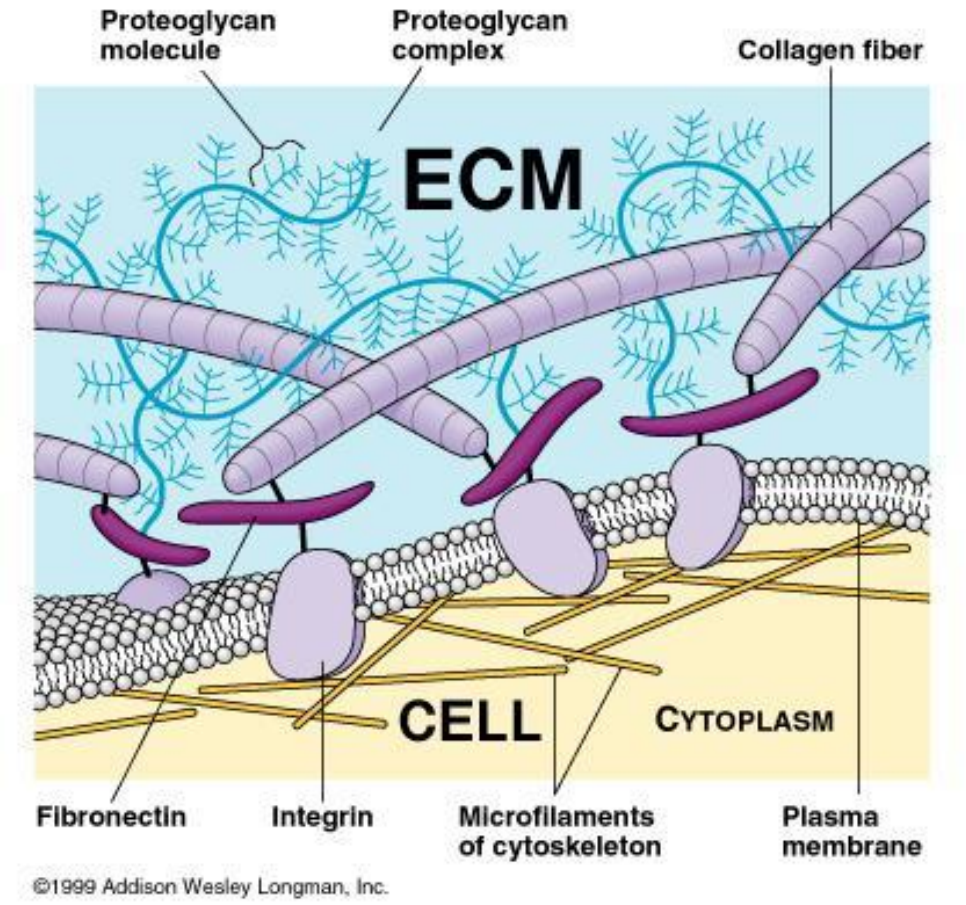

Figure 1. Diagram of extracellular matrix. The ECM is made up of proteins and carbohydrates that surround the cell. The composition of ECM is unique to different tissue and disease state (taken from Addison Wesley Longman. Inc. 1999).

1.2 General Properties and Structure of MMPs

Some unique proteolytic systems play important roles in modulating cell-matrix interactions, by regulating the composition and integrity of the ECM. Among these enzymes, the matrix metalloproteinases (MMPs) are a major group that participates in ECM degradation by cleaving all ECM proteins and some non-matrix proteins. MMPs belong to the superfamily of zinc-peptidases which include more than 50 families of enzymes. The human genome encodes MMPs, while additional MMPs have been identified in invertebrates and three in plants.

Human MMPs are multi-domain proteins that encompass three highly conserved domains: an amino-terminal propeptide which has a cysteine switch motif PRCGXPD maintaining MMPs in their zymogen form (proMMP); a catalytic domain that has the zinc-binding motif HEXGHXXGXXH, a sequence signature of zinc metalloproteins; and a hemopexin-like domain that is similar in sequence to the plasma protein, hemopexin. The zymogen forms of MMPs need to be activated in order to display proteolytic activity, by cleavage of removal of the propeptide (Hu et al., 2007). The catalytic domain of MMPs includes two zinc ions and at least one calcium ion. One of the two zinc ions, the catalytic zinc, has an essential role in MMP catalytic activity, while another zinc ion helps to stabilize the MMP structure. There are three histidine residues that coordinate with the catalytic zinc in the catalytic domain. The hemopexin-like domain is involved in specific substrate binding and/or in inhibition of MMPs by the tissue inhibitors of metalloproteinases (TIMPs).

Among the domains of MMP (Figure 2), the signal peptide is responsible of secretion of these enzymes and is removed by the action of signal peptidase in the endoplasmic reticulum; subsequently, the propeptide domain is removed when the enzyme is activated so that the catalytic domain can function as a protease (Creemers et al., 2001). During the evolution of modern MMPs additional domains were added and/or deleted to the core MMP structure to form various subgroups of MMPs (Woessner et al., 1991) .

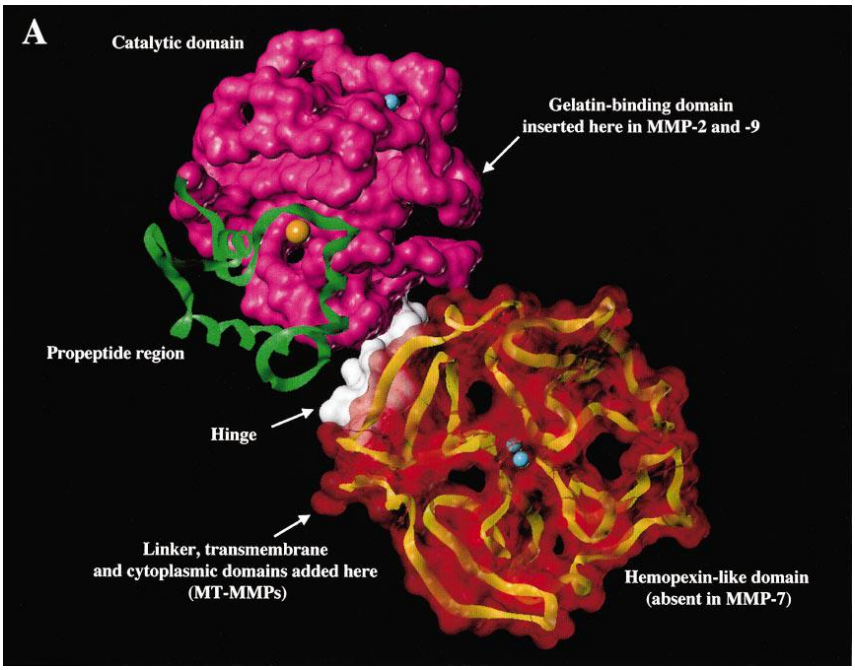

Figure 2. Basic domain structures of MMPs (Creemers et al., 2001)

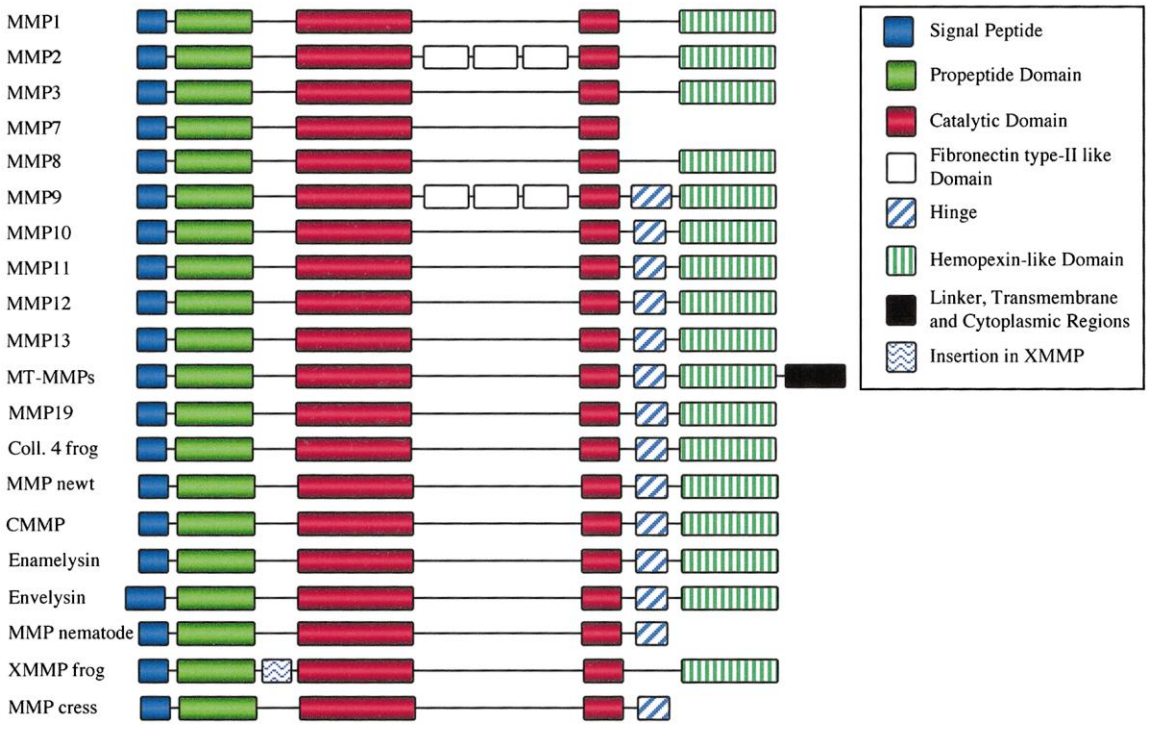

Figure 3. Schematics of the domain structures of the 23 representative MMPs. It shows Structural differences between the various classes of MMPs (Creemers et al., 2001)

MMPs can be classified into five subgroups based on their sequence similarity, domain structure and substrate specificity (Figure 3): Collagenases (MMP-1, -8, -13, and -18) are able to cleave fibrillar collagens, The gelatinases (MMP-2 and MMP-9) are able to digest collagen types IV, V, VII, and X, elastin, and denatured collagens. Stromelysins (MMP-3, -10 and -11) degrade proteoglycan core proteins, laminin, fibronectin, elastin, gelatin, and collagen types III, IV, V, VII, and IX while membrane-type MMPs (MMP-12, -14, -19 to -23, -27,and -28) can degrade several ECM components and, apart from MT4-MMP, are also capable of activating proMMP-2.

MMPs are involved in many biological processes ranging from regulation of tissue turnover and cellular homeostasis to many physiological and pathological processes, including cell growth, cell survival, inflammation, and angiogenesis.

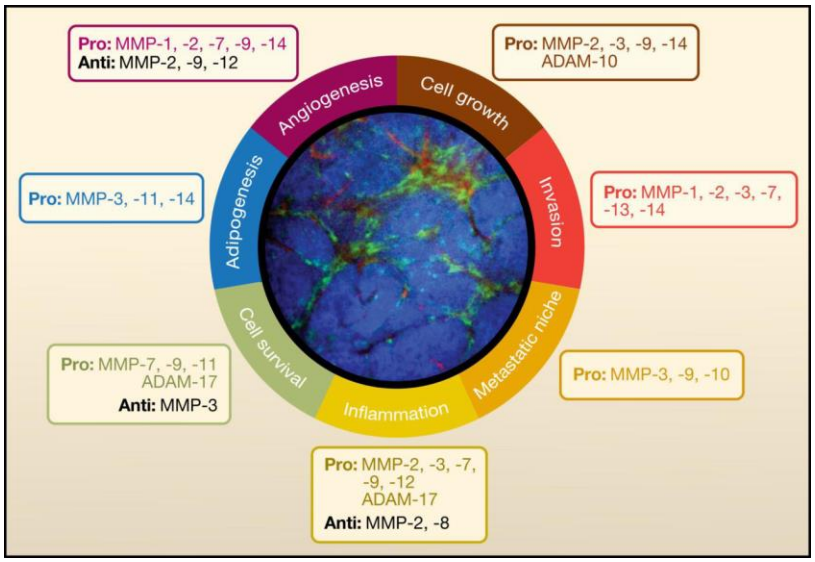

Figure 4. Modulation of the physiological and pathological processes by MMPs.Pro means promote, anti means suppress (Kessenbrock et al., 2010)

Growing evidence supports the view that many disease states are related to pathologically uncontrolled degradation of extracellular matrix proteins, and

subsequently to considering MMPs as possible therapeutic targets for many diseases. These include serious diseases such as cardiovascular disease, osteoarthritis, macular degeneration and cancer. Inhibition of one or several MMPs offers, in theory, an approach that may be utilized for future treatment of these diseases. Therefore, the rational design of MMP inhibitors becomes attractive, and such design requires detailed structural and biophysical information regarding MMPs, MMP inhibitors and their complexes.

Table 1. Major disease targets for inhibitors of matrix metalloproteinases (Rao et al. 2005)

MMP number	Enzyme name(s)	Therapeutic areas
MMP-1	collagenase-1 fibroblast collagenase (HFC)	Arthritis, cancer, periodontal disease
MMP-2	gelatinase A (Gel A) 72 kD gelatinase type IV	Cancer, MS, stroke, angiogenesis
MMP-3	stromelysin-1	Cancer, arthritis
MMP-7	matrilysin	Cancer
MMP-8	collagenase-2 neutrophil collagenase (HNC)	
MMP-9	gelatinase B (Gel B) 92 kD gelatinase	Cancer, MS, stroke
MMP-10	stromelysin-2	
MMP-11	stromelysin-3	Cancer
MMP-12	metalloelastase macrophase elastase	Emphysema
MMP-13	collagenase-3	Arthritis
MP-14-17	membrane-type	Cancer

1.3 Three-Dimensional (3D) Structures of MMPs

The first three-dimensional structure of the catalytic domains of two collagenases, MMP-1 and MMP-8 were revealed in 1994 (Lovejoy et al., 1994), and subsequently the crystal structures of proMMP-3 and full-length MMP-1 were reported in 1995 (Li et al., 1995). To date, a large number of 3D structures of MMPs in apo and inhibited forms have been determined by X-ray crystallography and NMR spectroscopy. There are more than 200 entries of MMP 3D structures in the protein databank. 187 of them were determined by X-ray crystallography, and 22 were determined by NMR. According to

these structures, all MMPs share a highly conserved polypeptide fold in their catalytic domains. Their structures show an α/β fold, consisting of three α-helices, a twisted 5-stranded β-sheet, and connective loops (Visse, et al., 2003).

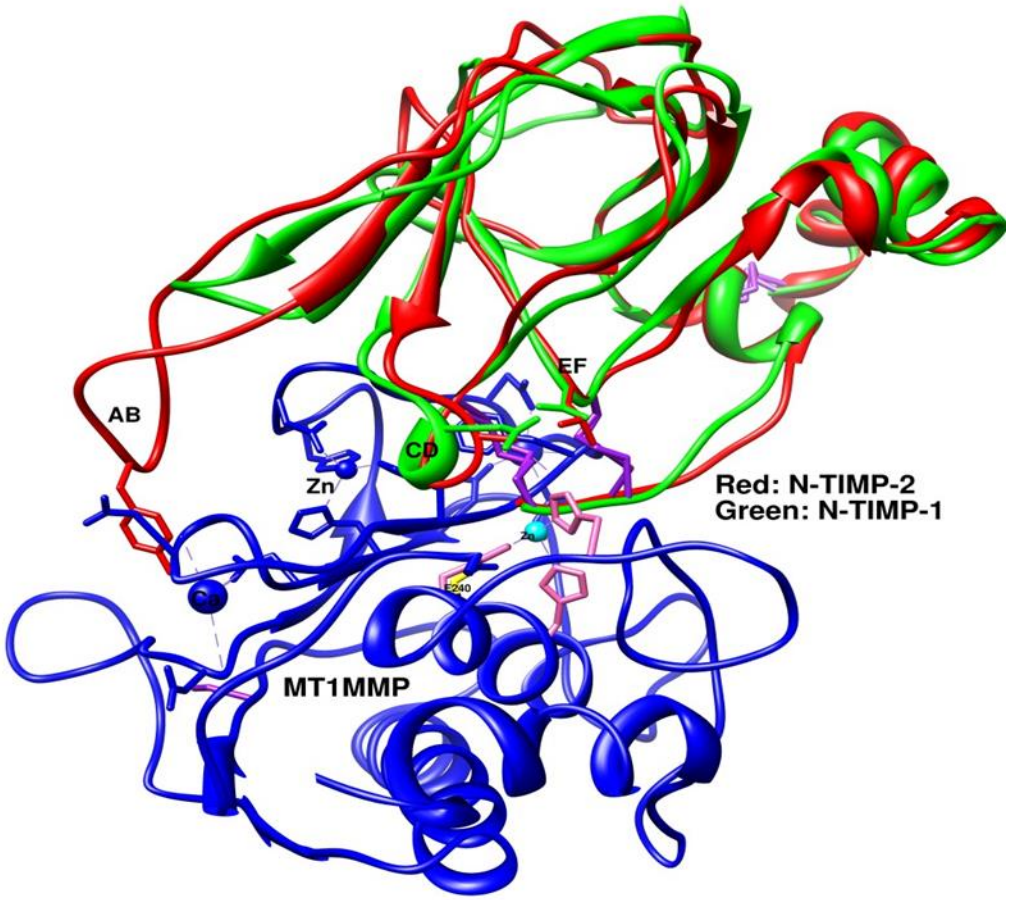

Figure 5. Model structures of complexes of MT1-MMP/N-TIMP-1,2

The structure is shown in Fig 5. Helix A is colored blue. Helix B yellow and helix C is orange; the five-stranded β-sheet is green/blue. The beta-strands are located near the N-terminus while helix C is located at the C terminus. The helices A and B are located centrally. The strands are, sequentially, β2 (light blue) β1 (blue) β3 (dark green) β5 (green) β4 (bright green), with β4 anti-parallel to the others. The amphipathic helix, A (blue) extends the full length of the sheet and is inserted between parallel β1 (blue) and

β2 (light blue) strands. The second helix B (yellow) is packed against the β-sheet, β4 and helix A (blue), and is positioned after a loop following β5 (green). The two His and Glu residues (shown as yellow sticks) of the Zn-binding sequence motif HExxHxxGxxH are part of the second helix B (yellow). A short turn at Gly of the same sequence brings the third His (shown as yellow sticks) together with the first two His side chains to coordinate catalytic Zn (shown as a purple sphere). The last part of the structure consists of the Met-turn (yellow), a defining feature of the Metzincin family, and a large loop (orange) and ends with the third helix, C (orange). The large loop is known as active site loop or S1' specificity loop. The enzymatic activity and inhibition profile of the recombinant catalytic domain of fibroblast collagenase is similar to that of corresponding full-length proteins so that the truncated domain is a suitable surrogate for the designing structure-based inhibitors for MMP-1.

Three histidine residues of the protein and atoms of the bound inhibitor chelate the catalytic zinc. Solution NMR studies underscores the flexibility of the active site of the MMP-1, suggesting that enzyme inhibition is achieved by stabilizing the mobile active site. Physiological inhibition of MMPs by the pro-peptide (during latency), and by endogenous inhibitors after activation, occur through the interaction of inhibitor atoms with the catalytic zinc.

1.4 Membrane Type MMPs

The membrane type MMPs (MT-MMPs) are a subgroup encompassing cell surface MMPs which are characterized by a short cytoplasmic tail at the C terminus and a trans membrane domain. Research has shown that when MT-MMPs are co-expressed with pro-gelatinase A (pro-MMP 2), they can cleave the propeptide sequence of pro-

gelatinase A to generate the mature enzyme, and this correlates with tumor spread and poor prognosis.

Membrane-type matrix metalloproteinase 1 (MT1-MMP) was identified as the first membrane-anchored type MMP and acts as a key enzyme in the degradation of the pericellular ECM. Compared with other MT-MMPs, MT1-MMP can digest the cartilage proteoglycan, fibronectin, vitronectin and type I and I11 collagen (Seiki et al., 1999). Tissue damage induces the expression of MT1-MMP in fibroblasts and this is combined with the expression of MMP-2 during the whole wound healing process (Okada et al., 1997). During angiogenesis, MT1-MMP is expressed in endothelial cells forming new blood vessels in both physiological and pathological situations (Gálvez, et al., 2001).

Because of its ability to activate gelatinase A, MT1-MMP also plays a crucial role in tumor cell invasion (Sato et al., 1994). MT1-MMP is expressed in tumor cells, as well as stromal cells in various organs, such as lung, breast (Polette et al., 1996), colon, liver, ovarian, cervical carcinomas (Harada et al., 1998), brain, head and neck (Yoshizaki et al., 1997)

1.5 MMP 1

Matrix metalloproteinase-1 (MMP-1), also known as interstitial collagenase, was identified in 1962 by Gross and Lapiere, who discovered this first MMP activity in the tail of a tadpole undergoing metamorphosis. MMP-1 degrades collagens type I, II, and III by cleaving the peptide bond between Gly775–Ile776 or Gly775–Lys776 (Lemaître et. al., 2006). Additionally, MMP-1 can also degrade the non-matrix constituents and activate cytokines (Gearing et al. 1994; Schönbeck et al. 1998). Owing to its unique ability to break the fibrillar collagen network, MMP-1 plays crucial roles in tissue remodeling

under physiological and pathological conditions, and in embryo development, morphogenesis, wound healing, and human diseases

MMP-1 can be synthesized and secreted in vitro by osteoblastic cells (Delaisse et. al., 1988). The expression levels of MMP-1 in tissues is extremely low under normal physiological conditions. However, environmental stimuli, reactive oxygen species production or certain pathophysiological processes can elevate MMP-1 levels dramatically (Kar et. al., 2010). Increased expression of MMP-1 is associated with many age-associated degenerative disease, such as Alzheimer's, skin aging, emphysema, atherosclerosis, and osteo-arthritis (Mercer et. al., 2004; Burrage et al., 2006; Fisher et al., 2009; Kar et al., 2010).

Studies of mice with human MMP-1 transgenes show that expression of human MMP-1 in mouse lungs causes cleavage of type III collagen in alveolar walls, leading to altered lung structure, and eventually causes pulmonary emphysema (D'Armiento, et.al., 1992). Additional studies revealed that transgenic expression of human MMP-1 in mouse hearts causes diastolic and systolic dysfunction, resulting in cardiac failure (Kim et al., 2000).

The tertiary structure of MMP-1 includes three α-helices, and a twisted, five-stand β-sheet which has four parallel strands and one antiparallel strand. Its N-terminal catalytic (Cat) domain, which is responsible for cleavage of a number of noncollagenous proteins including heat-denatured collagen, contains an active-site zinc ion. The structure of the C-terminal hemopexin (Hpx) domain, which is strictly required for efficient collagenolysis, is a four-bladed β-propeller stabilized by a calcium ion, (Li et al., 1995; Manka et al., 2012).

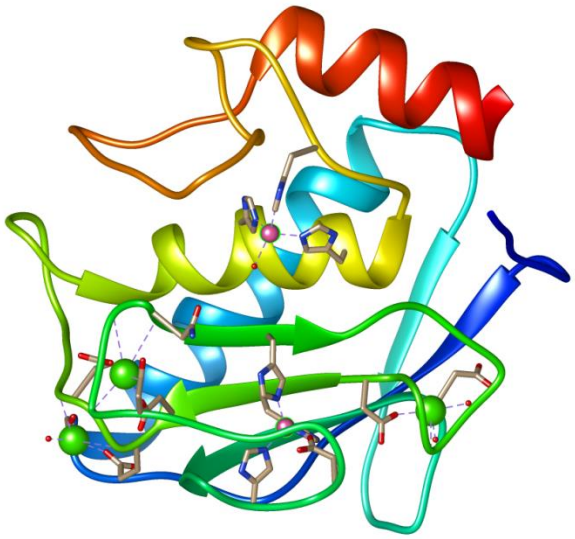

Figure 6. Structure of MMP-1 (made from PDB file 3SHI)

Figure 6 is the ribbon representation of the three-dimensional structure of human MMP-1 (E200A). There are four calcium ions and two zinc ions found in the structure that have been colored in green and magenta respectively. The secondary structural elements have been annotated: helices, strands of the catalytic domain and blades of the hemopexin domain.

2. Tissue Inhibitor of Metalloproteinases (TIMPs):

2.1 TIMP Research and Human Disease

MMPs are considered as promising targets for many diseases, such as cancer, arthritis and cardiovascular disease (Murphy et. al., 2008). Consequently, the development of inhibitors of specific MMPs has become an attractive area of research, and much effort has been applied to the elucidation of structures of MMP-inhibitor complexes to aid rational drug design (Fisher et. al., 2006).

The search for MMP inhibitors with high affinity and specificity which have the potential to be useful drugs has been in progress for four decades. Studies in this area

focus on two different types of inhibitor, synthetic metalloproteinase inhibitors (MPIs) and tissue inhibitors of metalloproteinase (TIMPs). MPIs were rapidly developed and tested in human clinical trials, however, all the trials failed with disappointing results (Coussens, et. al., 2002). The failure of MPIs in the clinic appears to be insufficient affinity for MMPs and inadequate selectivity.

TIMPs, the endogenous inhibitors of MMPs, play key roles as inhibitors of MMPs in tissues and in the ECM, helping to maintain the balance between ECM deposition and degradation in various physiological processes (Brew et. al., 2000). TIMPs can inhibit MMPs with high affinities in the nanomolar to subnanomolar range, making them attractive for future treatment of diseases associated with excess MMP activity. Additionally, TIMPs are involved in cell growth, apoptosis, angiogenesis, and other bioactivities as multifunctional proteins (Brew et al., 2000; Baker et. al., 2002; Brew et. al., 2010).TIMP-1 and TIMP-2 have been initially considered as potential therapies for cancer and other diseases (Stetler-Stevenson et al. 1989). Moreover, the fact that mutations in TIMP-3 cause Sorsby fundus dystrophy, as human disease that produces early onset macular degeneration diseases increases the interest in TIMPs structures, functions, and pathological roles (Brew et. al., 2000). The large-scale production of TIMPs, as well as their mutants, with the goal of using them in clinical trials have been striven by many R&D groups in Celltech, Molecular Oncology, Genetech , Rhone-Poulenc, and etc .

2.2 General Properties and Functions of TIMPs

TIMPs are ancient eukaryotic proteins with complex evolutionary history, being widely identified in invertebrates and nematodes, such as *C*. *elegans*, insect, as well as

vertebrates including birds and, fishes (Brew et. al., 2000) .In early 1970's, the inhibitory activity of TIMP-1 for collagenase (MMP-1) was discovered (Bauer et. al., 1975) and it was designated "tissue inhibitor of metalloproteinase-1", since it can inhibit not only collagenase, but also stromelysins and gelatinases. Four mammalian TIMPs isoforms, TIMP-1 to TIMP-4, are encoded, by the human genome; they show a high degree of similarity in sequence and structure. All four members of TIMP family inhibit MMPs, by forming stoichiometric non-covalent TIMP-MMP complexes in a 1:1 molar ratio. However, the affinities of different TIMP/MMP pairs varies (Brew et. al., 2010).

A

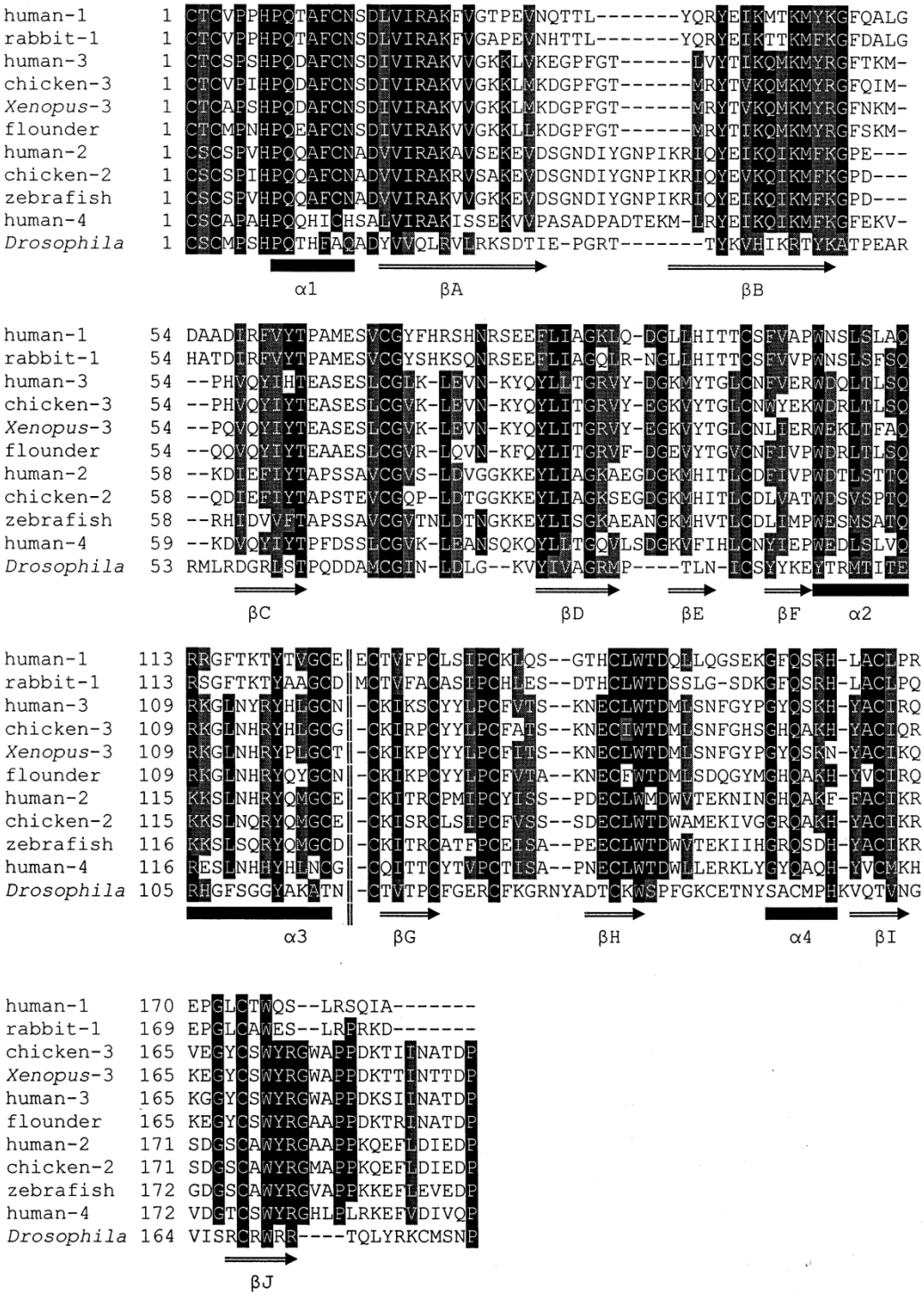
human-1 1 CTCVPPHPQTAFCNSDLVIRAKFVGTPEVNQTTL-------YQRYEIKMTKMYKGFQALG
rabbit-1 1 CTCVPPHPQTAFCNSDLVIRAKFVGAPEVNHTTL-------YQRYEIKTTKMFKGFDALG
human-3 1 CTCSPSHPQDAFCNSDIVIRAKVVGKKLVKEGPFGT------LVYTIKQMKMYRGFTKM-
chicken-3 1 CTCVPIHPQDAFCNSDIVIRAKVVGKKLMKDGPFGT------MRYTVKQMKMYRGFQIM-
Xenopus-3 1 CTCAPSHPQDAFCNSDIVIRAKVVGKKLMKDGPFGT------MRYTVKQMKMYRGFNKM-
flounder 1 CTCMPNHPQEAFCNSDIVIRAKVVGKKLLKDGPFGT------MRYTIKQMKMYRGFSKM-
human-2 1 CSCSPVHPQQAFCNADVVIRAKAVSEKEVDSGNDIYGNPIKRIQYEIKQIKMFKGPE---
chicken-2 1 CSCSPIHPQQAFCNADVVIRAKRVSAKEVDSGNDIYGNPIKRIQYEVKQIKMFKGPD---
zebrafish 1 CSCSPVHPQQAFCNADVVIRAKVVGKKEVDSGNDIYGNPIKRIQYEIKQIKMFKGPD---
human-4 1 CSCAPAHPQQHICHSALVIRAKISSEKVVPASADPADTEKM-LRYEIKQIKMFKGFEKV-
Drosophila 1 CSCMPSHPQTHFAQADYVVQLRVLRKSDTIE-PGRT-------TYKVHIKRTYKATPEAR
α1
βA
βB
human-1 54 DAADIRFVYTPAMESVCGYFHRSHNRSEEFLIAGKLQ-DGLLHITTCSFVAPWNSLSLAQ
rabbit-1 54 HATDIRFVYTPAMESVCGYSHKSQNRSEEFLIAGQLR-NGLLHITTCSFVVPWNSLSFSQ
human-3 54 --PHVQYIHTEASESLCGIK-LEVN-KYQYLLTGRVY-DGKMYTGLCNFVERWDQLTLSQ
chicken-3 54 --PHVQYIYTEASESLCGVK-LEVN-KYQYLITGRVY-EGKVYTGLCNWYEKWDRLTLSQ
Xenopus-3 54 --PQVQYIYTEASESLCGVK-LEVN-KYQYLITGRVY-EGKVYTGLCNLIERWEKLTFAQ
flounder 54 --QQVQYIYTEAAESLCGVR-LQVN-KFQYLITGRVF-DGEVYTGVCNFIVPWDRLTLSQ
human-2 58 --KDIEFIYTAPSSAVCGVS-LDVGGKKEYLIAGKAEGDGKMHITLCDFIVPWDTLSTTQ
chicken-2 58 --QDIEFIYTAPSTEVCGQP-LDTGGKKEYLIAGKSEGDGKMHITLCDLVATWDSVSPTQ
zebrafish 58 --RHIDVVFTAPSSAVCGVTNLDTNGKKEYLISGKAEANGKMHVTLCDLIMPWESMSATQ
human-4 59 --KDVQYIYTPFDSSLCGVK-LEANSQKQYLLTGQVLSDGKVFIHLCNYIEPWEDLSLVQ
Drosophila 53 RMLRDGRLSTPQDDAMCGIN-LDLG--KVYIVAGRMP----TLN-ICSYYKEYTRMTITE
βC
βD
βE
βF
α2
human-1 113 RRGFTKTYTVGCEICTVFPCLSIPCKLQS--GTHCLWTDQLLQGSEKGFQSRH-LACLPR
rabbit-1 113 RSGFTKTYAAGCDIMCTVFACASIPCHLES--DTHCLWTDSSLG-SDKGFQSRH-LACLPQ
human-3 109 RKGLNYRYHLGCNI-CKIKSCYYLPCFVTS--KNECLWTDMLSNFGYPGYQSKH-YACIRQ
chicken-3 109 RKGLNHRYHLGCGI-CKIRPCYYLPCFATS--KNECIWTDMLSNFGHSGHQAKH-YACIQR
Xenopus-3 109 RKGLNHRYPLGCTI-CKIKPCYYLPCFITS--KNECLWTDMLSNFGYPGYQSKN-YACIKQ
flounder 109 RKGLNHRYQYGCNI-CKIKPCYYLPCFVTA--KNECFWTDMLSDQGYMGHQAKH-YVCIRQ
human-2 115 KKSLNHRYQMGCEI-CKITRCPMIPCYISS--PDECLWMDWVTEKNINGHQAKF-FACIKR
chicken-2 115 KKSLNQRYQMGCEI-CKISRCLSIPCFVSS--SDECLWTDWAMEKIVGGRQAKH-YACIKR
zebrafish 116 KKSLSQRYQMGCDI-CKITRCATFPCEISA--PEECLWTDWVTEKIIHGRQSDH-YACIKR
human-4 116 RESLNHHYHLNCGI-CQITTCYTVPCTISA--PNECLWTDWLLERKLYGYQAQH-YVCMKH
Drosophila 105 RHGFSGGYAKATNI-CTVTPCFGERCFKGRNYADTCKWSPFGKCETNYSACMPHKVQTVNG
α3
βG
βH
α4
βI
human-1 170 EPGLCTWQS--LRSQIA-------
rabbit-1 169 EPGLCAWES--LRPRKD-------
chicken-3 165 VEGYCSWYRGWAPPDKTIINATDP
Xenopus-3 165 KEGYCSWYRGWAPPDKTTINTTDP
human-3 165 KGGYCSWYRGWAPPDKSIINATDP
flounder 165 KEGYCSWYRGAAPPDKTRINATDP
human-2 171 SDGSCAWYRGAAPPKQEFLDIEDP
chicken-2 171 SDGSCAWYRGMAPPKQEFLDIEDP
zebrafish 172 GDGSCAWYRGVAPPKKEFLEVEDP
human-4 172 VDGTCSWYRGHLPLRKEFVDIVQP
Drosophila 164 VISRCRWRR----TQLYRKCMSNP
βJ

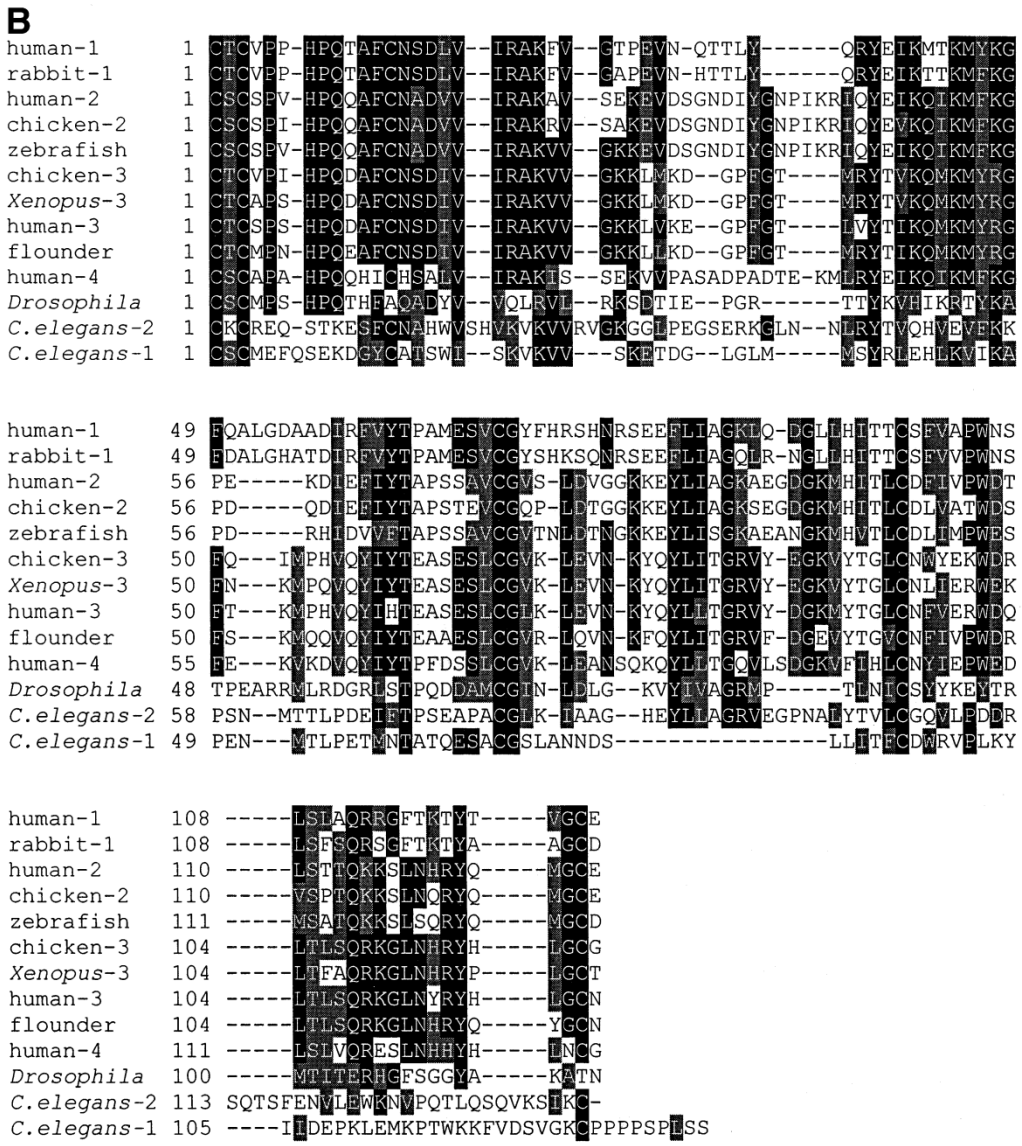

Figure 7. Alignment of full-length TIMPs (A) and Alignment of N-TIMPs (B), including C elegans. Constructed with CLUSTALW and shaded with BOXSHADE using the BCM (Baylor College of Medicine). Search Launch website (dot.imgen.bcm.tcm.edu:9331) (Brew et al.).

TIMP-3, has the broadest inhibition spectrum of the four mammalian TIMPs and can inhibit all the MMPs and several members of the ADAM and ADAM-TS families (disintegrin-metalloproteinases), including as ADAM10, 12, 17, 28 and 33, and ADAMTS-1, -2, -4 and -5 (Amour et al., 1998). In contrast to TIMP-3, TIMP-2 can inhibit all the MMPs, but only one ADAM, ADAM12 (Jacobsen et al., 2008). TIMP-2

also has a role in the cell surface activation of proMMP-2 (Visse et al., 2003); TIMP-1 is a tight inhibitor of most MMPs except MMP-14, -16, -19 and -24, and can inhibit ADAM10 (Amour et al., 2000); TIMP-4 is a tight inhibitor of most MMPs and ADAM 17, 28. ADAMs degrade the ECM and shed cell surface molecules, and differ from MMPs in domain structure, having EGF-like, disintegrin, cysteine-rich, and transmembrane domains C terminal to their catalytic domains (Brew et al., 2010).

There is increasing awareness that TIMPs are multifunctional proteins involved in cell growth, invasion, and migration, as well as anti-angiogenesis, anti- and pro-apoptosis. Some of these functions are independent of the inhibition of MMPs (Brew et al., 2010). TIMP-1 and TIMP-2 were shown to promote cell growth on keratinocytes, fibroblasts and metanephric mesenchyme cells (Bertaux et al., 1991, Barasch et al. 1999), and TIMP mutants which have reduced MMP-inhibitory activity can also retain such cell growth promoting ability (Chesler et al., 1995). In addition to its cell growth promoting activity, TIMP-1 also has anti-apoptotic effects on some cell types, by binding to CD63 to form a TIMP-1-CD63-integrin β1 complex which activates cell survival signaling (Liu et al., 2005). TIMP-2 inhibits angiogenesis, which may result from interactions between TIMP-2 andα3β1 integrin (Seo et al., 2006). Like TIMP-2, TIMP-3 is also a potent inhibitor of angiogenesis, by binding to angiotensin Π type 2 receptor (Kang et al., 2008) and/or VEGF receptor 2 (Qi et al., 2003). A study of the expression of human TIMP-3 in human DLD colon carcinoma cells showed that the inhibition of TACE (ADAM 17) by TIMP-3, together with subsequent stabilization of TNF receptor, may promote apoptosis (Smith et al., 1997).

A single mutation in the C-terminal domain of the human TIMP-3 gene can cause Sorsby fundus dystrophy (SFD), an autosomal dominant retinal disorder characterized by progressive degeneration of the central macula of the retina. The TIMP-3 mutants that cause SFD in different families are diverse, including a nonsense mutation, a splice mutation or a His158Arg mutation. SFD has similar clinical symptoms to those of age-related macular degeneration (AMD) (Brew et al., 2010). However, it affects patients at earlier ages than AMD (Weber et al., 1994). SFD TIMP-3 mutants form odd number of cysteines in C-terminal domain of TIMP-3 possibly resulting in intermolecular disulfides that stabilize dimers or multimers of TIMP-3 (Li et al., 2005). In another early onset macular degeneration disease, Malattialeventinese, retinal dystrophy is also linked with TIMP-3. This disease is caused by a mutation in the gene for a binding partner of TIMP-3, an ECM protein also called EGF-containing fibulin-like extracellular matrix protein 1 (EFEMP 1) (Stone et al., 1999). Studies of Malattialeventineseretinal dystrophy have shown that the EFEMP 1 mutant cannot be secreted effectively, resulting in accumulation in the endoplasmic reticulum, as well as activation of the unfolded protein response and production of vascular endothelial growth factor (VEGF) (Roybal et al., 2005).

2.3 Three-Dimensional Structures of TIMPs

In 1994, Williamson et al. reported a multidimensional NMR study of the N-terminal domain of TIMP-2 (Williamson et al., 1994), which might be considered as the first three-dimensional structure reported for a TIMP molecule (Brew et al., 2000). To date, there are 14 entries of TIMP 3D structures in the protein databank. 11 were determined by high resolution crystallographic studies, including the TIMP-1/MT1-MMP complex at 2.05 Å (PDB entry 3MA2) (Grossman et al., 2010), N-TIMP-1/MMP-1CD

complex at 2.54 Å (PDB entry 2J0T) (Iyer et al., 2007), TIMP-1/MMP-3 CD complex at 2.80 Å (PDB entry 1UEA) (Gomis-Rüth et al., 1997), TIMP-1/MMP-10CD complex at 1.90 Å (PDB entry 3V96) (Batra et al., 2012),TIMP-2/MT1-MMP complex at 2.75 Å resolution (PDB entry 1BQQ/1BUV) (Fernandez-Catalan et al., 1998), TIMP-2/MMP-13 complex at 2.00 Å (PDB entry 2E2D) (Maskos et al., 2007), TIMP-2/ProMMP-2 complex at 3.10 Å (PDB entry 1GXD) (Morgunova et al., 2002), and N-TIMP-3/TACE complex at 2.30 Å (PDB entry 3CKI) (Wisniewska et al., 2008). In 3 cases the structures related to TIMP were determined by NMR methods, such as N-TIMP-1 (PDB entry 1D2B) (Wu et al., 2000), N-TIMP-2 (PDB entry 2TMP) (Muskett et al., 1998) and the N-TIMP-1/MMP-3CD complex (PDB entry 1OO9) (Arumugam et al., 2003).

All four mammalian TIMPs share a two-domain structure, having an N-terminal domain and a C-terminal domain, each of which is stabilized by three disulfide bonds. The three-dimensional structure of TIMP is wedge-shaped. Crystallographic studies of free TIMPs, N-TIMPs and TIMP/MMP complex reveal that the N-terminal region is highly conserved and plays a crucial role in the inhibition of MMPs (Brew et al., 2010). As illustrated by the crystallographic structure of TIMP-2 (Figure 8), the N-terminal domain of TIMPs encompasses an oligosaccharide binding (OB) fold, a five-stranded β-barrel (formed from β-strands A through F)twisted with a Greek key topology, and three small α-helices. The five-stranded β-barrel is relatively rigid, compared with the N-terminal end and the loop connecting β-strands A and B. One of the three small α-helices is located close to N-terminal region and precedes β-strand A while another two follow β-strand F and form part of interface with the C-terminal domain (Nagase et. al., 2002).

The C-terminal domain of TIMP-2 (Figure 8), with about 65 residues, is composed of a pair of parallel β-strands (G and H), another two antiparallel β-strands (I and J), and a small α-helix. β-strands G and H are connected by a loop, followed by helix 5Й, while β-strands I and J are connected by a β-hairpin (Brew et. al., 2010). The core of C-terminal domain is covalently fastened by two disulfide bonds, Cys127-Cys174 and Cys145-Cys166, and shows an increasing flexibility towards the C-terminus (Brew et al., 2000).

The structure of TIMP-1 shows cysteines Cys1 and Cys3 are attached to two other cysteines, Cys70 and Cys99, respectively, to form two disulfide bonds. Cys1-Cys70 and Cys3-Cys99 disulfide bonds connect N-terminal region with the CD loop and EF loop, and together they contribute to the formation of the molecular edge (Gomis-Rüth et al., 1997). In TIMP-1, five residues, Cys1-Thr-Cys-Val-Pro, another five residues, Met66-Glu-Ser-Val-Cys70, and CD loop are covalently connected by the Cys1-Cys70 disulfide bond, and form a continuous ridge to insert into the active site of MMPs. As the result of this insertion, Cys1 located in N-terminal domain of TIMP-1, lies above the catalytic zinc ion of MMPs, the second residue Thr interact with S1' specificity pocket of the MMP, residues Cys3-Val-Pro5 interact with the S3' pocket in MMP active site, Ser68 interacts with the MMP S2 subsite and Val69 interacts with MMP S3 subsite (Figure 8) (Brew et al., 2010). This core of TIMP-1-MMP interaction interface which is highly conserved in all TIMP/MMP complexes, including N-TIMP-3/ADAM17, makes 60-75% interactions between TIMP-1 and MMPs (Brew et al., 2010).

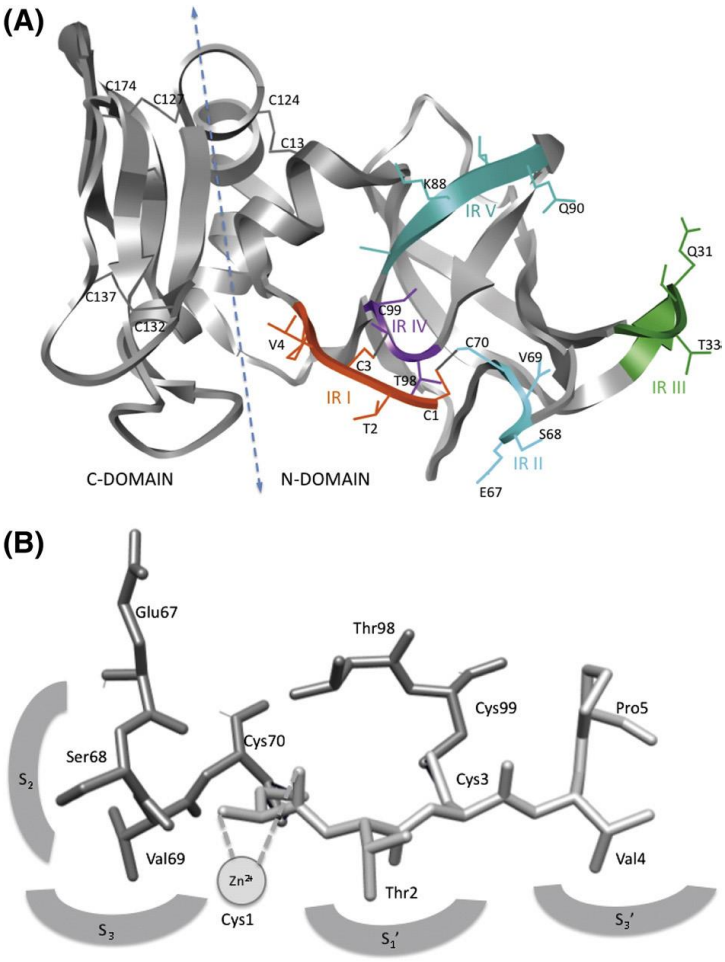

Figure 8. The crucial amino acid residues in the interfaces of TIMP-MMP complex (Brew et al., 2010)

Besides the core interaction interface, the AB loop (IR III) and EF loop (IR II) also contribute to the interaction between TIMP and MMP (Figure 8 A). Although the four human TIMPs share a high level of sequence identity (41%-52%) and have highly conserved structures and similar interactions in the core of their complex with MMPs, the size of AB loop in different TIMPs varies, resulting in variations in the interactions between TIMPs and MMPs. Some contacts formed between C-terminal domain of TIMP and the catalytic domain of MMP are on the periphery of interaction site (Gomis-Rüth et al. 1997, Fernandez-Catalan et al. 1998, Maskos et al., 2007), do not play important roles

in formation of complex since truncated N-TIMPs can still bind to MMPs in high affinity (Brew et al., 2010).

2.4 Structural basis for inhibition of MMPs by TIMPs

The X-ray structure of the MMP-3/TIMP-1 complex reveals that the wedge-shaped TIMPs bind with their edge into the active-site cleft of the cognate MMPs catalytic domain (Gomis-Rüth et al., 1997). During the formation of MMP-3/TIMP-1 complex, four polypeptide segments provided by N-terminus of TIMP-1 together with another two C-terminal polypeptide segments of TIMP-1 interact with MMP-3 catalytic domain (Figure 9). The N-terminal segment and the C-connector loop of TIMP-1 provide most of the intermolecular contacts. The N-terminal segment of TIMP-1, Cys 1-Thr 2-Cys 3-Val 4 interacts with the active-site cleft of MMP3, and inserts into two MMP-3 peptide backbones of S162–S166 and S220–S223 to make more intermolecular contacts with the bottom of MMP-3 active-site cleft and border it as well.

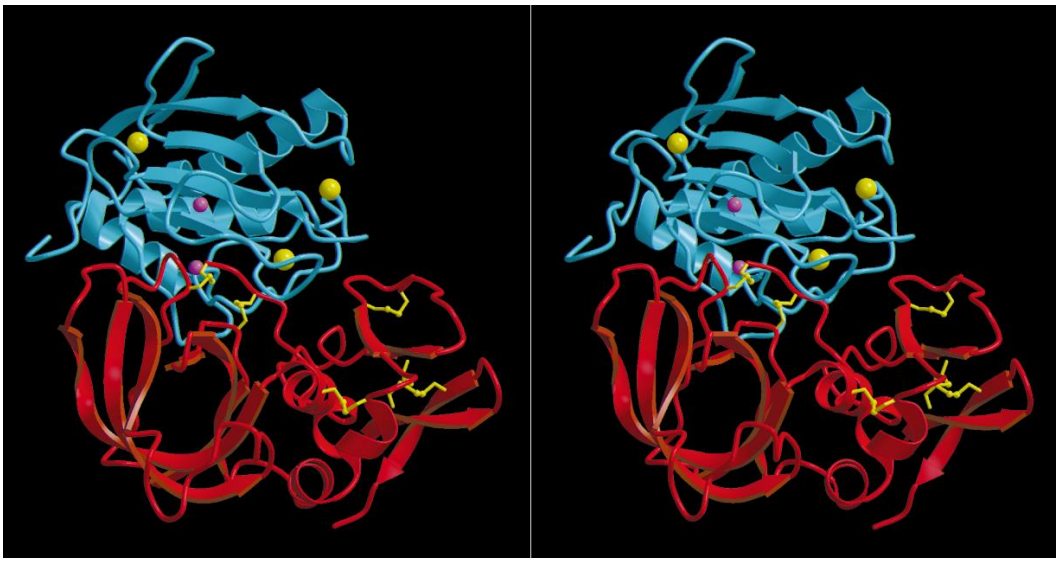

Figure 9. Stereo ribbon diagram of the complex formed between TIMP-1 (red) and MMP-3 (blue) (Gomis-Rüth et al., 1997)

Yellow bonds indicate disulphide bridges, and the spheres represent theMMP-3 bound 2 zinc (pink) and 3 calcium (yellow) ions. The active-site cleft of MMP-3 is directed halfway towards the bottom and the viewer. The MMP-3 polypeptide chain starts with a 'cap-like' structure on the left. Cys 1 of TIMP-1 is located on top of the catalytic zinc (centre of the complex). Its first four residues insert between the 'edge' strand (above, front) and the strand blocking off the specificity pocket (below, back) of MMP-3 (Gomis-Rüth et al., 1997), before the TIMP-1 chain deviates from the active-site cleft to form the N-terminal subdomain (left, bottom) and the C-terminal subdomain (right, bottom). Figure 9 was drawn with MOLSCRIPT and rendered with RASTER3D. (Gomis-Rüth et al., 1997).

The N-terminal TIMP-1 residue, Cys 1, is located directly over the catalytic zinc ion of MMP-3, and the N-terminal alpha-amino and carbonyl group interact with the zinc, which is also coordinated by another three imidazole nitrogens of MMP His s201, His s205 and His s211. The unprotonated α-amino group of Cys 1 forms hydrogen bonds to MMP-3 residues, Ser 68 and Glu 202. Mutational studies reveal that substitution of Thr to Ala on position 2 decreases the affinity of TIMP-1 to MMP-3 for 100-fold (Huang et al., 1997, Nagase et al., 2002) and the TIMP-1 mutant of Cys1 or Cys70 also shows more than 3- fold reduction in affinity to MMP-3 (Williamson et al., 1994), suggesting that residues around Cys1-Cys 70 which is disulfide bounded in TIMP-1 play critical roles when TIMP-1 interacting with MMP-3 (Nagase et al., 2002)

The side chains of TIMP-1 residues, Val 4 and Pro 5 just touch the surface of MMP-3. while the side chain of Thr 2 of TIMP-1 extends into S1′, a large specificity

pocket of MMP-3, with its β methyl group fitting in a hydrophobic niche and its β-hydroxy group facing the more polar entrance neck of S1′ (Gomis-Rüth et al., 1997). Towards the active-site cleft of MMP-3, which is represented by a solid surface coloured according to the electrostatic potential. The view is similar to that of Fig. 1. For simplicity, TIMP-1 (with carbons in green, oxygens in red, nitrogens in blue, and sulphurs in yellow) is represented only by the disulphide connected segments Glu 67–Gly 71 (left), Cys 1–Cys 3(right), and Thr 98–Cys 99 (bottom segment). The N-terminal TIMP-1 residue, Cys 1, is located on top of the catalytic zinc (pink sphere), liganding it through its a-amino and its carbonyl group; Thr 2 extends towards the deep S19 pocket of MMP-3 (right). The TIMP-1 side chains of Ser 68 and Val 69 (left) nestle towards the shallow S2 subsite and the S3 pocket ofMMP-3, respectively. Figure prepared using GRASP30. (Gomis-Rüth et al., 1997). The N terminus of TIMP-1 (only shown from Cys 1 to Cys 3) runs antiparallel to the MMP-3 ‘edge’ strand Leu S164–Tyr S168 (top) and parallel to segment Pro S221– Tyr S223 blocking off the specificity pocket (bottom, right)14 making six and two inter-main-chain hydrogen bonds, respectively (white dashed lines, not all of them visible). The catalytic zinc is coordinated by the a-amino group and the carbonyl oxygen of Cys 1 (visible only up to Cb) and by the three imidazole nitrogens of His S201, His S205 and His S211 (arranged anti-clockwise) in atrigonal–bipyramidal manner. The four zinc–ligand interactions visible are indicated by pink dashed lines. Contour is at 1j, and the orientation is as in Figs 1 and 3. (Gomis-Rüth et al.,1997).

The C-connector loop of TIMP-1 forms contacts with part of MMP-3 substrate-binding site that includes residues 83–86, 154–155, 163–167, 205 and 210–211. The

disruption of the salt bridge formed by the Phe 83 α-amino group and the Asp 237 side chain carboxyl group in MMP-3, a rearrangement of the N-terminal segment of MMP-3, and the movement of MMP-3 Phe 210 side chain phenyl ring result in the formation of a hydrophobic cap-like structure by the N-terminal segment of MMP-3, Phe 83-Pro 90. The side chains of Met 66 and Val 69 of TIMP-1 extend into this "cap", and most of the interactions of TIMP-1 residues with this region are hydrophobic. Also, the A–B loop of TIMP-1, particularly Val 29, Thr 33–Tyr 35, interacts with MMP-3 segments 85–86 and 154–155; and the Thr98 and Cys99 of the E–F loop of TIMP-1, Thr 98, is interacts with MMP-3 residues 221–223. Parts of the TIMP-1 C-terminal domain make weak hydrophobic interactions with MMP-3, an open loop, Leu133 and Ser 134, with MMP-3 residues 190–192; and the multiple-turn region, Gln 150–Leu 152, with MMP-3 residues 223–228 that are located near the C-terminus of MMP-3 (Figure 9) (Gomis-Rüth et al., 1997; Maskos et al., 2013).

In the MT1-MMP-TIMP-2 complex (Figure 10) the long A-B hairpin loop of TIMP-2 is located alongside the S-loop of the MT1-MMP active site cleft, to the β-sheet (Fernandez-Catalan et al., 1998) . Although the structure of MT1- MMP-TIMP-2 complex is similar to that of MMP-3–TIMP-1 complex, the elongated sA–sB loop of TIMP-2 and a MT-characteristic insertion loop of MT1-MMP are noteworthy differences (Gomis-Rüth et al., 1997). As in the MMP-3–TIMP-1 complex, most of the intermolecular contacts are made by the TIMP-2 N-terminal segment Cys1-Pro5, the C–connector loop and the disulfide bridge. TIMP-2 interacts with MT1-MMP through six separate segments, similar to TIMP-1 interaction with MMP-3 (Fernandez-Catalan et al. 1998).

Figure 10. Crystal structure of the MT1-MMP–TIMP-2 complex (Fernandez-Catalan et al. 1998)

3. Engineering of Proteins for Increased Selectivity and Affinity

3.1 Directed Evolution and Rational Protein Design

The introduction of mutations in the gene that encodes a target protein provides an effective method of engineering novel molecules with modified functional or physical properties using information derived from experimental data and by computation. Currently, many industrial enzymes are engineered, for example, to enhance their stabilities and the ability to modify proteins for different purposes has practical applications in the medical and agricultural fields. Protein engineering has deepened our understanding of the fundamental properties of proteins in relation to activity, stability, folding, and diseases associated with protein misfolding and dysfunction. The acquisition of detailed information on protein structures and developments in high-throughput

technology have expanded the capabilities of protein engineering. However, it remains challenging to identify modifications that are required for chosen functions, as well as to predict the effects of mutations. The main strategies for protein engineering to solve these problems are directed evolution and rational design.

During the last decade, directed evolution, a mimic of natural Darwinian evolution, has developed rapidly as the result of advances in high-throughput methods. Directed evolution relies on the Darwinian principle of selecting mutants with desired properties from large combinatorial libraries as opposed to applying knowledge of structure-function relationships in a protein. As shown in Figure 1, directed evolution involves creating a library of mutant proteins using repeated rounds of randomly mutating genes via the mutagenesis and recombination of their DNA, the expression of mutated genes in host cells, followed by screening and selection to identify mutants with the desired properties (Turner et al., 2009). In each cycle, a new library is created using, as templates, improved mutants that were selected in the previous round. Directed evolution is applied for cases in which the desired properties of the protein can be only obtained by multiple mutations. The results of directed evolution studies reveal that the new characteristics of proteins, such as high stability can be achieved by many different "structural routes" (Giver et al., 1998, Zhao et al., 1999, Spiller et al., 1999, Miyazaki et al., 2000, Martin et al., 2002, Wintrode et al., 2000). Random mutagenesis makes a major contributes to the success of direct evolution. This approach does not rely on detailed information about the structural basis of interactions that underlie the function of the target protein. Because only a very limited number of mutations can yield a large increase in stability or selectivity, screening more mutants can increase the success rate

for finding mutants with the desired properties. Unfortunately, the difficulty to refold the aggregated mutations limits the mutation library size, due to our insufficient knowledge of protein folding. (Eijsink et al., 2004).

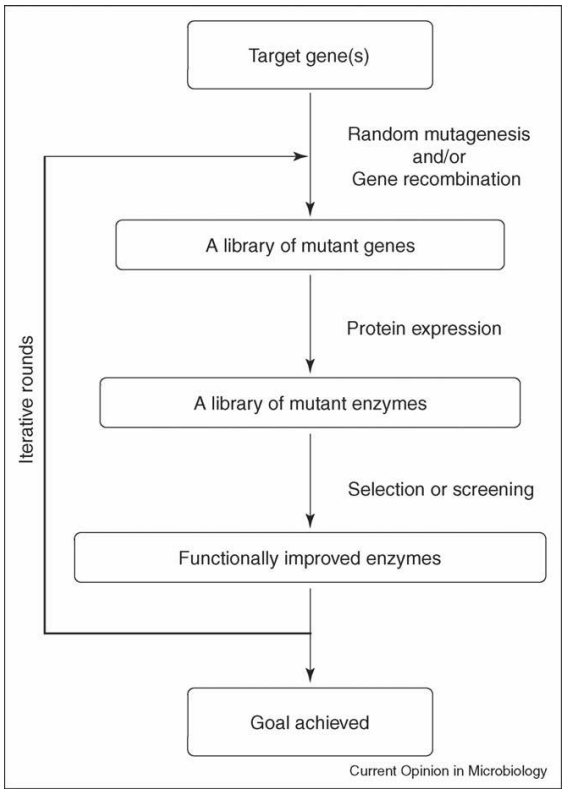

Figure 11. General scheme of directed evolution (Johannes et al. 2006)

Unlike directed evolution, rational protein design is based on protein structural information, such as knowledge of the functional effects different mutations, crystal structure data on proteins or structural models obtained by homology modeling, and information on structure-function relationships obtained by experiments or computation (Lu et al. 2009, Lu et al. 2001). The recent progress of rational protein-design includes three methodologies: design using scaffolds developed *de novo*, design using native protein scaffolds and the design of novel proteins containing unnatural amino acids or non-native cofactors (Lu et al. 2009). Among these three design strategies, *de novo*

design, also called design “from scratch”, is the most challenging. In de novo design, a polypeptide sequence not directly related to any natural occurring protein is constructed, with the goal of making the novel protein sequence fold into a defined three dimensional structure with the desired function. Most *de novo* design involves in searching for lowest free-energy states which relies on physics-based force fields. However, the current difficulty is to accurately design the force fields to describe the atomic interactions of the novel proteins, as well as the their correct folds (Mitra et al., 2013). Exciting developments in this field include a designed three-stranded coiled-coil protein that binds arsenic with a tris Cys metal-binding site (Touw et al., 2007), and RM1, a designed β-structure protein, mimicking the redox active protein, rubredoxin, that binds iron and reversibly cycles between the FeII and FeIII) oxidation states (Nanda et al., 2005). *De novo* design offers the complete control over the structure of the protein to achieve a goal, however, our current limited knowledge of protein folding restricts the *de novo* designed scaffolds to a few types. When compared to proteins designed from native scaffolds, *de novo* designed proteins can be hard to fold and crystallize to allow characterization of the 3D structure. Therefore, design using naturally evolved protein as templates results in a wider choice of scaffolds that are sufficiently stable and more tolerant of mutations. Moreover, the resulting designed protein tends to form the globular structure which can be studied by spectroscopic and X-ray crystallographic method more easily (Lu et al., 2001) . In this approach, site-directed mutagenesis is used to confer a new function on a protein scaffold by introducing chosen residues. This methodology relies on knowledge/experience derived from previous research, such as structural, computational, and thermodynamic studies as well as molecular dynamics simulations. This approach

does not replace biochemical and biophysical studies of native proteins, but requires to incorporate all the structural features to create novel or improved function. (Lu et al. 2009). Besides using protein scaffolds that have been generated de novo or are natural, protein engineers can incorporate unnatural amino acids or cofactors into the scaffolds to expand the potential properties of polypeptides. Mills JH et al. reported a successfully example to incorporated metal-chelating unnatural amino acids in the designed metalloenzyme , which is aided by an computational design programs with atomic level accuracy (Mills et al., 2013) .

3.2 Protein engineering of the Tissue Inhibitors of Metalloproteinase

A molecule that has the potential to be used as a drug should bind to its target with high affinity and selectivity. Because they are generally lack of selectivity as MMPs inhibitors, wild-type TIMPs show little clinical promise. However, TIMPs that have been engineered to be highly selective and efficacious inhibitors of selected MMPs, may be utilized for future treatment of diseases.

Previous studies have shown that residues 2, 4, 68 and 98 are pivotal in the inhibitory specificity of TIMP-1 and the A-B loop may modulate the effects of crucial site mutations on TIMPs affinity to MMPs (Meng et al., 1999, Wei et al., 2003, Hamze et al., 2007). The results of two types of study have provided information that is used for rational engineering of TIMPs for increased selectivity and/or affinity: 1. Mutational studies using site-direct mutagenesis that provide information about the roles of specific residues in the affinity for different MMPs; 2. Computational protein designs that predict the effect of various mutations and optimize the sequence of TIMPs to yield required structures. Computational methods for structure prediction can be considered as a good

starting point for the further experimental determination of the protein structures, since these methods are significantly faster and cheaper than experimental ones. However, these are few examples in which this tool has been successfully applied in TIMPs engineering, possibly due to the inaccuracy of current computational approaches.

3.3 Mutational Studies of the Tissue Inhibitors of Metalloproteinase 1 (TIMP-1) Inhibitory Domain

Mutational studies of N-TIMP-1 have shown that the side chain of residue 2 which, in currently known TIMP/MMP complexes binds to the large S1´ specificity pocket of MMPs which is a key to MMP substrate specificity, has a major influence its and selectivity for MMPs (Meng et al, 1997). Such conclusion is supported by a series of research data, including the observation that the absence of the side chain of residue 2 as the result of a Thr2 to Gly mutation decreases the affinity for MMPs by three to five orders of magnitude, resulting in a loss of 33–55% of the free energy of interaction (Meng et al, 1999). Investigations of the effect of the side chain of this position in N-TIMP-1 by substituting Thr with another fifteen different amino acids indicate that TIMP variants with larger side chains at their position 2 may have higher selectivity for MMPs. Among all those fifteen TIMP variants, apart from the Gly mutant which has the weakest inhibitory activity for all three MMPs, MMP-1, MMP-2 and MMP-3, the Ala2 mutant also has reduced affinity for all three MMPs (Table 2).

Table 2. Ki values of the N-terminal domain of tissue inhibitor of metalloproteinases 1 (N-TIMP-1) and its variants.Ki values of the N-terminal domain of tissue inhibitor of metalloproteinases 1 (N-TIMP-1) and its variants (Meng et al., 1999)

Variant	MMP-1	MMP-2	MMP-3
N-TIMP-1	3.0	1.1	1.9
Thr2 to Serine	25	2.1	0.5
Thr2 to glycine	18000	103000	1400
Thr2 to alanine	2090	307	126
Thr2 to leucine	93	1.0	3.2
Thr2 to isoleucine	236	5.6	20
Thr2 to valine	1.6	4.5	3.0
Thr2 to methionine	11	0.7	0.7
Thr2 to phenylalanine	42	17	13
Thr2 to asparagine	1970	16	44
Thr2 to glutamine	870	12	29
Thr2 to aspatic acid	8130	1250	1110
Thr2 to glutamic acid	5730	433	468
Thr2 to lysine	1670	31	70
Thr2 to arginine	5010	12	28
Thr2 to Leucine Val4 to Serine Ser38 to alanine	More than 2000	6.8	196

In addition to the substitutions for residue 2, mutants with substitutions at residue 4 and 68 also alter the affinity and selectivity of N-TIMP-1 for MMPs. Moreover, double and triple mutations with combination of substitutions at position 2 with position 4 and/or 68 resulted in engineered N-TIMP-1 with higher binding affinity and selectivity for individual MMPs (Table 3)

Table 3. Ki (app) (nM) of N-TIMP-1 combined mutants against MMP-1 (5 nM), MMP-2, and MMP-3 (1 nM each). (Wei et al. 2003b)

Mutant	MMP-1	MMP-2	MMP-3
Wild type	0.4 ± 0.02	0.4 ± 0.04	0.2 ± 0.002
T2L	37 ± 6	0.4 ± 0.04	1.3 ± 0.2
V4S	2.1 ± 0.2	0.4 ± 0.04	1.7 ± 0.2
T2L/V4S	140 ± 6	0.3 ± 0.01	6.0 ± 0.6
S68A	14 ± 1	5.2 ± 0.7	32 ± 0.7
T2L/V4S/S68A	≥3000	4.0 ± 0.2	14 ± 0.4
T2S	5.9 ± 0.8	0.8 ± 0.1	0.2 ± 0.04
V4A	0.4 ± 0.05	0.5 ± 0.02	0.1 ± 0.02
T2S/V4A	3.3 ± 0.6	0.4 ± 0.1	0.1 ± 0.006
S68Y	61 ± 11	2.7 ± 0.3	0.3 ± 0.02
T2S/V4A/S68Y	15 ±0.6	0.1 ±0.006	0.05 ±0.004
T2R	≥2000	4.8 ± 0.2	11 ± 0.8
V4I	6.4 ± 0.7	0.3 ±0.008	0.2 ±0.01
T2R/V4I	NIDb	10 ± 0.6	4.0 ±0.1

Some membrane-type MMPs, such as MT1-MMP are efficiently inhibited by TIMP-2, -3, and -4, but not TIMP-1(Stracke et al., 2000). Although the overall structure of TIMP-1 is closely similar to that of TIMP-2, a major difference in their structures is the size of the loop between β-strands A and B. In the crystallographic structure of the TIMP-1/MT1-MMP complex, the longer and more flexible A-B loop of TIMP-2 extends into the MT domain of MT1-MMP, making extensive residue contacts with the MT1-MMP catalytic domain (Fernandez-Catalan et al. 1998; Maskos et al. 2007), while there is no explanation as to why TIMP-1 has low activity against MT1-MMP. Moreover, grafting the longer AB loop from TIMP-2 into N-TIMP-1 did not improve the interaction between N-TIMP-1 and MT1-MMP (Hamze et al., 2007). In study conducted by Lee et al, MT1-MMP binding ridge of TIMP-1 was divided into five divisions: the "N terminus" division, the "Pro6" division, the "AB-loop" division, the "CD-loop" division, and the "EF-loop" division. Each division had one or more amino acid residues chosen for mutagenesis (Table 4). Among the mutants created, the substitution of Leu for Thr98 lowered the Ki for MT1-MMP from 178 to 51nM (Hamze et al., 2007). Thr98 is located in the EF-loop, and is adjacent to the Cys3–Cys99 disulfide bond and above the interface of N-TIMP-1-MT1-MMP complex. The more than 2-fold improvement of inhibitory ability of N-TIMP-1 T98L mutant for MT1-MMP indicates that Thr98 is one determinant of the weak binding of N-TIMP-1 to MT1-MMP (Lee et al., 2003) . In addition to the enhanced inhibition for MT1-MMP, the N-TIMP-1 T98L mutant was found to have a similar effect on binding to MMP-3 with approximately threefold reductions in the Ki (from 0.2nM to 0.06nM). The combination of three mutations, V4A plus P6V plus T98L improves N-TIMP-1 binding to MT1-MMP to 16nM (Hamze et al, 2007).

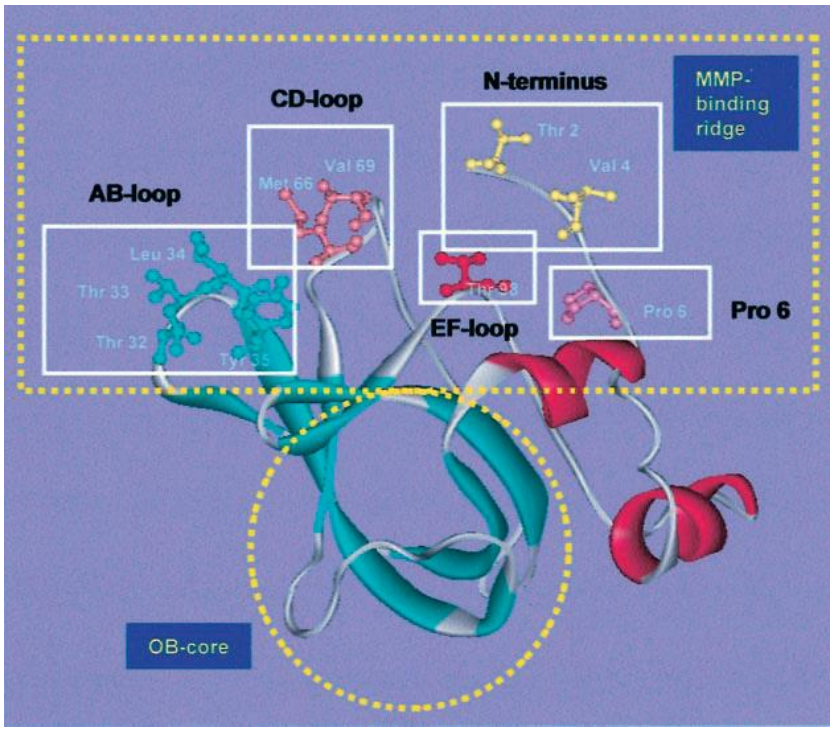

Figure 12. Anatomy of N-TIMP-1.TIMPs inhibit metalloproteinases by inserting the MMP-binding ridge into the active site of the enzyme. The inactivity of TIMP-1 against MT1-MMP is most likely to be due to the presence of obstructive epitopes at the MMP-binding ridge of the molecule. Hence, the ridge is divided into five "divisions," each composed of one or more independent epitopes. The amino acid residues chosen for mutagenesis in this work are highlighted in the *ball-and-stick* format.(Lee et al., 2003).

Table 4. Ki (app) (nM) of N-TIMP-1 mutants against MT1-MMP (Lee et al. 2003; Hamze et al., 2007).

	Ki app (n M)
Pro6 mutants	
P6V	78 ± 4
P6S	95 ±5
P6A	165 ± 13
AB-loop mutants	
T2-AB-loop	77 ± 6
Long T2-AB-loop	117 ±18
T3-AB-loop	106 ± 7
T4-AB-loop	170 ± 13
CD loop mutants	
M66K	462 ±103
M66D	≥500
M66L	237 ± 18
M66I	146 ± 10
M66V	183 ± 13
M66A	199 ± 20
M66G	254 ± 28
V69L	259 ± 30
EF-loop mutants	
T98L	51 ± 7
N-terminal mutants	
T2S	220 ± 20
V4A	66 ± 6
V4S	81 24

4. Protein-Protein Binding Energetics

During protein-protein interactions, the interplay between some physical forces and proteins results in the formation of protein complexes, which have unique structures. Moreover, the changes of the proteins' energy landscape may induce some structural changes in the interacting molecules. Therefore, a true understanding of protein-protein interaction requires its characterization related to two factors: first, the principle physical forces acting on the binding process and, second, the changes in conformation and dynamics of the polypeptide chains during binding. Such characterization not only is used for the understanding of the protein structures in details, but also contributes to some applied research areas, such as protein engineering and rational drug design. One can use thermodynamic approaches to characterize the physical forces involved in protein binding by studying the dependency of the binding's general energetic properties on temperature and concentration of the reaction system.

4.1 Thermodynamic Parameters

A complete thermodynamic profile for a binding interaction is composed of the binding free energy, enthalpy, entropy, and heat capacity change. Among them, the Gibbs free energy (symbolized by G), can be used for doing non-expansion jobs in biological systems, such as motivating chemical processes or changing molecular conformations. Meanwhile, the Gibbs free energy change (symbolized by ΔG) accompanying the protein binding process reflects the binding strength (affinity).

In relation to TIMP/MMP interactions, the Gibbs free energy change (ΔG) can be determined by using this equation: $\Delta G = - RT \ln (1/K_i)$ (Equation 1). Where R is the

universal gas constant (1.989 cal/mol K)), and T is the temperature in K. At room temperature (289 K), RT ≈ 0.6 Kcal/mol. K_i is the binding/inhibition constant generated from fluorescence assays.

The Gibbs free energy change of the protein-protein interaction system provides valuable information to predict the binding affinity, the relative stability of states, and the direction of the interaction process. Moreover, the Gibbs free energy change is made up of contributions from changes in two other thermodynamic quantities, enthalpy (H) and entropy (S). At constant temperature, the changes of these three thermodynamic quantities follow this relationship: $\Delta G = \Delta H - T\Delta S$ (Equation 2)

The enthalpy change (ΔH) and entropy change (ΔS) associate with specific features of the binding system. Enthalpy (H) relates to the internal energy (E), pressure (P), and volume (V) of the system: $H = E + PV$ (Equation 3).

Since the pressure and volume of the protein binding system are constant, the changes of enthalpy (ΔH) of the protein binding come from changes in the internal energy of the whole system. The internal energy of the system (E) is composed with two contributions: potential energy (U) and kinetic energy (K): $E = U + K$ (Equation 4).

The potential energy (U) is the sum of all the atom-field effects in the system, which can be represented by all covalent bonds and most non-covalent interactions in the protein binding process (Schonbrun et al., 2003). Meanwhile, the kinetic energy, K, is determined by thermally induced atomic motions in molecules. Therefore, the enthalpy change (ΔH) is associated with formation or breaking of covalent bonds, formation of

hydrogen bonds or van der Waals contacts, and changes of thermally induced atomic motions.

Entropy (S), a concept provided by statistical thermodynamics, is related to the number of possible configurational states of the whole system, which can be considered as a measure of disorder in the system. Thus, entropy change (ΔS) represents changes in the freedom of movement of the solute atoms or the solvent atoms during the binding process (Pierce et al., 2011).

The changes in two thermodynamic quantities, enthalpy change (ΔH) and entropy change (ΔS), can be tracked by measuring the heat transferring between the system and its surroundings. Another thermodynamic quantity called heat capacity (C_p) refers to the amount of heat required to be transferred for elevating the system to a certain temperature. The heat capacity (C_p) can also be considered as the change of enthalpy per change of temperature of 1 mol of substance by 1 K (Prabhu et al., 2005): $\Delta C_p = \Delta H/\Delta T$ (Equation 5).

In the protein binding system, heat energy is needed to drive the endergonic reaction of breaking non-covalent interactions. Therefore, the heat capacity can be used to measure the number of non-covalent interactions in the system. One of the energetic changes associated with protein-protein interactions is often a large negative heat capacity change, which is provided by burial of one or more hydrophobic surfaces (Pierce et al., 1999).

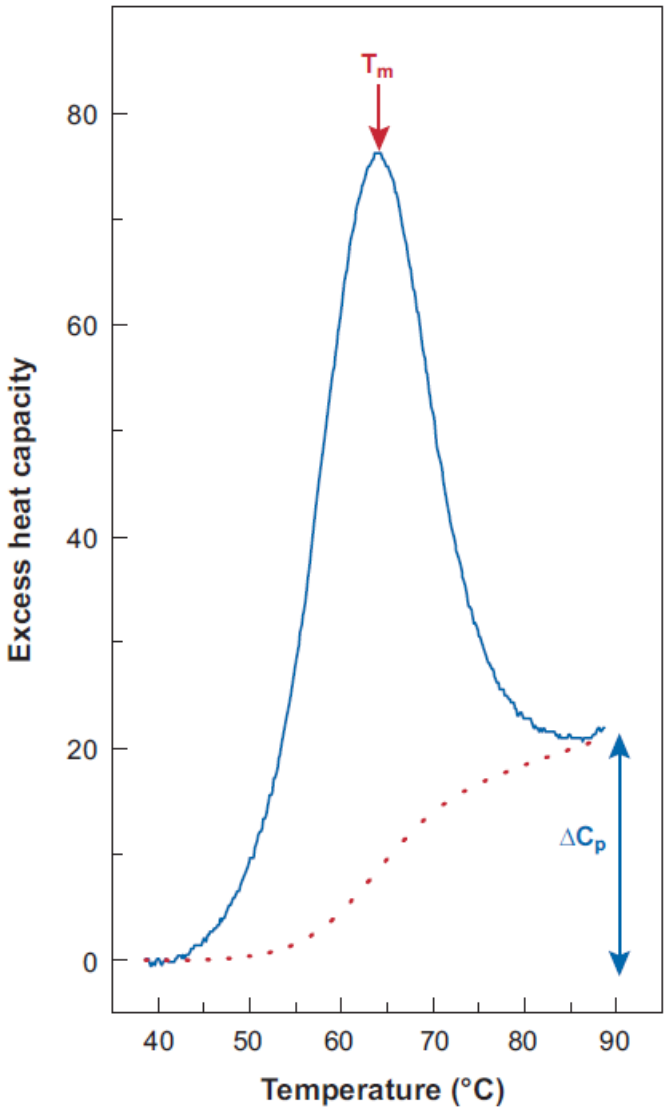

Figure 13. Representative DSC data shows the relationship between the melting transition temperature (Tm) and the heat capacity change (ΔCp)The curve depicts the heat capacity (C_p) as a function of temperature (Chaires et al., 2008)

4.2 Correlation of Interactions in the Structures of Protein/Protein Complexes with Thermodynamic Profiles

The binding process between two biomolecules at the atomic level involves the formation or elimination of many individual non-covalent bonds both between the interacting molecules and with the solvent (Ladbury et al., 2010). Protein-protein

interactions involve the burial of solvent-exposed surfaces with release of solvent molecules and the formation of hydrogen bonding networks and van der Waals interactions. Correlations between thermodynamic data and structure may enhance our understanding of protein interactions and provide a useful tool to aid drug development (Ladbury et al., 2010).

Thermodynamically speaking, protein-protein interactions are analogous to the process of protein folding, in several ways. First, both cases involve a cooperative array of polar and non-polar interactions. Second, in both cases the process has conformational adjustments resulting from changes in the system's degree of order. Protein-protein interactions display diversity in their binding affinities, with binding energies ranging from -2.5 to -22 kcal/mol (Dunn et al., 2001). Most protein-protein interactions are non-covalent, and their specificities and affinities are mainly the result of non-covalent interactions. The non-polar residues located in protein-protein interfaces are mainly responsible for driving the binding process via hydrophobic effects (Jones et al., 1996; Bogan et al., 1998), while the polar residues are involved in binding specificity and affinity via electrostatic interactions (Sheinerman et al., 2000).

Because the binding affinity is related to ΔG, and ΔG is made up of two different contributions (ΔH and ΔS), the same energy and so the same binding affinity can be obtained by the different combinations of enthalpy and entropy contributions. (Sarver et al., 2007). Polar groups which are able to establish hydrogen bonds and van der Waals interactions might contribute significantly to a favorable enthalpy change (negative value). However, the desolvation of polar groups or structural changes carry the

unfavorable enthalpy change (positive value). The entropy change of binding is also made up of two major contributions: the conformational entropy change (ΔS_{conf}) and the solvation entropy change (ΔS_{solv}). ΔS_{conf} represents the changes in number of accessible inter-convertible conformations. Favorable ΔS_{solv} results from the release of water molecules from nonpolar groups in binding interfaces. Loss of translational and rotational degree of freedom and the rigidification of groups, as well as the decrease in the accessible conformational space resulting from the binding process, may cause unfavorable entropy changes. Meanwhile, favorable entropy change are associated with the hydrophobic effect and increased conformational entropy (summarized by Figure 14) (Kawasaki et al., 2011).

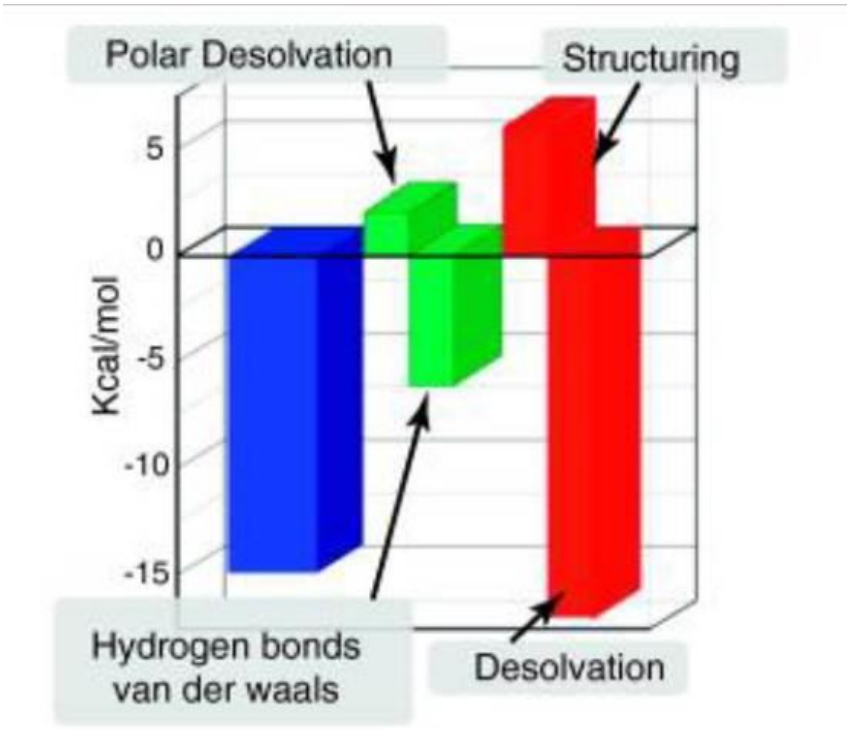

Figure 14. Typical contributions to the thermodynamic signature of protein-protein interactions Favorable enthalpic interactions (ΔH; green bars) originate primarily from hydrogen bonding and van der Waals interactions. Unfavorable enthalpic interactions, by contrast, originate from the desolvation of polar groups or structural changes. Favorable entropic contributions ($-T\Delta S$, red bars) are due to desolvation of nonpolar functionalities, whereas unfavorable entropic contributions originate from the structuring of residues in the protein or the compound itself. *Abbreviation*: ΔG, Gibbs energy of binding (blue bars) (Kawasaki et al., 2011).

High binding affinity can be obtained by optimizing the entropy change by increasing the hydrophobic effect of nonpolar groups. However, an increase in the hydrophobic effect tends to make proteins less soluble and to make protein-protein interactions less specific. As opposed to entropic optimization, enthalpic optimization may increase selectivity by improving binding affinity for specific targets. The introduction of nonpolar and polar functionalities may improve binding affinity and selectivity in different ways. A nonpolar functionality can be introduced to fill a cavity in

order to improve affinity to the target protein with a favorable combination of entropy and enthalpy changes. (Kawasaki et al., 2011).

A nonpolar group that fills a cavity with good shape complementarity will increase the binding affinity to the target protein (blue) by a combination of enthalpic and entropic gains (Figure 14, top). If the functionality does not fill the cavity tightly for an off-target protein (Figure 14, center) a smaller affinity gain will be observed, thus contributing to selectivity. If the cavity in the off-target protein is smaller and the functionality does not physically fit, an affinity decrease can result with a larger selectivity gain. (Figure 14, top) shows the effects of a polar functionality that establishes two strong hydrogen bonds with the target protein (blue) that is partially compensated by an opposite entropic penalty (this situation is common, but other outcomes are also possible). If one of the hydrogen-bonding partners is not present or if its location is not similar in an off-target protein (Figure 14, bottom), the enthalpic desolvation penalty will predominate, causing a decrease in binding affinity to the off-target molecule (Kawasaki et al., 2011).

4.3 Isothermal Titration Calorimetry (ITC): A Quantitative Means for Measuring the Thermodynamic Properties of a Protein-Protein Interaction

Isothermal titration calorimetry (ITC) can dissect the sources of the free energy changes for protein interactions with other macromolecules and ligands (Campoy et. al., 2005), providing a full thermodynamic characterization of molecular interactions, including stoichiometry, Gibbs free energy, enthalpy, entropy, ionization and heat capacity changes (Falconer et al, 2010). The binding process between two biomolecules

at the atomic level involves the formation or elimination of many individual non-covalent bonds both between the interacting molecules and with the solvent (Ladbury et al., 2010). Isothermal titration calorimetry (ITC) can dissect the sources of the free energy of protein interactions with other macromolecules and ligands. Measurements of the heat released or absorbed during the titration of a protein with a binding partner can quantify the enthalpy of binding (ΔH), association constant Ka, and stoichiometry (N), allowing the calculation of the changes in free energy (ΔG) and entropy (ΔS) of binding. Titrations in buffers with different ΔH of ionization provide information about ionization changes associated with binding while the heat capacity change for binding, ΔC_p, is quantified as the temperature-dependence of ΔH and can be used to estimate the solvation entropy of binding (ΔS_{solv}). These parameters can be correlated with the composition of the interaction interface and changes in dynamics and solvation associated with the interaction. Correlations between thermodynamic data and structure may enhance our understanding of protein interactions and provide a useful tool to aid drug development (Ladbury et al., 2010).

The major part of an ITC instrument is an adiabatic jacket, which contains two lollipop- shaped cells: a reference cell and a sample cell. Both cells are made of highly efficient conducting materials. In an ITC experiment, the sample cell is used to hold the macromolecule solution while the reference cell contains buffer, water or ligand. There is a heater inside the jacket to supply a small continuous power on reference cell. Sensitive thermopile/thermocouple detectors detect temperature differences between the reference and sample cells, and between the two cells and jacket which is usually cooled by a circulating water bath. In the experiment, the constant power applied on the reference cell

produces the signals prior to the injection of titrant, which direct the feedback circuits to activate the heater of the sample cell. Such direct can be measured and be considered as the time-dependent input of power to maintain the same temperature of sample cell and reference cell.

During the injections, an endothermic reaction has a decreased temperature on sample cell, so that the feedback power will be activated to increase the temperature of sample cell to maintain the equal temperature of two cells. For an exothermic reaction, an increased temperature of sample cell causes feedback circuits be deactivated in order to maintain the same temperatures between sample cell and reference cell (Pierce et al., 1999).

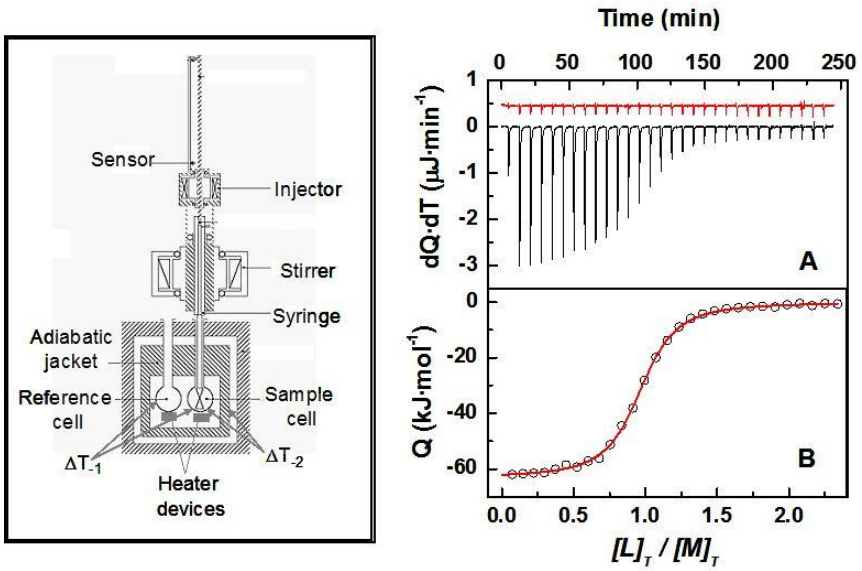

Figure 15. A schematic diagram of the main components of a titration calorimeter *(left side)*. *a titration calorimetry experiment of a protein with a ligand (right side)* (Pierce et al., 1999).

In panel A) the titration thermogram is represented as heat per unit of time released after each injection of the ligand into the protein (black), as well as the dilution

of ligand into buffer (red). In panel B) the dependence of released heat in each injection *versus* the ratio between total ligand concentration and total protein concentration is represented. Circles represent experimental data and the line corresponds to the best fitting to a model considering *n* identical and independent sites (Pierce et al., 1999).

II THERMODYNAMIC ORIGINS OF SELECTIVITY IN THE INTERACTIONS OF N-TIMPS AND MT1-MMP CATALYTIC DOMAINS

1. Introduction

While all the four TIMPs (-1 to -4) can inhibit most MMPs, there are some differences in specificity between them and their specificity as inhibitors of individual MMPs has not been fully discovered (Brew et al., 2010). A good example of differences in specificity is the efficient inhibition of MT1-MMP by TIMP-2, -3, and -4, but not by TIMP-1 (Stracke et al., 2000), which raises interesting questions regarding the structural basis of specificity of TIMP/MMP interactions. Previous structural studies indicate that in the complex of TIMP-2 with MT1-MMP, the solvent-exposed surface of each component is reduced by ~1250 $Å^2$ during their interaction (Fernandez-Catalan et al, 1998), while the interaction shows a similar mode of inhibition to that in the TIMP-1/MMP-3 complex (Gomis-Rüth et al., 1997; Fernandez-Catalan et al, 1998). A comparison of the structures of N-TIMP-2 and N-TIMP-1 indicates that N-TIMP-2 is longer by 7 residues and has a longer flexible AB loop than N-TIMP-1, which makes multiple contacts with MT1-MMP (Maskoset al, 2007; Fernandez-Catalan et al, 1998). However, the low affinity of TIMP-1 for MT1-MMP cannot be readily explained by the surface features of the complex. Calorimetric studies of the interactions of N-TIMP-1variants and -2 variants to MT1-MMP cd will illuminate the correlations between the thermodynamic profiles of the

binding process and structural features of complex which may help to explain how differences in TIMPs structure contribute to the their affinities and specificity for MMPs.

Previous calorimetric studies of the interactions of N-TIMP-1 and N-TIMP-2 with the catalytic domains of MMP-3 and MMP-1 (Arumugam et al., 2003, Wu et al., 2011) show that all these interactions are associated with unfavorable or small favorable enthalpy changes and are driven by entropy increases arising from solvent (estimated from the ΔC_p) and/or increased conformational dynamics.

In this section, I focus on the investigation of the thermodynamic profiles of the N-TIMP-1/MT1-MMPcd and N-TIMP-2/MT1-MMPcd interactions, including determining the heat capacity changes and the ionization changes on complex formation. Our data show that a large conformational entropy penalty is responsible for the weak inhibition of MMP-14 by N-TIMP-1. Together with the previous study of the interactions between N-TIMP-1, N-TIMP-2 and MMP-1, MMP-3cd (Wu et al., 2011), the thermodynamic profiles of N-TIMP-1 and N-TIMP-2 with MT1-MMPcd interactions indicate that the interactions of N-TIMPs with MMPs are driven by entropy increases that are partitioned between solvent and conformational entropy.

2. Materials and Methods

2.1 Construction of N-TIMPs, MMPs and Their Mutants

Wild-type N-TIMP-2 and its mutants (S2D, and S2D/S4A), wild type N-TIMP-1 and its T98L mutant as well as MMP-1cd, MMP-3cd and MT1-MMP were expressed using the pET-42b vector. Superdex-75 was purchased from Amersham Biosciences and Centriplus YM-3 centrifugal filter devices were from Millipore. Isothermal titration

calorimetry studies were carried out using a MicroCal VP-ITC Microcalorimeter. All other reagents and cells were from the same sources as in previous studies (Wu et al., 2011).

The N-TIMP-1 and N-TIMP-2 mutants were generated using QuikChange II Site-Directed Mutagenesis Kits (Agilent Technologies). Primers were designed using web-based primer design program (http://labtools.stratagene.com/QC). PCR reactions were carried out at 95 °C for 30 sec, 55 °C for 1 min and 68 °C for 5 min, for 30 cycles after a 3-min hot start at 95 °C. The PCR products were cloned back into pET-42b vector (Novagen) for expression.

2.2 Expression, Purification, and in Vitro Folding of N-TIMPs, MMPs and Their Mutants

N-TIMPs wild type, MMPs CD and their mutants were expressed in Escherichia coli BL21(DE3) cells as inclusion bodies and extracted and folded as described previously (Arumugam et. al. 2003). The native N-TIMPs were purified by medium pressure cation exchange chromatography as described (Wu et al., 2011) using the cellulose cation exchange mediumCM-52. The concentration of active N-TIMPs were determined by ITC and activity titration, were about 44% of the total in most preparations. MMPs were purified by ion exchange chromatography in 8M urea followed by folding gel filtration and a column (2.5×35cm) of Superdex‐75, pre-equilibrated and eluted with 20 mM HEPES buffer, pH 7.4, containing 250 mM NaCl and 20 mM $CaCl_2$. The eluate was collected in 6-ml fractions at a flow rate of 0.5 ml/min. Fractions containing

folded N-TIMPs were identified by polyacrylamide gel electrophoresis, pooled and concentrated using Centriplus YM-3 centrifugal filter devices (Millipore).

2.3 Fluorescence Assays for N-TIMPs Activity

The inhibition of MMPs by wild type N- TIMP- 1, N-TIMP-2 and their variants were measured by assaying MMP activities for hydrolysis of fluorogenic substrates using a PerkinElmer LS50B luminescence spectrometer. Assays were conducted in HEPES buffer (20 mM) pH 7.4, containing 250 mM NaCl, 10 mM CaCl2, and 50 μM ZnCl2 which was used also for the dilution of MMP and TIMP samples. To determine the Ki(app) of N- TIMP- 1 wild type for MT1-MMP CD at 25 ° C (298 K), various concentrations of inhibitor were incubated with 5 nM enzyme at 25 ° C for 3h before addition of Knight substrate for MT1-MMP CD and MMP-1cd or, for MMP-3cd, the NFF-3 substrate (Mca-Arg-Pro-Lys-Pro-Val-Glu-Nva-Trp-Arg-Lys(Dnp)-NH2)to a final concentration of 3μM. Catalytic activity was determined by measuring the increase in fluorescence intensity as described above.

Reaction velocities were measured as the slope of the linear portion of the fluorescence vs time curve. The percentage of residual MMP activity was calculated by dividing the velocities measured with inhibitor by the velocities measured without inhibitor (v/v_0).

$K_{i(app)}$ values were calculated by fitting inhibition data into the following equation,

$$v/v_0 = \frac{E - I - K + ((E - I - K)^2 + 4EK)^{0.5}}{2E} \quad \text{(Equation 6)}$$

where v is the experimentally determined reaction velocity, v_0 is the activity in the absence of inhibitor, E is enzyme concentration, I is inhibitor concentration, and K is the apparent inhibition constant, $K_{i(app)}$ (Wei et al., 2005).

For stoichiometric titrations, the inhibitors, N-TIMP-1, N-TIMP-2 wild type and their variants at various concentrations were incubated with 500 nM MMPs at room temperature (310K) for 4 h. The mixtures were diluted 300-fold with TNC buffer, and immediately assayed with 1.5 μM Knight Substrate for MMP-1cd and MT1-MMP cd and NFF-3 substrate for MMP-3cd as described above. Residual MMP activity (%) was calculated as described above and plotted against the molar ratio of TIMP/MMP (0–4 in this case). The stoichiometry was determined by linear regression analysis of the appropriate data points using Sigma Plot™.

2.4 Isothermal Titration Calorimetry of N-TIMP/MMP cd Interactions

Protein solutions were dialyzed extensively against various buffers at 20 mM concentration containing 250 mM NaCl, 10 mM $CaCl_2$, and 50 μM $ZnCl_2$ at pH 7.4 and degassed prior to use. N-TIMPs were titrated with the MMP cd (120–300 μM) at different temperatures using a MicroCal VP-ITC microcalorimeter as described previously.

The titrations of N-TIMPs were conducted at pH 7.4 to avoid solubility problems at the protein concentrations required for ITC. The instrument, MicroCal VP-ITC microcalorimeter was programmed to carry out 14 injections of 20 μl each over 40 s, spaced at 300 s intervals. The stirring speed was 300 rpm. Heats of binding were calculated by integrating the signal from the calorimeter, and binding isotherms were

determined by plotting the heats of binding against the ratio of enzyme to inhibitor. The data were analyzed by the software package Origin 5.0 from Microcal Inc. which was used to calculate the enthalpy changes (ΔH) and stoichiometry (N).

The following relationship was used to determine the heat capacity (ΔC_p):

$$\Delta C_p = \delta\Delta H / \delta T \qquad \text{(Equation 7)}$$

ΔH was measured at a series of temperatures and ΔC_p was determined by linear regression analysis.

2.5 Correlation of Thermodynamics with Structure

As discussed previously (Arumugam, et al., 2003, Wu, et al., 2011) the ΔCp^o value for a protein-protein interaction can be interpreted in a number of ways but is generally considered to be related to changes in non-polar and polar accessible surface area, ΔASA_{np} and ΔASA_{pol} on complex formation (where surface burial has a negative sign) (Spolar et al., 1992; Baker et al., 1998):

$$\Delta C_p = a*\Delta ASA_{npol} + b*\Delta ASA_{pol} \qquad \text{(Equation 8)}$$

This relationship has been widely used for analyzing interactions. The parameterizations of the coefficients for changes in nonpolar and polar surface used here were a=0.28±0.12 cal mol^{-1} K-1 $Å^{-2}$ and b= -0.09±.30 cal mol^{-1} K^{-1} $Å^{-2}$ (Higashi et. al., 1999). The enthalpy of binding (ΔH_o) at 60° was calculated using the relationship (Baker et al., 1998):

$\Delta Ho\ (60°C) = c*\Delta ASA_{npol} + d*\Delta ASA_{pol}$ (Equation 9)

3. Results

The thermodynamic profiles of interactions of MT1-MMPcd with N-TIMP-1 and N-TIMP-2 both have large positive enthalpy changes compensated by favorable positive entropy changes. Their free energies of binding (ΔG), were calculated from the Ki values determined by inhibition kinetics at 298K (N-TIMP1/MT1-MMP, K_a : $3.1*10^6$, ΔG: -8.6 kcal/mol; N-TIMP-2/MT1-MMP, K_a : $1.8*10^{10}$, ΔG: -13.7 kcal/mol). The analysis of the data shows that the interactions have an unfavorable (positive) enthalpy changes of about 6.1 kcal/mol, with that for N-TIMP-1 being less unfavorable than that for N-TIMP-2 (6.1 VS 8.0 kcal/mol) (Table 5).

Isothermal titrations at 291 K in buffers with different enthalpies of ionization show the contribution of buffer protonation or deprotonation to $\Delta H_{obs,}$ arising from the release or uptake of protons on complex formation (Table 5). The enthalpy change independent of buffers ,ΔH_{int} , and the number of protons, $N_{H+,}$ taken up or released to the buffer, were analyzed by linear regression based on the relationship (Baker et al., 1998):

$\Delta H_{obs} = \Delta H_{int} + N_{H+} \times \Delta H_{ion,}$ (Equation 10)

There are 1.02 protons taken up for the interaction of N-TIMP-1 with MT1-MMP, but an insignificant uptake (0.08) protons on N-TIMP-2 binding to MT1-MMP (Table 5)

Table 5. Enthalpy of binding for the interactions of N-TIMP-1 and N-TIMP-2 with MT1-MMPcd in buffers of different enthalpies of ionization at 291 K and calculated intrinsic enthalpy change (ΔHint) and ionization change (NH+)

Buffer	ΔH_{ion}	N-TIMP-1/MT1-MMPcd	N-TIMP-2/MT1-MMPcd
		ΔH_{obs} (kcal/mol)	
PIPES	2.726	11.77±0.37	10.17±0.10
HEPES	4.94	13.82±0.24	10.38±0.09
BES	5.993	14.61±0.62	10.44±0.11
ACES	7.497	16.81±0.30	10.51±0.06
ΔH_{int} (kcal/mol)		8.87±0.54	10.00±0.05
N_{H+}		1.02±0.10	0.08±0.01

Table 6. Enthalpies of interaction of N-TIMPs with MT1-MMPcd at different temperatures. ΔC_p was determined by linear regression of ΔH_{obs} vs K and ΔS_{solv} and used to calculate ΔS_{solv} at 298K ($=\Delta C_p * \ln(T/Ts^*)$, where Ts* is the reference temperature (385K) at which the hydrophobic contribution to ΔS is zero.

Temperature (K)	MT1-MMPcd	
	N-TIMP-1	N-TIMP-2
	ΔH_{obs} (cal/mol)	
291	13.82±0.24	10.38±0.09
298	10.77±0.09	8.69±0.04
303	9.04±0.09	7.27±0.03
310	6.18±0.07	4.90±0.02
ΔC_p (cal/mol/K)	-398±11	-288±17
ΔS_{solv} (cal/mol)	102	74

Table 7. Thermodynamic profiles for interactions of N-TIMP-1 and N-TIMP-2 with MT1-MMPcd, and MMP-3cd

MMP	MT1-MMPcd		MMP-3cd[a]	
N-TIMP	N-TIMP-1 (WT)	N-TIMP-2 (WT)	N-TIMP-1 (WT)	N-TIMP-2 (WT)
ΔH_{int} (kcal/mol)	6.1±0.5	8.0±0.1	6.5±0.3	5.5±0.2
Ka	$3.1*10^{6}$	$1.8*10^{10}$	$3.5*10^{8}$	$2.3*10^{8}$
ΔG_{1M}(kcal/mol)	-8.6	-13.7	-11.7±0.1	-11.1±0.2
$T\Delta S_{int}$ (kcal/mol)	14.7±0.5	21.7±0.05	18.2±0.4	16.6±0.2
ΔC_p (kcal/mol)	-398±11	-288±17	-50±6	-47.2±3.7
$T\Delta S_{solv}$(kcal/mol)	32.4±0.9	23.5±1.4	3.8	3.6±0.3
$T\Delta S_{conf}$(kcal/mol)	-14.7±1.0	1.2±1.4	17.4	16

ΔH_{obs} values from titrations in HEPES buffer at four different temperatures: 291 K, 298K, 303 K and 310 K were used to determine the heat capacity change (ΔC_p) of interactions between N-TIMP-1 and N-TIMP-2 with MT1-MMP by linear regression analysis. The heat capacity of binding, from which the hydrophobic contribution to binding ($T\Delta S_{solv}$) is estimated, is more negative for N-TIMP-1 and MT1-MMP interaction than for N-TIMP-2 and MT1-MMP interaction (-398 kcal/mol vs -288 kcal/mol) (Table 7). Because the ΔG values were determined at 298 K, the ionization-independent enthalpy changes of ΔH_{int}, at 291 K for N-TIMP-1 with MT1-MMP is 8.87 kcal/mol and the ΔH_{int} of interaction between N-TIMP-2 and MT1-MMP is 10.00 kcal/mol (Table 5). The ΔH_{int} value at 291 K were used to calculate ΔH_{int} at 298 K using the value of ΔC_p (N-TIMP-1/MT1-MMP: 6.1 Kcal/mol; N-TIMP-2/MT1-MMP: 8.0 Kcal/mol). $T\Delta S$int for both interactions were calculated from ΔG and ΔHint values at 298 K (N-TIMP-1/MT1-MMP: 14.7 kcal/mol VS N-TIMP-2/MT1-MMP: 21.7 kcal/mol) (Table 7).

Further analysis clarified the source of the entropy driving the interactions of the N-TIMP-1 and N-TIMP-2 with MT1-MMP. The overall entropy change, ΔS_{int}, includes contributions from the interacting proteins ($\Delta S_{protein}$) and solvent (ΔS_{solv}), of which the latter can be estimated from the heat capacity for the interaction ($\Delta S_{solv} = \Delta Cp^0 * \ln(T/Ts^*)$), where Ts^* is the reference temperature (385 K) at which the hydrophobic contribution to ΔS is zero. $\Delta S_{protein}$ includes negative, unfavorable effects arising from the loss of translational and rotational freedom T ($\Delta S_{trans} + \Delta S_{rot}$) in the complex, that has been estimated to be about 3 (± 2.4) kcal/mol for the N-TIMP-1/MMP-

3cd interaction (Arumugam et al., 2003) and will be similar for other N-TIMP/MMP interactions (Wu et al., 2011). It also contains the change in conformational entropy, ΔS_{conf}, that is expected to include an unfavorable loss of entropy originating from increased rigidity in the interaction sites of the two proteins plus any favorable entropy increase resulting from increased dynamics in regions distant from the interaction sites in the bound protein populations (Arumugam et al., 2003; Wu et al., 2011). The values for $T\Delta S_{conf}$ at 298 K indicate that the conformational entropy increase contributes about -14.7 kcal/mol to the ΔG for interaction of N-TIMP-1 with MT1-MMP, contrasting with N-TIMP-2/MT1-MMP interaction, the weaker binding of the N-TIMP-1 to MT1-MMPcd reflects a more favorable (less positive) ΔH_{int} that is compensated by a large unfavorable $T\Delta S_{conf.}$ .For comparison, the thermodynamic parameters previously determined for the interactions of N-TIMP-1 and -2 with MMP-3cd (Wu et al., 2011) are also given in Table 7.

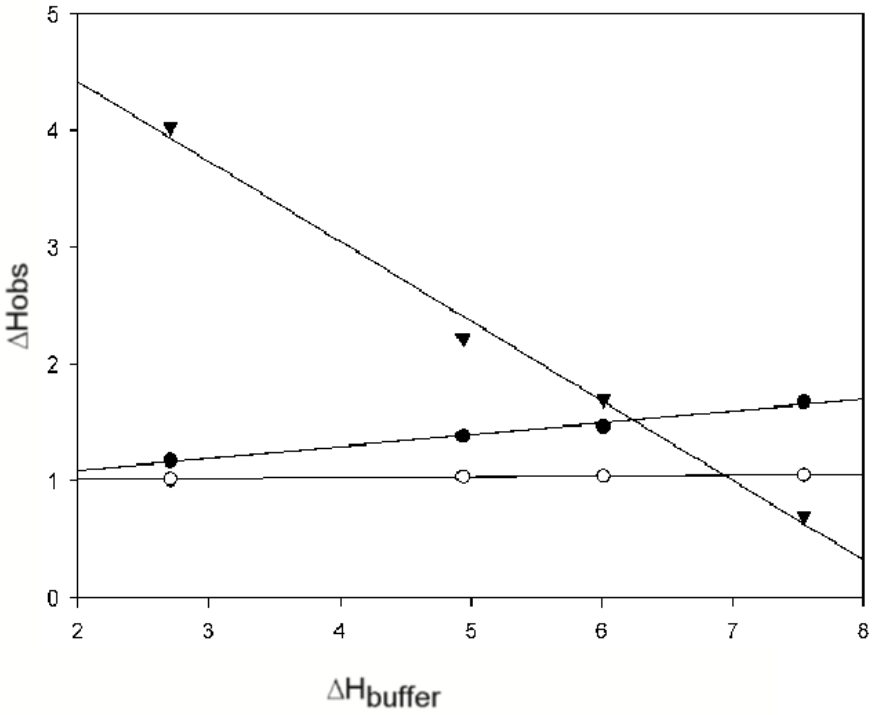

Figure 16. Relationship of buffer enthalpy of ionization (ΔHion) on ΔHobs for different N-TIMP/MMPcd interactionsSymbols the different interactions are: N-TIMP-1/MT1-MMPcd (open circles) N-TIMP-2/MT1-MMPcd (closed circles), N-TIMP-2/MMP-3 (closed squares).

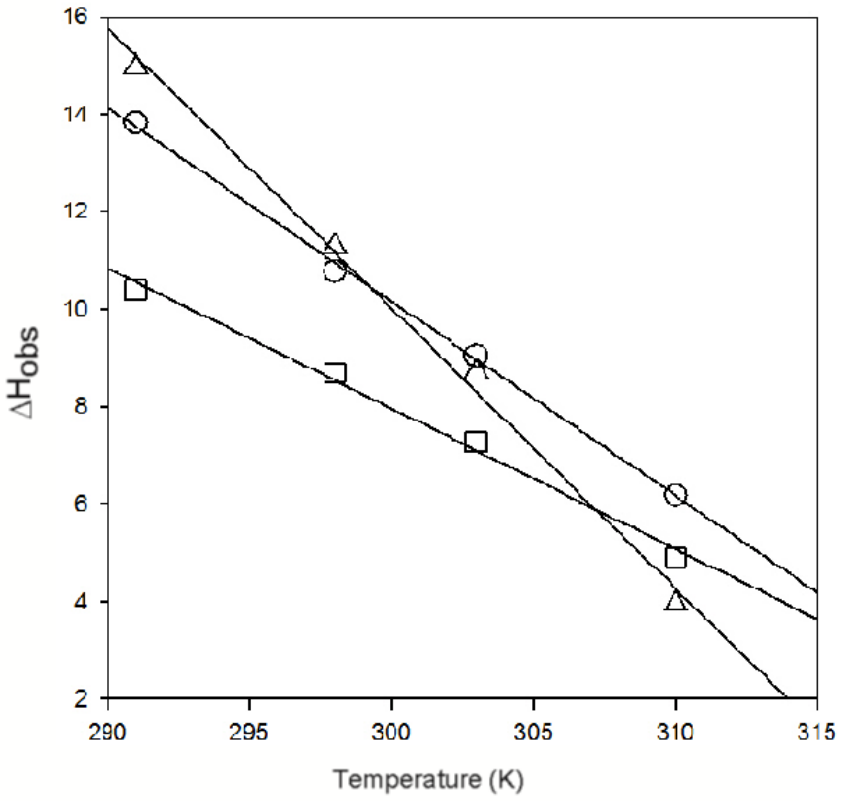

Figure 17. Temperature dependence of the enthalpy of binding. The heats of binding were measured in HEPES buffer (pH 7.4) at four different temperatures (291K, 298K, 303K and 310K) ΔC_p was determined from the slope of the plot: N-TIMP-1 to MT1-MMPcd (open circles), N-TIMP-2 to MT1-MMPcd (closed circles) and N-TIMP-2 to MMP-3cd (closed squares).

4. Discussion

4.1 Sources of Binding Energy for the Different N-TIMP/MMPcd Interactions

Previous studies of the interactions of N-TIMP-1 and N-TIMP-2 with MMP-1cd and MMP-3cd showed similar binding thermodynamic profiles to the interactions of N-TIMP-1 and N-TIMP-2 with MT1-MMPcd: an unfavorable (positive) enthalpy change compensated by a large favorable entropy change of which a big fraction appears to arise from the hydrophobic effect ($T\Delta S_{solv}$). This suggests that hydrophobic effect is the driving force for the interactions of N-TIMP-1 and N-TIMP-2 with MT1-MMPcd.The

thermodynamic profiles (Table 5-7) show that although N-TIMP-1 is a weak inhibitor of MT1-MMPcd, the ionization-independent enthalpy for this interaction is slightly less unfavorable than that of N-TIMP-2 binding to MT1-MMPcd (6.1 kcal/mol vs 8.0 kcal/mol).

The interaction of N-TIMP-1 with MT1-MMPcd is characterized by the uptake of about one proton. ΔHobs for both interactions show strong negative dependence on temperature (Figure 17), giving large negative values for the heat capacity change for those two interactions. Based on the values of heat capacity change, two estimated $T\Delta S_{solv}$ show that for the N-TIMP-1/MT1-MMPcd interaction has a larger magnitude than that of N-TIMP-2 with MT1-MMPcd interaction, which indicates there is a larger hydrophobic effect when N-TIMP-1 binds to MT1-MMPcd compared with N-TIMP-2/MT1-MMPcd binding (32.4 kcal/mol vs 23.5 kcal/mol) (Table 7). The more than 1000-fold lower K_a for N-TIMP-1 relative to N-TIMP-2 binding to MT1-MMPcd stems from a less favorable $T\Delta S_{int}$ (14.7 kcal/mol vs 21.7 kcal/mol) and a large conformational entropy penalty ($T\Delta S_{conf}$ of -11.9 kcal/mol) for the N-TIMP-1/MT1-MMPcd interaction compared with +3.2 kcal/mol for N-TIMP-2 binding to MT1-MMPcd) (Table 7) is responsible for the weak inhibition of MT1-MMPcd by N-TIMP-1.

During the interactions of N-TIMP-1 and N-TIMP-2 with MMP-1cd, MMP-3cd and MT1-MMPcd, the entropy increases arising from solvent and/or increased conformational dynamics show mutually compensating effects and indicate a strong influence of the MMP; interactions with MMP-3 have the highest contributions from

conformational entropy and least from solvent entropy. Interactions with MMP-1 are intermediate between the other two.

4.2 Structural Correlations with Thermodynamics

Like the previously studied interactions of N-TIMP-1 and N-TIMP-2 with MMP-1cd and MMP-3cd (Arumugam et. al., 2003; Wu et. al., 2011) the interactions of N-TIMP-1 and N-TIMP-2 with MT1-MMPcd have minimal to strongly positive enthalpy change values and are driven by large entropy increases. Crystallographic structures for the N-TIMP-1/MMP-1 and TIMP-1/MMP-3 complexes have been reported (Gomis-Rüth et al., 1997; Iyer et al., 2007). Other crystallographic structures relevant to the interactions between TIMPs include the complex of MT1-MMP with full-length TIMP-2, pdb 1BUV, and with the V4A/P6V/T98L triple mutant of N-TIMP-1, pdb 3MA2 (Fernandez-Catalan et al., 1998; Grossman et al., 2010). A model of the complex of N-TIMP-1 T98L mutant with MMP-3cd was generated from pdb 1UEA, the TIMP-1 complex with MMP-3cd (Gomis-Rüth et al., 1997), by deleting residues 126 to 180, mutating residue 98 to Leuand subjecting the structure to energy minimization. The V4A, P6V and T98L mutations in N-TIMP-1individually reduce the K_i for MT1-MMP by 1.5, 2.4 and 2.9, respectively, consistent with the view that they contribute additively to the about 10-fold increase in affinity of the triple mutant (Hamze et al., 2007). Therefore, it appears that the mutations do not cooperatively generate a major conformational change in the complex with MT1-MMP, suggesting that the 3MA2 structure (Grossman et al., 2010) is a reasonable template for generating model of complex of N-TIMP-1 with MT1-MMPcd (Figure 18). The modeled complex was analyzed to obtain the areas of apolar and polar surface in the interfaces and to predict the values of ΔC_p and ΔH (298 K) for

the interactions of N-TIMP-1 and N-TIMP-2 with MT1-MMPcd (Coussens et. al., 2002; Pavlaki et. al., 2003) for comparison with those determined experimentally (Table 8).

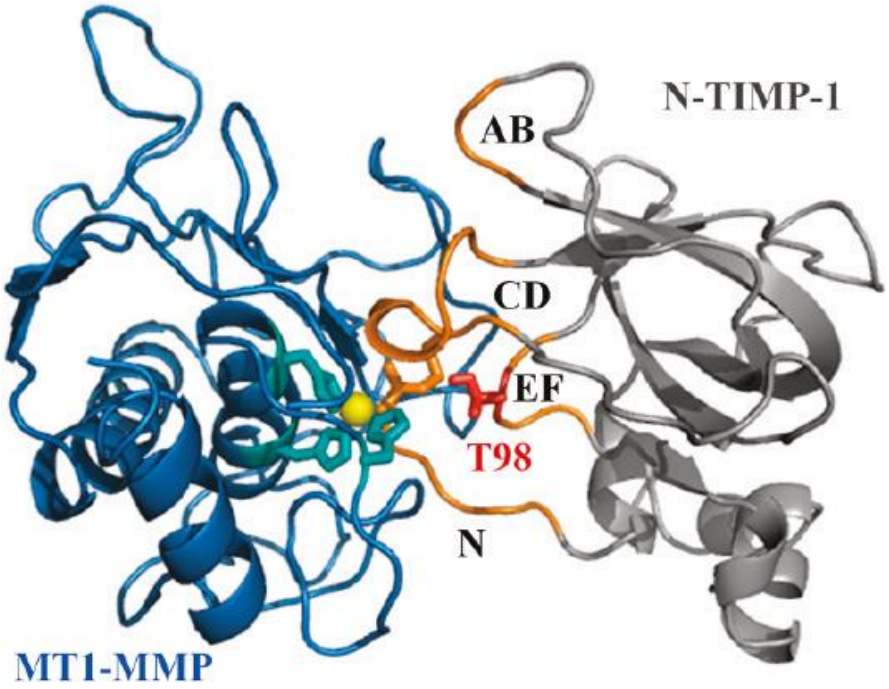

Figure 18. Model of binding of N-TIMP-1 to MMP 14.Complex derived from homology modeling, generated from pdb 3MA2 (Grossman et al., 2010).

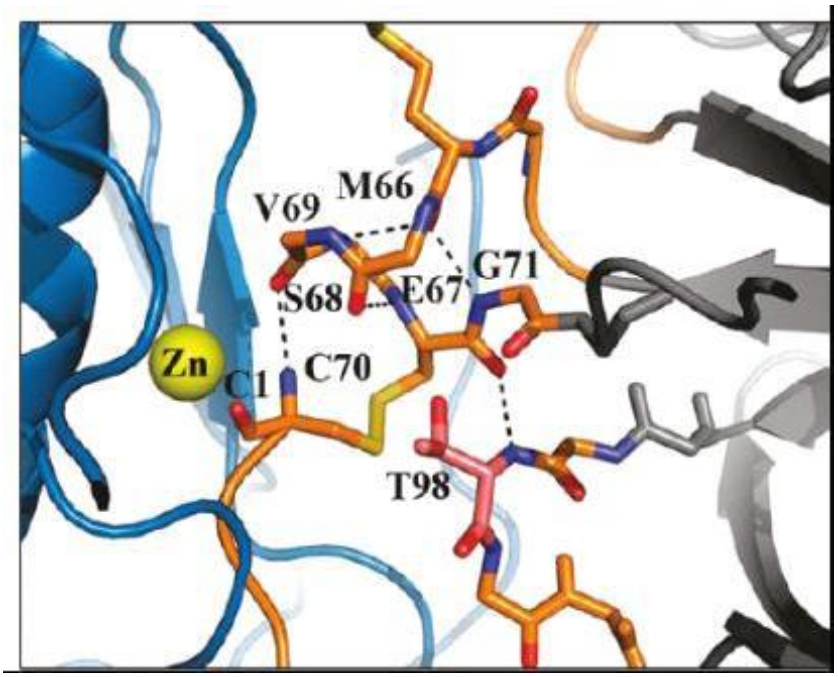

Figure 19. Crystal structure of N-TIMP-1 intramolecular hydrogen bond network.(in orange sticks), when bound to MT1-MMP generated from 3MA2 (Grossman et al., 2010)

Table 8. Characteristics of interaction interfaces and calculated and empirical ΔCp and ΔH for the association of N-TIMP-1 and N-TIMP-2 with MT1-MMPcd

COMPLEX	**Polar**	**Apolar**	**$\Delta C_{p\ (calc)}$**	**$\Delta C_{p\ (exp)}$**	**$\Delta H_{(calc)}$**	**$\Delta H_{(exp)}$**
Buried Surface areas/Parameters	$Å^2$	$Å^2$	Kcal/mol	Kcal/mol	Kcal/mol	Kcal/mol
N-TIMP-1/MT1-MMPcd	512 (30%)	1205(70%)	-292	-398	+4.1	+6.1
N-TIMP-2/MT1-MMPcd	659(28%)	1661(72%)	-391	-289	+3.9	+8.0

* ΔH(332)=-7.27x ΔASAnp +29.16 x ΔASAp

ΔH(298) = ΔH(332)-35 x ΔCp

ΔCp = a x ΔASAnp + b x ΔASAp;

a=0.28, b=-

III THERMODYNAMIC SOURCES OF MMP-SPECIFICITY IN MUTANTS OF N-TIMP-1

1. Introduction

Mutational studies of N-TIMP-1 suggest that the weak binding affinity of TIMP-1 for MT1-MMP, partly arises from multiple (>3) sequence differences in the interaction sites, compared with other TIMPs/MMPs (Hamze et al. 2007). Thr98 has been proposed to be a key residue determinant of the weak interaction between N-TIMP-1 and MT1-MMP (Lee et al. 2004). The substitution of Leu for Thr98 of NT1 has been shown to enhance its affinity for MMP-14 (2 to 3-fold) and additional substitutions of Ala for Val4 and Val for Pro6 further increase the affinity, reflected in improvement of the K_i from 150 nM for WT to 16 nM for the triple mutant (Lee et al. 2004; Hamze et al.,2007). However, this mutant is a 280-fold weaker inhibitor of MT1-MMP than N-TIMP-2. A crystallographic structure of the complex of the highest affinity triple mutant of NT1 with MT1-MMP has been determined (Grossman et al. 2010).

The effects of these specific amino acid substitutions on the thermodynamics of N-TIMP- 1 binding to MT1-MMPcd have not been investigated. The thermodynamic parameters for N-TIMP-1 mutant T98L/MT1-MMP investigated together with the wild type N-TIMP-1/MT1-MMPcan help us to understand the biophysical basis of the TIMP-1/MT1-MMP interaction and how this can be enhanced by mutagenesis. Such

correlations of structure with thermodynamics for N-TIMP-1 mutant T98L containing specific amino acids that modulate its inhibitory activity to MT1-MMP cd may help us design N-TIMP-1 variants with increased selectivity and binding affinity towards MT1-MMP.

2. Materials and Methods

2.1 Construction of N-TIMPs, MMPs and their mutants

Wild-type N-TIMP-1 and its T98L mutant as well as MMP-3cd and MT1-MMP were expressed using the pET-42b vector. Superdex-75 was purchased from Amersham Biosciences and Centriplus YM-3 centrifugal filter devices were from Millipore. Isothermal titration calorimetry studies were carried out using a MicroCal VP-ITC Microcalorimeter. All other reagents and cells were from the same sources as in previous studies (Arumugam et al. 2003; Hamze et al., 2007; Wu et al., 2011).

The N-TIMP-1 T98L mutant was generated using QuikChange II Site-Directed Mutagenesis Kits (Agilent Technologies). Primers were designed using web-based primer design software program (http://labtools.stratagene.com/QC). PCR reactions were carried out at 95 °C for 30 sec, 55 °C for 1 min and 68 °C for 5 min, for 30 cycles after a 3-min hot start at 95 °C. The PCR products were cloned back into pET-42b vector (Novagen) for expression.

2.2 Expression, Purification, and in vitro Folding of N-TIMPs, MMPs and their Mutants

N-TIMP-1 T98L mutant was expressed in Escherichia coli BL21(DE3) cells as inclusion bodies. The proteins were partially purified and folded as described earlier in this dissertation.

2.3 Fluorescence Assays for N-TIMP Activities

The inhibition of MMPs by N-TIMP-1 wild type and its T98L mutant were measured by assaying MMP activities for hydrolysis of fluorogenic substrates using a PerkinElmer LS50B luminescence spectrometer. Assays were conducted in HEPES buffer (20 mM) pH 7.4, containing 250 mM NaCl, 10 mM $CaCl_2$, and 50 μM $ZnCl_2$ which was used also for the dilution of MMP and TIMP samples. To determine the $K_{i(app)}$ of N-TIMP-1 T98L mutant for MT1-MMP CD at 25°C (298 K), various concentrations of inhibitor were incubated with 5 nM enzyme at 25 °C for 3h before addition of Knight substrate for MT1-MMP CD and, for MMP-3cd, the NFF-3 substrate (Mca-Arg-Pro-Lys-Pro-Val-Glu-Nva-Trp-Arg-Lys(Dnp)-NH2) to a final concentration of 3μM. Catalytic activity was determined by measuring the increase in fluorescence intensity as described above. Reaction velocities were calculated as previously described.

2.4 Isothermal Titration Calorimetry of N-TIMP-1 T98L/ MMP-3 cd Interactions

Protein solutions were dialyzed extensively against various buffers at 20 mM concentration containing 250 mM NaCl, 10 mM $CaCl_2$, and 50 μM $ZnCl_2$ at pH 7.4 and degassed prior to use. N-TIMP-1 T98L (12–30 μM) was titrated with the MT1-MMPcd and MMP-3 cd (120–300 μM) at different temperatures using a MicroCal VP-ITC

microcalorimeter. The instrument was programmed to carry out 14 injections of 20 µl each over 40 s, spaced at 300-s intervals. The stirring speed was 300 rpm. The data were analyzed by the software package Origin 5.0 from Microcal Inc. and was used to calculate the enthalpy changes (ΔH) and stoichiometry (N). The heat capacity and intrinsic enthalpy change were determined as previously described.

3. Results

3.1 Thermodynamic Profiles for the Interaction of the N-TIMP-1 T98L Mutant with MMP-3cd

Here, we have investigated how the effects of the T98L mutation in N-TIMP-1 that modify MMP selectivity affect the thermodynamics of N-TIMP/MMP interactions, focusing on its inhibition of MT1-MMPcd and MMP-3cd. Like previously studied N-TIMP/MMP interactions, these are driven by increases in entropy. The entropy change for the interaction (ΔS_{int}) and the change in solvent entropy (ΔS_{solv}, estimated from ΔC_p) can be used to assess the entropy change arising from differences in conformational dynamics between the free and bound proteins (ΔS_{conf}). The effect of N-TIMP mutations on both ΔS_{solv} and ΔS_{conf} for the interactions with different MMPs are important for changes in the selectivity. Large negative ΔC_p values for all N-TIMP interactions with MT1-MMPcd are greater (more negative) than for the other MMPs, and, using these to estimate ΔS_{solv} and, from this and ΔS_{int} to calculate ΔS_{conf}, the weak binding of N-TIMP-1 to MT1-MMPcd is found to arise from a large negative ΔS_{conf}, in contrast to N-TIMP-2 which has a small negative value. However, the T98L mutation does not reduce the conformational entropic cost of binding by increasing interaction site rigidity in the unbound protein, as previously proposed from dynamics simulation studies (Grossman. et

al. 2010), but increases ΔS_{solv} (the hydrophobic effect) estimated from the larger negative ΔC_p.

The isothermal titration of N-TIMP-1 T98L mutant by MMP-3cd in 3 different buffers (HEPES, PIESE and MOPS) at 291 K shows that the interaction has an unfavorable (positive) ΔH of 6.11 kcal/mol (Table 9), compensated by a large favorable (positive) ΔS. The enthalpy change was determined at four different temperatures (Figure 21). Unexpectedly, ΔH_{obs} for the N-TIMP-1 T98L interaction with MMP-3cd increases with temperature indicating a positive ΔC_p value of 115 kcal/mol (Table 10), compared to -50.4 kcal/mol for the heat capacity change of the interaction between wild type N-TIMP-1 and MMP-3cd. It is unusual for a protein-protein interaction to have a positive heat capacity change which is generally interoperated as reflecting the increased exposure of non-polar groups, raising the possibility that this interaction results in an analogous process. This could arise from structural adjustment and exposure of hydrophobic groups during complex formation, because of the threonine to leucine substitution.

Based on the positive ΔC_p, N-TIMP-1 T98L interacting with MMP-3cd appears to generate an unfavorable hydrophobic effect with an estimated $T\Delta S_{solv}$of-8.8 kcal/mol, to ΔG of -12.3 kcal/mol that is compensated by a $T\Delta S_{conf}$ of 32kcal/mol. In contrast, the interaction between wild type N-TIMP-1 and MMP-3cd has a favorable $T\Delta S_{solv}$ of 3.8 kcal/mol and a less favorable $T\Delta S_{conf}$ of 17.4 kcal/mol (Table 11).

To determine the contribution to ΔH_{obs} of binding of N-TIMP-1 T98L with MMP-3cd from enthalpy changes arising from the release or uptake of protons on complex

formation, isothermal titrations were performed at 291 K in buffers with different enthalpies of ionization (Table 9). A linear regression based on these data shows the N-TIMP-1 T98L/MMP-3cd interaction releases 0.65 protons compared to an insignificant uptake (0.058 protons) during the binding of wild type N-TIMP-1 to MMP-3cd. However, the ionization-independent enthalpy change, ΔH_{int}, for the mutant is 6.11 kcal/mol, similar to the 6.26 kcal/mol value for wild-type (Table 9).

A B

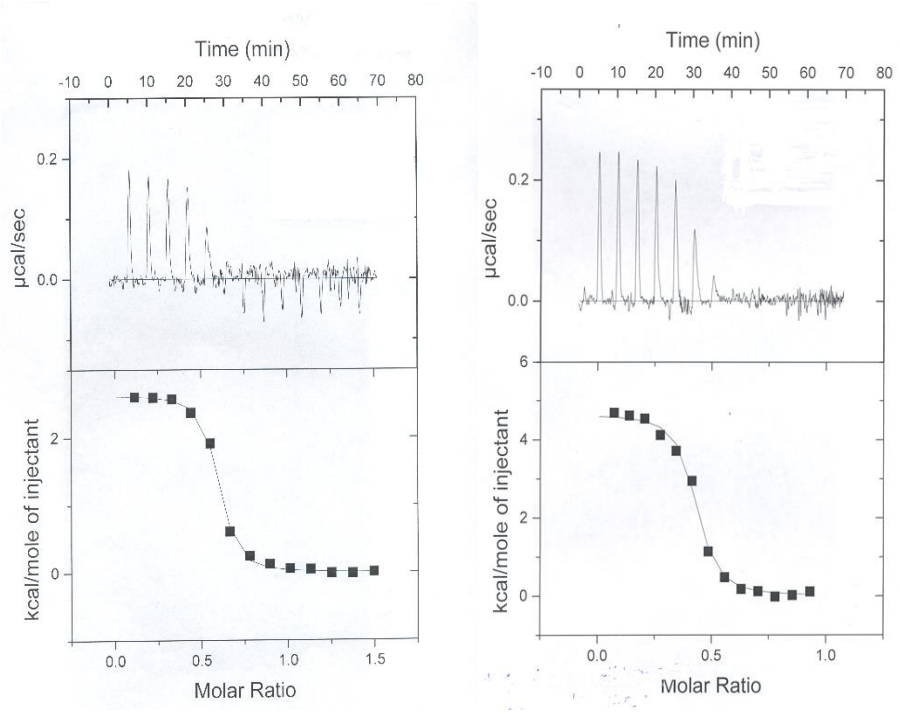

Figure 20. Isothermal calorimetric titration of N-TIMP-1 T98L mutant with MMP-3cd at 291K in HEPES buffer (A) and PIPES buffer (B). Aliquots (20 ul) of MMP-3cd (150 uM) were injected into N-TIMP-1 T98L (30uM) in HEPES buffer, pH 7.4 and the heats of binding were measured with a MicroCal VP-ITC micro calorimeter as described in Experimental Procedures.

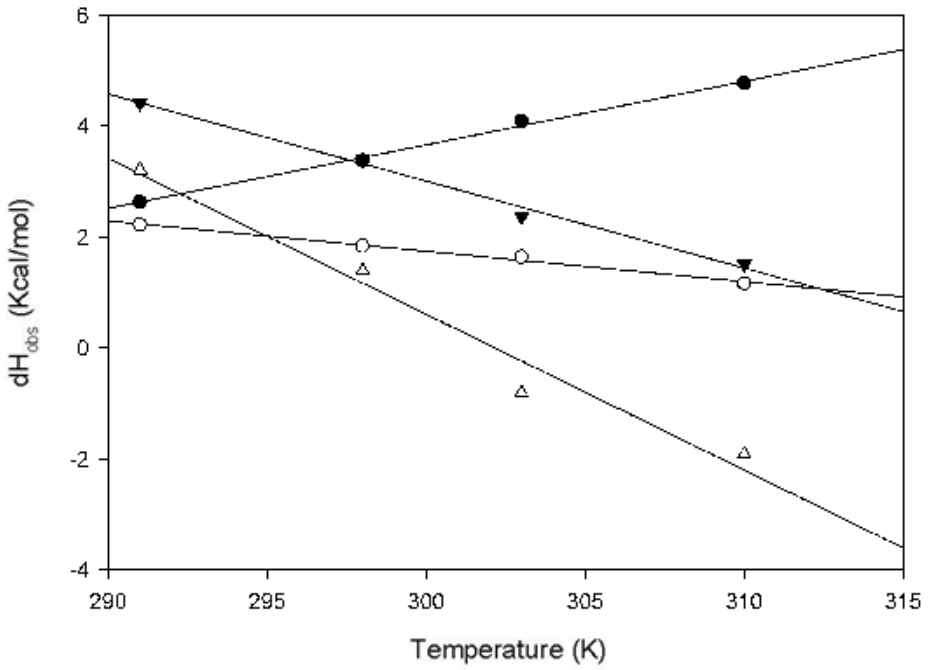

Figure 21. Temperature dependence of the enthalpy of binding. The heats of binding were measured in HEPES buffer (pH 7.4) at different temperatures. Cp was calculated as the slope of the plot. Symbols for the different interactions are: N-TIMP-1 T98L/MMP-3cd (open triangles), N-TIMP-2 /MMP-3cd (closed circles), N-TIMP-1 /MMP-1 cd (open circles), and N-TIMP-2/MMP-1cd (closed triangles).

Table 9. Enthalpies of binding for different N-TIMP variants /MMP-3cd interactions. Experiments are conducted at 291 K. The studies with N-TIMP-1 were conducted at pH 6.8 and those with N-TIMP-1 T98L at pH 7.4 a Data from (Arumugam et al., 2003) at 298K.

Buffer	ΔH_{ion}	N-TIMP-1 T98L/ MMP-3cd	N-TIMP-1/MMP-3cd[a]
		Hobs (kcal/mol)	
PIPES	2.726	4.65±0.08	6.42±0.23
HEPES	4.94	2.63±0.03	6.57±0.38
MOPES(N-TIMP-1T98L)	5.20	2.48±0.03	--
BES(N-TIMP-1)	5.993	--	6.60±0.27
ACES	7.497	16.81±0.30	6.70±0.25
ΔH_{int} (kcal/mol)		6.11±0.62	6.26±0.14
N_{H+}		-0.65±0.11	0.058±0.002

Values taken from Wu et al. (2011)

Table 10. Enthalpies of interaction of N-TIMP-1 T98L and N-TIMP-2 with MMP-3cd at different temperatures. ΔCp was determined by linear regression of ΔHobs vs K and ΔSsolv and used to calculate ΔSsolv at 298K (=ΔCp*ln(T/Ts*), where Ts* is the reference temperature (385K) at which the hydrophobic contribution to ΔS is zero.

Temperature (K)	MMP-3cd	
	N-TIMP-1 T98L	N-TIMP-2[a]
	ΔHobs (kcal/mol)	
291	2.63±0.03	2.222±0.015
298	3.38±0.04	1.838±0.011
303	4.09±0.08	1.639±0.030
310	4.77±0.14	1.162±0.037
ΔC_p (kcal/mol)	115±5	-54.8±3.7

Values taken from Wu et al (2011)

Table 11. Thermodynamic profiles for interactions of N-TIMP-1 variants with MMP-3cd

MMP	MMP-3cd	
N-TIMP	N-TIMP-1 (WT)[a]	N-TIMP-1 T98L
ΔH_{int} (kcal/mol)	6.5±0.25	6.9±0.6
Ka	$3.5*10^{8}$	$1.6*10^{9}$
ΔG_{1M}(kcal/mol)	-11.7±0.1	-12.3
$T\Delta S_{int}$ (kcal/mol)	18.2±0.4	19.2±0.6
ΔC_p (kcal/mol)	-50±6	115±5
$T\Delta S_{solv}$(kcal/mol)	3.8	-8.8±0.5
$T\Delta S_{conf}$(kcal/mol)	17.4	31.0±0.5

a.Values taken from Wu et al (2011)

3.2 Thermodynamic profile for N-TIMP-1 T98L mutant and MT1-MMPcd Interaction

Compared to the interaction of wild type N-TIMP-1 with MT1-MMPcd, the mutant T98L binding to MT1-MMPcd has a larger unfavorable enthalpy change (10.7 kcal/mol vs 6.1 kcal/mol) which is compensated by a larger favorable entropy change. The free energies of binding for both interactions were calculated from the Ka values determined by inhibition kinetics at 298 K (N-TIMP1 (WT) /MT1-MMP, Ka: $3.6*10^{6}$, ΔG: -8.6 kcal/mol; N-TIMP-1 T98L/MT1-MMP, Ka: $6.7*10^{6}$, ΔG: -9.1 kcal/mol) (Table 14).

The titrations performed in buffers with different enthalpies of ionization yielded an insignificant 0.06 protons taken up upon T98L binding to MT1-MMPcd, while 1.02 protons are taken up for the interaction of wild type N-TIMP-1 (Table 12). Titrations performed at different temperatures gave a value for the heat capacity change of -576 kcal/mol that is more negative compared to N-TIMP-1 wild type, -398 kcal/mol (Table 13), indicating a larger increase of 14 kcal/mol in the free energy contribution from the solvent entropy increase, $T\Delta S_{solv,}$ which exceeds an 8 kcal/mol increase (from 12 kcal/mol to 20 kcal/mol) in the conformational entropy penalty, $T\Delta S_{conf}$ (Table 14).

Table 12. Enthalpy of binding for the interactions of N-TIMP-1 variants with MT1-MMPcd in buffers of different enthalpies of ionization at 291 K and calculated intrinsic enthalpy change (ΔHint) and ionization change (NH+).

Buffer	ΔH_{ion}	N-TIMP-1/MT1-MMPcd	N-TIMP-1 T98L/MT1-MMPcd
		ΔHobs (kcal/mol)	
PIPES	2.726	11.77±0.37	14.83±0.37
HEPES	4.94	13.82±0.24	14.96±0.25
BES	5.993	14.61±0.62	15.04±0.25
ACES	7.497	16.81±0.30	15.10±0.20
ΔH_{int} (kcal/mol)		8.87±0.54	14.68±0.003
N_{H+}		1.02±0.10	0.06±0.003

Table 13. Enthalpies of interaction of N-TIMP-1 variants with MT1-MMPcd at different temperatures. ΔCp was determined by linear regression of ΔHobs vs K and ΔSsolv and used to calculate ΔSsolv at 298K (=ΔCp*ln(T/Ts*), where Ts* is the reference temperature (385K) at which the hydrophobic contribution to ΔS is zero.

Temperature (K)	MT1-MMPcd	
	N-TIMP-1 (WT)	N-TIMP-1 T98L
	ΔHobs (cal/mol)	
291	13.82±0.24	14.96±0.25
298	10.77±0.09	11.28±0.18
303	9.04±0.09	8.70±0.10
310	6.18±0.07	3.96±0.14
ΔC_p (cal/mol/K)	-398±11	-575±29
ΔS_{solv} (cal/mol)	102	148

Table 14. Thermodynamic profiles for interactions of N-TIMP-1 variants with MT1-MMPcd

MMP	MT1-MMPcd	
N-TIMP	N-TIMP-1 (WT)	N-TIMP-1T98L
ΔH_{int} (kcal/mol)	6.1±0.5	10.7±0.02
K_a	$3.1*10^6$	$6.7*10^6$
ΔG_{1M}(kcal/mol)	-8.6	-9.1
$T\Delta S_{int}$ (kcal/mol)	14.7±0.5	19.8±0.0
ΔC_p (kcal/mol)	-398±11	-575±29
$T\Delta S_{solv}$(kcal/mol)	32.4±0.9	46.8±2.4
$T\Delta S_{conf}$(kcal/mol)	-14.7±1.0	-24.0±2.4

4. Discussion

4.1 Sources of Binding Energy for the Interactions of N-TIMP-1 Variants with MMP-3cd and MT1-MMPcd

The T98L mutation in N-TIMP increases the affinity for MMP-3cd. For this interaction, a more unfavorable ΔH_{int} (8.2 kcal/more for T98L vs 6.0 kcal/mol for WT) is compensated by an increase in $T\Delta S_{int.}$ A comparison of the thermodynamic profile for the interaction of the N-TIMP-1 T98L mutant/MMP-3cd with that for the WT N-TIMP-1/MMP-3cd interaction shows that the N-TIMP-1 T98L mutation enhances binding to MMP3 by increasing $T\Delta S_{conf}$ by 13.6 kcal/mol (from 17.4 kcal/mol to 31.0 kcal/mol) for the interaction.

Comparison of the thermodynamic parameters for the N-TIMP-1 T98L mutant/MT1-MMPcd with those for WT N-TIMP-1/MT1-MMPcd reveals that it has a more unfavorable ΔH_{int} (10.7 vs 6.1 kcal/mol), compensated by an increase in $T\Delta S_{int}$ (14.7 to 19.8 kcal/mol), which indicates that the interaction of N-TIMP-1 T98L with MT1-MMP is driven by favorable entropy change; the increased affinity derives from an greater increase in solvent entropy on binding, reflected in a more negative ΔC_p (-576 vs -409 cal/mol/K). Compared to wild type N-TIMP-1, the N-TIMP-1 T98L mutation increases the large ΔS_{conf} cost for binding to MMP14 but this is offset by a greater increase in ΔS_{solv} . Previous studies of the interactions of N-TIMPs with MMPs indicates a similar pattern to the interactions of N-TIMP-1 variants with MMP-3cd and MT1-MMPcd.

4.2 Relationship of Thermodynamic Profiles to Interface Structures

A model complex of N-TIMP-1 T98L mutant with MMP-3cd (Figure 23) was generated from the crystallographic structure of TIMP-1/MMP-3cd complex, 1UEA (Gomis-Rüth. et al., 1997), and a model structure of N-TIMP-1 T98L/MT1-MMPcd (Figure 24) was generated based on a template, the 3MA2 structure (Grossman. et al., 2010).

The modeled complexes were analyzed, as described, to obtain the areas of apolar and polar surface in the interfaces and to predict the values of ΔC_p and ΔH (25 °C) for the interaction (Baker et al., 1998; Spolar et al., 1994) for comparison with those determined experimentally (Table 15). The experimental and calculated values show reasonable agreement for the MT1-MMP complexes but the experimentally determined ΔC_p values for the MMP-3 complexes are consistently far more positive than those calculated from the structures. Most notably, the experimentally-determined ΔC_p value for the interaction of the N-TIMP-1 T98L with MMP-3 is unusual in being positive (+124), but the calculated value is -388 (cal/mol/K). The model for the structure of this complex suggests that Leu98 is less than 4 Å from Pro221 and Leu222 of MMP-3; Thr98 of WT N-TIMP-1 is similarly close to Pro221 of MMP-3 but does not interact with Leu222. The interaction of MMP-3 with the T98L mutant, unlike that with WT N-TIMP-1, is linked with the release of 0.65 protons which may arise from the deprotonation of His224, adjacent to this region, in the more apolar environment produced by the introduction of Leu98.

Table 15. The areas of apolar and polar surface in the interfaces of the modeled complexes of N-TIMPs/MMPcd , and the predicted values of ΔCp and ΔH(25 °C) for the interactions

COMPLEX	Polar	Apolar	ΔCp (calc)	ΔCp (exp)	ΔH (calc)	ΔH (exp)
	Å2	Å2	cal/mol/K	cal/mol/K	kcal/mol	kcal/mol
MMP1/NTIMP-1[a]	564	971	-221	-194	-0.9	+0.5
MMP3/NTIMP-1[a]	514	1525	-381	-51	+9.4	+6.5
MMP3/NTIMP-1T98L	558	1532	-388	+124	+10.1	+6.9
MMP14/NTIMP-1T98L*	505	1218	-296	-576	+4.5	+10.7

a: Taken from Wu et. al., 2011

ΔH(332)=-7.27x ΔASAnp +29.16 x ΔASAp

ΔH(298) = ΔH(332)-35 x ΔCp

ΔCp = a x ΔASAnp + b x ΔASAp;

a=0.28, b=-0.09

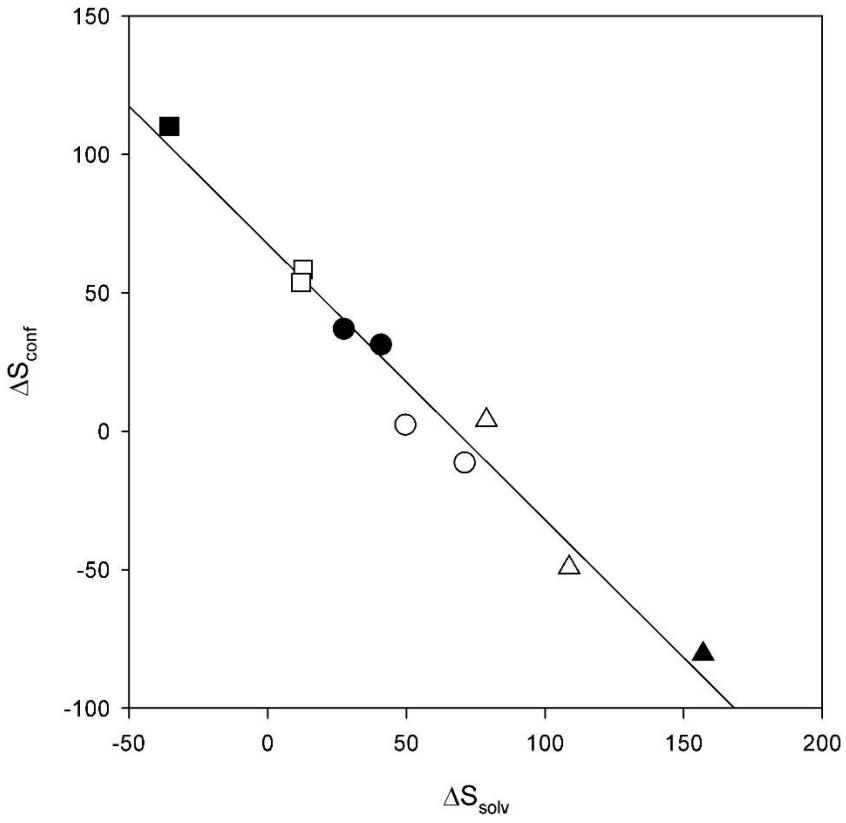

Figure 22. Relationship between ΔSsolv and ΔSconf for all characterized N-TIMP/MMP interactions. Data for interactions with MMP-1 are denoted by circles, MMP-3 by squares and MMP14 by triangles; Wild-type N-TIMPs are represented by open symbols and engineered N-TIMPs by filled symbols. The units of ΔS are cal/mol. The line, generated by regression analysis represents the relationship: $\Delta S_{conf} = 67.6 - \Delta S_{solv}$.

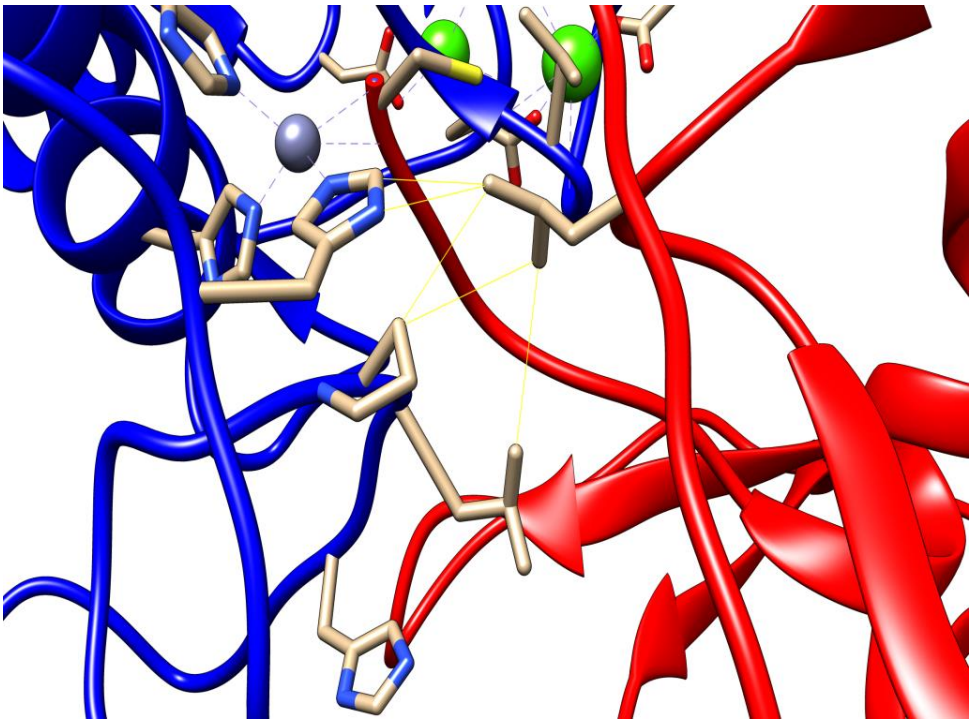

Figure 23. Modeled complex of N-TIMP-1 T98L with MMP-3cd. N-TIMP-1 T98L is displayed in red. The catalytic domain of MMP-3 (including the S1′ specificity pocket) is shown in blue.

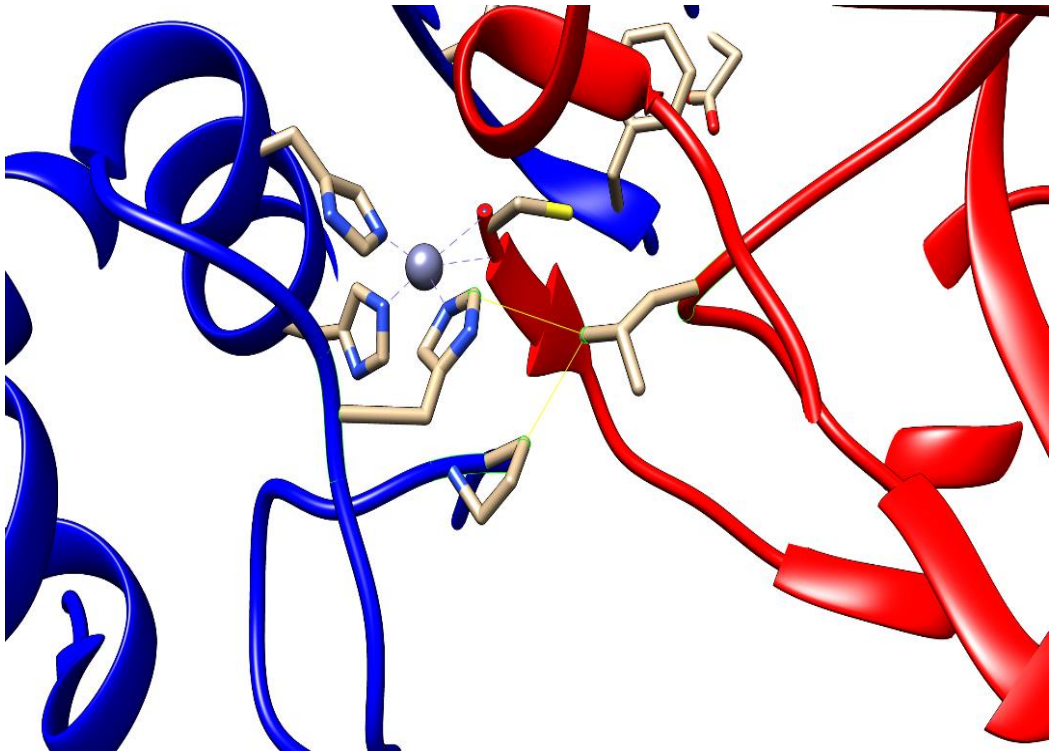

Figure 24. Modeled complex of N-TIMP-1 T98L with MT1-MMPcd.N-TIMP-1 T98L is displayed in red. The catalytic domain of MT1-MMP is shown in blue.

4.3 Conformational Dynamics and Selectivity in MMP Inhibition

The poor agreement between the experimental and calculated values for ΔC_p for the N-TIMP-1/MMP-3 interaction (Table 15) was previously attributed to large conformational changes that occur in both proteins on complex formation (Arumugam et. al., 2003; Wu et. al., 2011) including rearrangements of the N-terminal region and S1' loop of the protease and in the MMP-binding ridge, A-B and C-D loops of N-TIMP-1 (Arumugam et.al., 1998; Wu et., al., 2000; Gomis-Rüth et. al., 1997). As a result, the surfaces of the two proteins buried in the interface of the complex do not correspond to those present in the free molecules and an analysis of the crystallographic complex provides misleading information about the areas of polar and apolar surface areas that are

buried during the interaction (Wu et al., 2011). In contrast, in the N-TIMP-1/MMP-1 complex, there appear to be only minor differences between the structure of the free proteins and those in the complex (Iyer et al., 2007). Crystallographic structures provide limited information about the dynamics of proteins and are averages of the array of conformers that are present in a population of protein molecules. The roles of conformational and solvent dynamics in complex stabilization, as well as NMR structures of TIMP/MMP complexes (Arumugam et. al., 2003, Grünberg et al., 2006, Chen et al. 1999) are consistent with the "conformer selection model" of protein-protein interactions (Kumar et al. 2000) as opposed to "induced fit". Based on the dynamic nature of protein structures, the conformer selection model considers two interacting proteins as ensembles of conformers with similar free energies that differ in enthalpic and entropic stabilization, and interconvert on varying timescales. Initial interactions occur between compatible conformer subgroups of each protein, to form a complex that refolds to form the final structure (Grünberg et al. 2004). The protein-protein complex contains populations of conformers that differ from those in the free proteins. Changes in conformational equilibria between free and bound forms help to explain the low negative and positive ΔC_p values for interactions involving MMP-3. Figure 3 indicates that the structures of N-TIMP-1 from the crystallographic structures of various MMPcd complexes show large differences, particularly in the loops between β-strands A and B, B and C which include the absence of electron density, suggesting local unfolding, which can expose apolar groups, making a positive contribution to ΔC_p. It has been shown by Eftink and coworkers that if an interacting protein has two conformational states that both interact with a binding partner with different affinities, indicating non-mandatory coupling

between binding and conformational change, ΔC_p can have positive or negative values, depending on the values of parameters relating to the conformational transition (Eftink et al., 1983). This provides an explanation for the "anomalous" ΔC_p values for N-TIMP interactions with MMP-3cd, particularly the positive value, +124 kcal/mol, for the ΔC_p of interaction with the N-TIMP-1 T98Lmutant and fits with the previously discussed structural changes observed in the free and bound forms of MMP-3cdand TIMP-1in its complex with TIMP-1 (Gomis-Rüth et al., 1997).

Previously reported dynamics simulations with wild type N-TIMP-1 and its T98L mutant suggested that the mutation reduced the flexibility of its interface for MMP-14, including the highly flexible N-terminal region, leading to a lower ΔS_{conf} penalty for binding (Grossman et al., 2010). Our results provide direct experimental evidence that WT N-TIMP-1 binding carries a large entropic penalty, showing that there is a $T\Delta S_{conf}$ penalty of -12 kcal/mol for the interaction. However, the T98L mutation in N-TIMP-1 increases this penalty by 8 kcal/mol and the increased affinity comes from an increase in solvent entropy ($T\Delta S_{solv}$), reflected in the more negative ΔC_p. This apparent anomaly may be linked to changes in the conformer assemblies of both the N-TIMP-1 and MMP14 components and associated solvent molecules in the complex with the N-TIMP-1 T98L mutant that result in a greater reduction in conformational entropy that is more than balanced by increased solvent entropy. This is consistent with the 3MA2 structure, which shows an interaction between Leu98 of the N-TIMP-1 mutant and Leu 222 of the MMP that is not present in the complex with wild type N-TIMP-1, which has the smaller polar Thr98.

The combined data for the interactions of three MMPs with WT and mutant forms of N-TIMPs-1 and -2 do not include all possible mutant N-TIMP/MMP combinations. However, there is a similar correlation in the data for the interactions of the two WT N-TIMPs with all three MMPs. It should be noted that ΔS_{solv} and ΔS_{int} are used to estimate ΔS_{conf} and that $T\Delta S_{int}$ for the ten interactions has a low variance (mean 17.2, SD 2.8) so that the apparent compensation between ΔS_{solv} and ΔS_{conf} is not surprising. It also follows that ΔS_{conf} has a direct positive correlation with ΔC_p suggesting a correlation with polar surface desolvation during the protein-protein interaction (Prabhi et al., 2005). This may be associated with the formation of new H-bonds and electrostatic interactions in the interface that generate structural changes and increases in dynamics.

$T\Delta S_{solv}$ and $T\Delta S_{conf}$ show mutual compensation for all interactions, with characteristic ranges for each MMP (Figure 22). These results are consistent with a possibility that distinct electrostatic and dynamic features of MMPs are key factors in their selective inhibition. Interactions with MMP-3 have the highest $T\Delta S_{conf}$ and lowest $T\Delta S_{solv}$ values while interactions with MT1-MMP have the lowest (mostly negative) $T\Delta S_{conf}$ and highest $T\Delta S_{solv}$. This is consistent with our previous observation that the character of the MMP has a dominant effect on the source of entropy driving its interaction with TIMPs (Wu et. al., 2011). It suggests MMP-3 has the greatest flexibility and MT1-MMP the least among these three MMPs with respect to adapting to TIMP binding partners. Difference in flexibility and dynamics among MMPs is clearly a factor to consider in designing specific inhibitors.

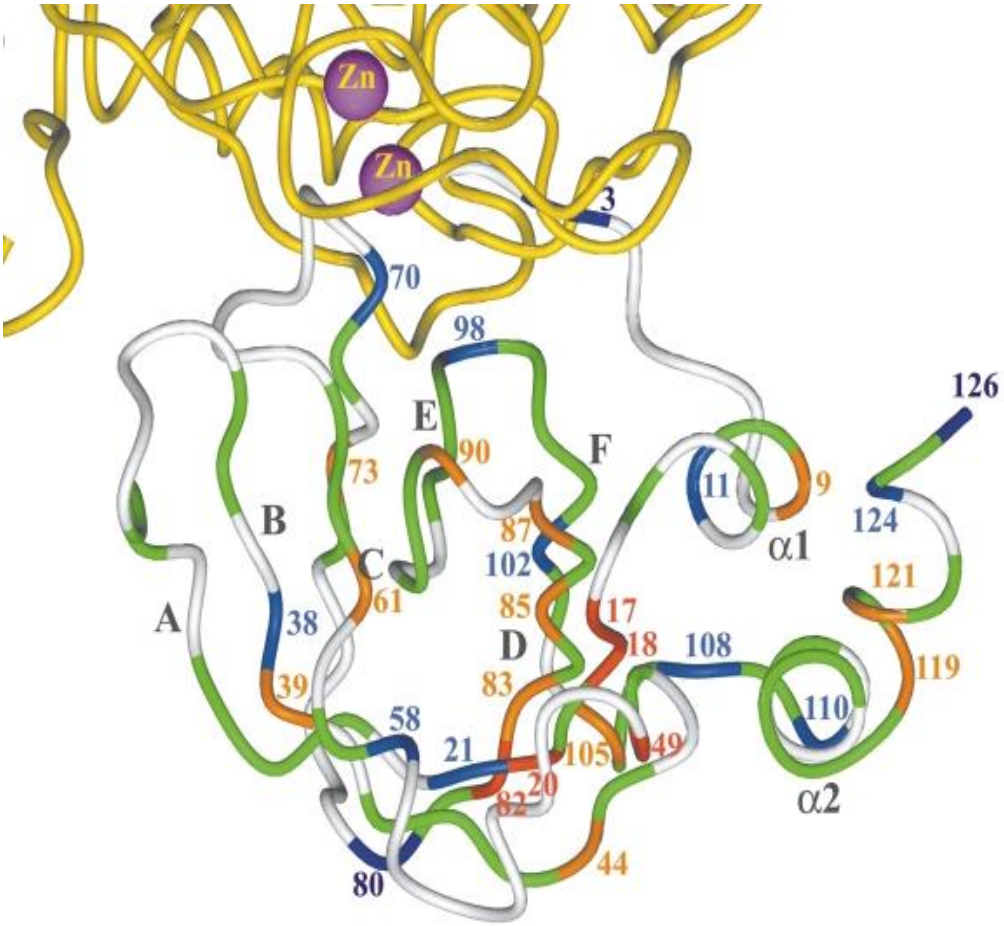

Figure 25. Sites of MMP-3-induced changes in N-TIMP-1 backbone flexibility (Arumugam et al., 2003) shows large conformational differences of protein structures in their free and complexed states

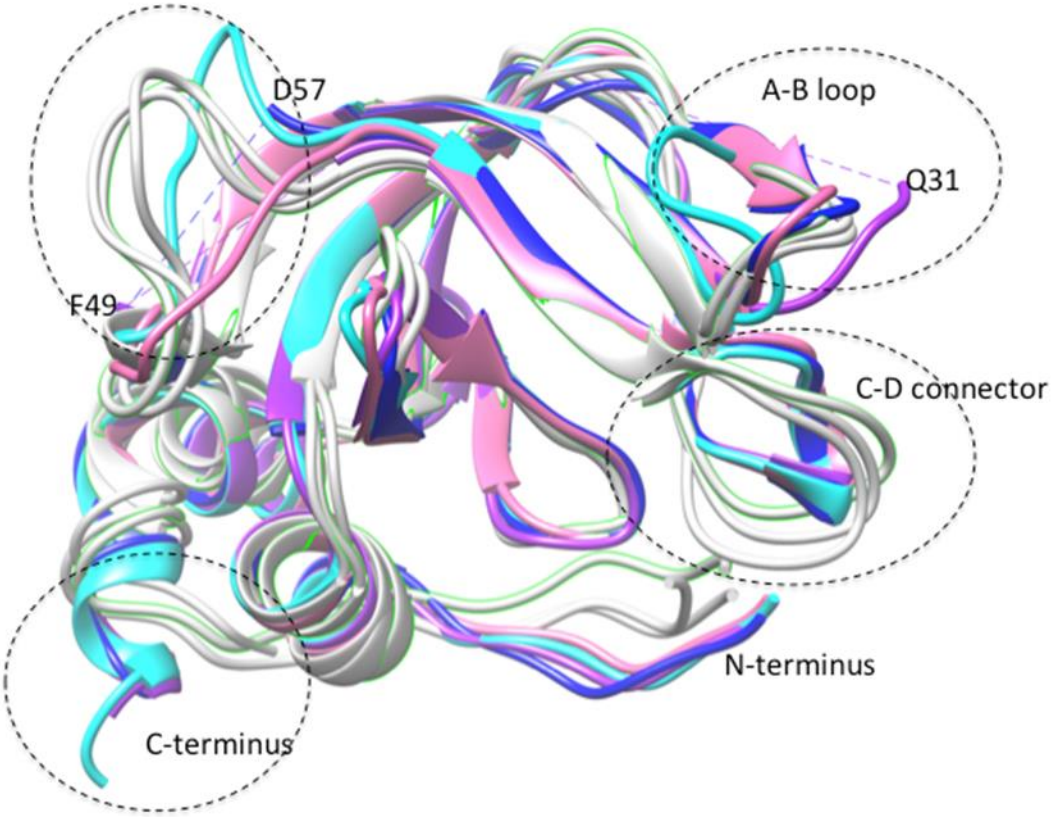

Figure 26. Superimposed ribbon structures of NT1 extracted from crystallographic structures of different complexes and solution NMR structures of the free protein.The structures from the complexes are colored as follows: MMP1c (2jot) pink; MMP3c (1uea), cyan; MMP14c (3ma2), blue; MMP10c (3v96), purple. The free NT1 structures were chains 1, 20 and 29 from 1d2b, and are colored light grey. The structures were superimposed and displayed using CHIMERA (Pettersen et. al., 2004)

IV THERMODYNAMIC STUDIES OF THE ROLE OF THE ACTIVE SITE RESIDUE GLU202 OF STOMELYSIN-1 (MMP-3) IN HIGH-AFFINITY BINDING OF N-TIMPS

1. Introduction

Our previous projects revealed that distinct electrostatic and dynamic features of MMPs are key factors in their selective inhibition and the interactions between N-TIMPs and MMP-3cd have "anomalous" thermodynamic profiles compared with other N-TIMP/MMPcd interactions. Previous structural studies also show a major interaction-induced structural transition in MMP-3cd during the formation of its complex with TIMP-1 (Gomis-Rüth et al., 1997; Iyer et al., 2007), while this large structural adjustment has not been observed in other N-TIMP/MMPcd interactions. Therefore, a redistribution of dynamics when MMP-3cd binds to N-TIMPs may contribute to their "anomalous" thermodynamic parameters.

The crystallographic structures of the N-TIMP-1/MMP-3 complex, indicates that during the formation of complex, Glu202 in MMP-3 forms a hydrogen bond with the α-amino group of Cys1 of N-TIMP-1 with a distance 3.33 Å, as well as six van der Waals interactions with Cys1 and Thr2 of N-TIMP-1 (Arumugam et al., 2003). In the TIMP-MMP interactions, the side chain of this Glu202 moves closer to TIMP and this motion excludes the zinc-bound water molecule normally found in the enzyme (Gomis-Rüth et

al., 1997). Previously published mutagenesis studies reports the replacement of Glu202 in stromelysin-1 by aspartic acid, alanine and lysine. The aspartic acid mutant reduced enzyme activity to about 15% compared with the wild type stromelysin-1, while both the alanine and lysine mutants lost all the catalytic activity (Arza et al., 2001).

These previous studies illustrate the important role of the glutamic acid 202 in the catalytic activity, which raises the question of how MMP-3 contribute to TIMP/MMP interactions which can be investigated by determine how substitutions for the glutamic acid 202 affect MMPs and TIMP interactions.

This chapter reports an investigation of the thermodynamic profile of the interaction of MMP-3 mutant E202A with wild type N-TIMP-2. This mutant shows an favorable (negative) enthalpy change and a large negative conformational entropy change for interacting with wild type N-TIMP-2. Our data shows a large conformational entropy penalty might be the reason for the reduced affinity of MMP-3cd mutant E202A to wild type N-TIMP-2.

2. Materials and Methods

N-TIMP-2 and MMP-3 E202A were expressed as described earlier in this dissertation. ITC studies were carried out using a MicroCal VP-ITC Microcalorimeter. All other equipment, reagents, and cells were from the same sources as in previous studies.

a. Construction of MMP-3 E202A

The MMP-3 E202A was generated using QuikChange II Site-Directed Mutagenesis Kit (Agilent Technologies). Primers were designed using web-based primer design software program (http://labtools.stratagene.com/QC). PCR reactions were carried out at 95 °C for 30 sec, 55 °C for 1 min and 68 °C for 5.5 min, for 30 cycles after a 3-min hot start at 95 °C. The PCR products were cloned back into pET-42b vector (Novagen) for expression.

PCR reactions were carried out at 95 °C for 30 sec, 55 °C for 1 min and 68 °C for 5 min, for 30 cycles after a 3-min hot start at 95 °C. The PCR products were cloned back into pET-42b vector (Novagen) for expression.

b. Isothermal Titration Calorimetry of N-TIMP-2/MMP-3 E202A cd Interaction

Protein solutions were dialyzed extensively against various buffers at 20 mM concentrations containing 250 mM NaCl, 10 mM $CaCl_2$, and 50 μM $ZnCl_2$ at pH 7.4 and degassed prior to use. Solutions of N-TIMP-2 (12–30 μM) were titrated with the MMP-3 E202A cd (120–300 μM) at different temperatures using a MicroCal VP-ITC microcalorimeter. The instrument was programmed to carry out 14 injections of 20 μl each over. The heat capacity change, intrinsic enthalpy change and intrinsic entropy change were determined or calculated as previously described.

3. Results and Discussion

Compared to the wild type MMP-3cd, the mutant E202A binds weakly to wild type N-TIMP-2 with a K_a of $1.118*10^6$, and its interaction with N-TIMP-2 has a small favorable enthalpy change (-2.3 kcal/mol) compared with an unfavorable +5.46 kcal/mol

together with a less favorable entropy change (5.4 kcal/mol vs 16.6 kcal/mol). The heat capacity change (ΔC_p), measured as the temperature-dependence of ΔH_{obs}, is negative and similar in magnitude to that for binding to wild-type MMP-3 (-49 vs -55 cal/mol/K) indicating a similar ΔS_{solv}. Using these parameters, we calculate that the interaction of N-TIMP-2 with the E203 mutant has an unfavorable conformational entropy contribution ($T\Delta S_{conf}$) of -4.5 kcal/mol as compared with the strongly favorable conformational entropy contribution (16.8 kcal/mol) for binding to wild-type MMP-3. The crystallographic structure of the TIMP-1/MMP-3 complex (Gomis-Rüth et al., 1997) reveals that the MMP undergoes significant conformational changes on binding to TIMP-1, which can help to explain why the negative ΔC_p for this interaction is much less than that predicted from the non-polar and polar surface areas buried on complex formation (Wu et al, 2011) but the source of the unfavorable enthalpy of binding is not clear (Arumugam et al, 2003). While the interaction of N-TIMP-2 with MMP-3 has a similar unfavorable ΔH_{int}, its interaction with the E203A mutant has a favorable value of -2.3 kcal/mol, suggesting that interactions with residue Glu 202 of MMP-3cd might be linked to the "anomalous" unfavorable enthalpy of binding to N-TIMPs.

The interaction between wild type MMP-3 and N-TIMP-2 interaction releases 0.68 protons to the solvent, whereas the mutant E202A is associated with the release of much less protons (0. 2) which shows a probable relation to the substitution of Ala residue with a smaller side chain for Glu202. Possibilities include the displacement of the water molecule from the MMP active site on TIMP binding, since this water molecule may be absent in the mutant enzyme, or distortion of the TIMP N-terminal region associated with interactions with Glu203.

A B

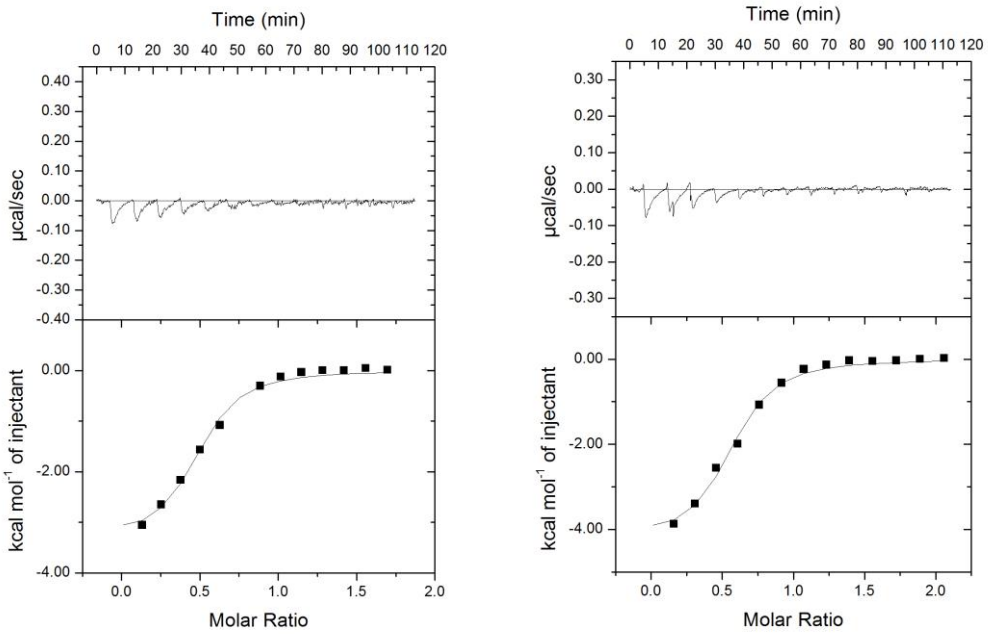

Figure 27. Isothermal calorimetric titration of N-TIMP-2 with catalytic domain of MMP-3 E202A in HEPES buffer at 291K (A) and 310 K (B).Aliquots (20 ul) of MMP-3cd (150 uM) were injected into N-TIMP-1 T98L (30uM) in HEPES buffer, pH 7.4 and the heats of binding were measured with a MicroCal VP-ITC micro calorimeter as described in Experimental Procedures.

Table 16. Enthalpy of binding for the interactions of MMP-3cd variants with N-TIMP-2 in buffers of different enthalpies of ionization at 291 K and calculated intrinsic enthalpy change (ΔHint) and ionization change (NH+).

Buffer	ΔH_{ion}	MMP-3cd WT[a]	MMP-3cd E202A
		ΔH_{obs} (kcal/mol)	
PIPES	2.726	4.028±0.03	-3.758±0.08
HEPES	4.94	2.222±0.02	-3.336±0.16
BES	5.993	1.698±0.05	-3.137±0.05
ACES	7.497	0.702±0.02	-2.341±0.04
ΔH_{int} (kcal/mol)		5.78±0.24	-2.27±0.26
N_{H+}		-0.68±0.04	-0.2±0.10

a Values taken from Wu et al.(2011)

Table 17. Enthalpies of interaction of MMP-3cd variants with N-TIMP-2 at different temperatures.ΔC_p was determined by linear regression of ΔH_{obs} vs K and ΔS_{solv} and used to calculate ΔS_{solv} at 298K ($=\Delta C_p * \ln(T/Ts^*)$, where Ts* is the reference temperature (385K) at which the hydrophobic contribution to ΔS is zero.

Temperature (K)	N-TIMP-2	
	MMP-3cd (WT)[a]	MMP-3cd E202A
	ΔH_{obs} (cal/mol)	
291	2.222±0.02	-3.336±0.16
298	1.838±0.01	-3.675±0.15
303	1.639±0.03	-3.941±0.17
310	1.162±0.04	-4.255±0.18
ΔC_p (cal/mol/K)	-54.8±3.7	-48.68±1.05
ΔS_{solv} (cal/mol)	14.0	13.63±0.42

Table 18. Thermodynamic profiles for interactions of N-TIMP-2 with MMP-3cd variants.

N-TIMP	N-TIMP-2	
MMP	MMP-3cd (WT)[a]	MMP-3cd E202A
ΔH_{int} (kcal/mol)	5.46±0.24	-2.27±0.26
K_a	$2.3*10^8$	$1.118*10^6$
ΔG_{1M}(kcal/mol)	-11.1±0.15	-7.8
$T\Delta S_{int}$ (kcal/mol)	16.6	5.4±0.26
ΔC_p (kcal/mol)	-56	-48.68±1.05
$T\Delta S_{solv}$(kcal/mol)	3.6	3.9±0.12
$T\Delta S_{conf}$(kcal/mo)	16.0	-4.53±0.13

a Values taken from Wu et al.(2011)

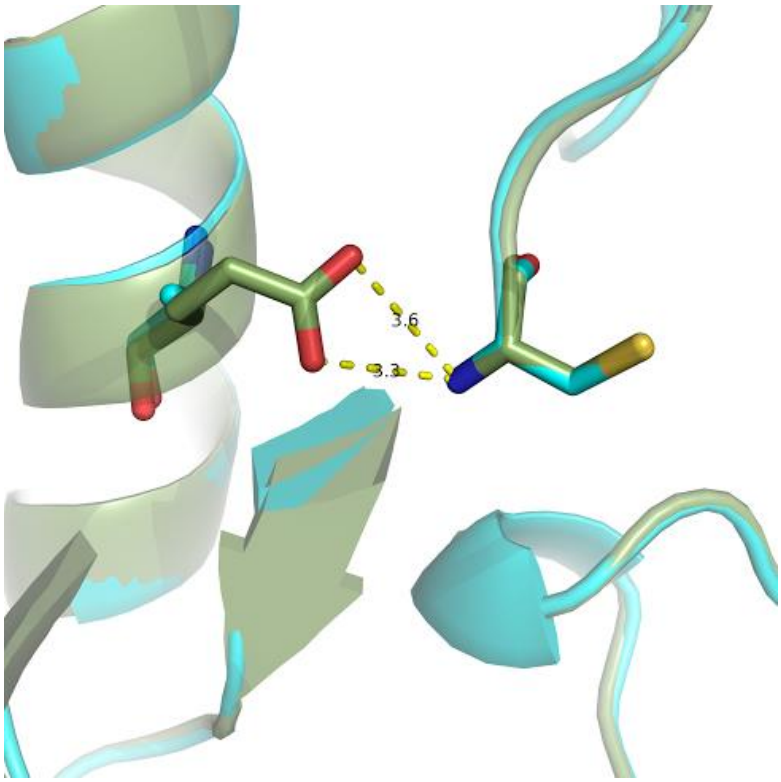

Figure 28. Complex of MMP-3E202A modeled with N-TIMP-2 wild-type. N-TIMP-2 wild-type is displayed in green, and MMP-3 E202D is colored in cyan. Weak hydrogen bonding is shown in yellow. Chimera 1.6rc.

V APPENDICES

Appendix A Sample concentrations for ITC of N-TIMP-1 / MT1-MMP CD interaction

MT1-MMP CD (mM)	N-TIMP-1 (mM)	Buffer	Temperature (K)
0.12	0.023	HEPES	291
0.12	0.023	HEPES	296
0.12	0.023	HEPES	303
0.12	0.023	HEPES	310
0.093	0.023	PIPES	291
0.097	0.023	BES	291
0.091	0.023	ACES	291

Appendix B Sample concentrations for ITC of N-TIMP-2/ MT1-MMP CD interaction

MT1-MMP CD (mM)	N-TIMP-2 (mM)	Buffer	Temperature (K)
0.15	0.02	HEPES	291
0.14	0.012	HEPES	296
0.15	0.016	HEPES	303
0.15	0.016	HEPES	310
0.12	0.012	PIPES	291
0.15	0.016	BES	291
0.15	0.016	ACES	291

Appendix C Sample concentrations for ITC of N-TIMP-1 T98L/ MT1-MMP CD interaction

MT1-MMP CD (mM)	N-TIMP-1 T98L (mM)	Buffer	Temperature (K)
0.12	0.022	HEPES	291
0.12	0.022	HEPES	296
0.12	0.022	HEPES	303
0.12	0.022	HEPES	310
0.10	0.022	PIPES	291
0.095	0.022	BES	291
0.093	0.022	ACES	291

Appendix D Sample concentrations for ITC of N-TIMP-1 T98L/ MMP3 CD interaction

MMP 3 CD (mM)	N-TIMP-1 T98L (mM)	Buffer	Temperature (K)
0.13	0.021	HEPES	291
0.13	0.021	HEPES	296
0.13	0.021	HEPES	303
0.13	0.021	HEPES	310
0.13	0.021	PIPES	291
0.12	0.021	MOPS	291
0.13	0.021	ACES	291

Appendix E Sample concentrations for ITC of N-TIMP-2/ MMP3 E202A CD interaction

MMP 3 E202A CD (mM)	N-TIMP-2 (mM)	Buffer	Temperature (K)
0.175	0.019	HEPES	291
0.152	0.017	HEPES	296
0.150	0.018	HEPES	303
0.165	0.0165	HEPES	310
0.2	0.03	PIPES	291
0.19	0.031	BES	291
0.2	0.03	ACES	291

Appendix F Copyright Permissions

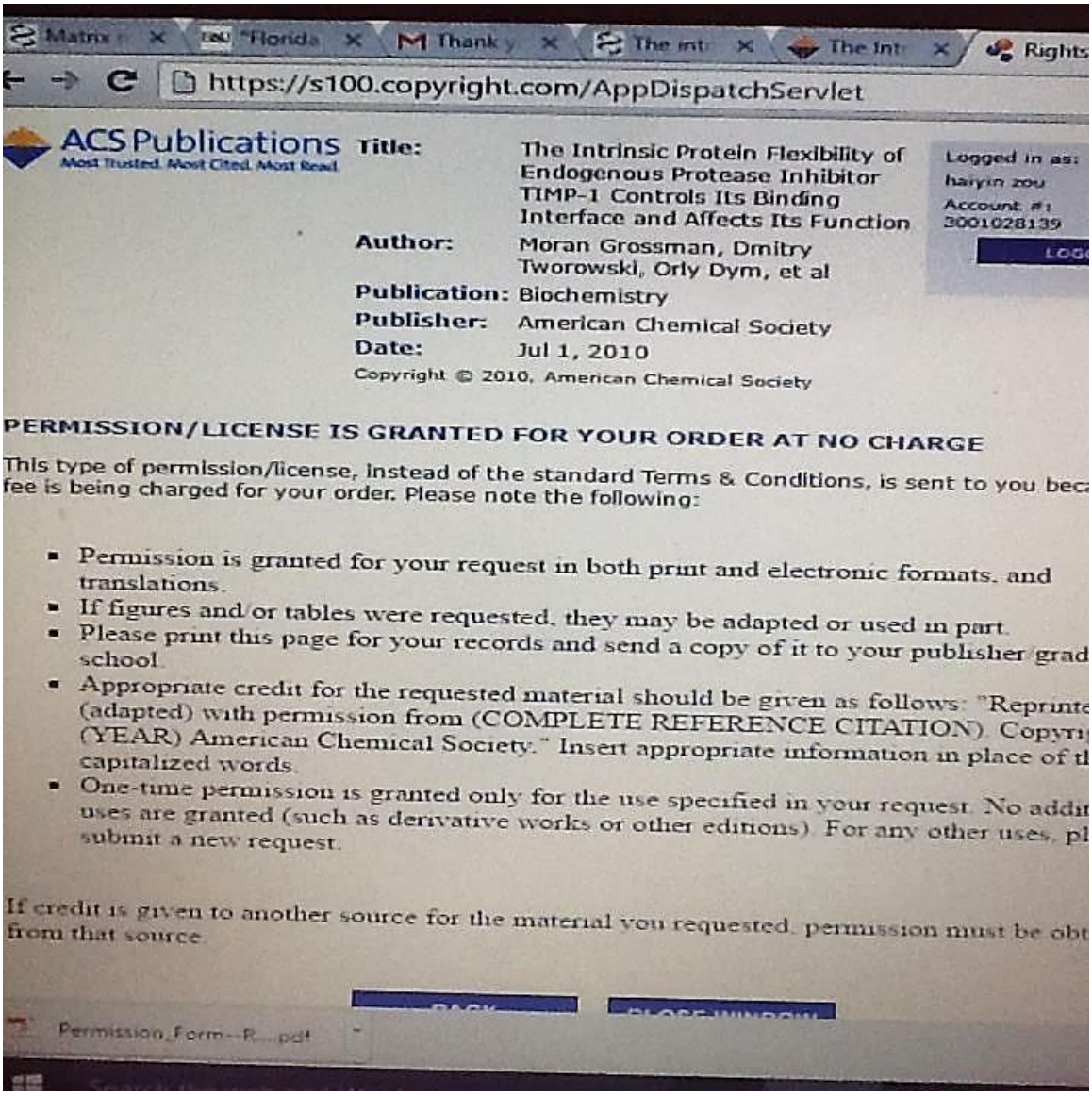

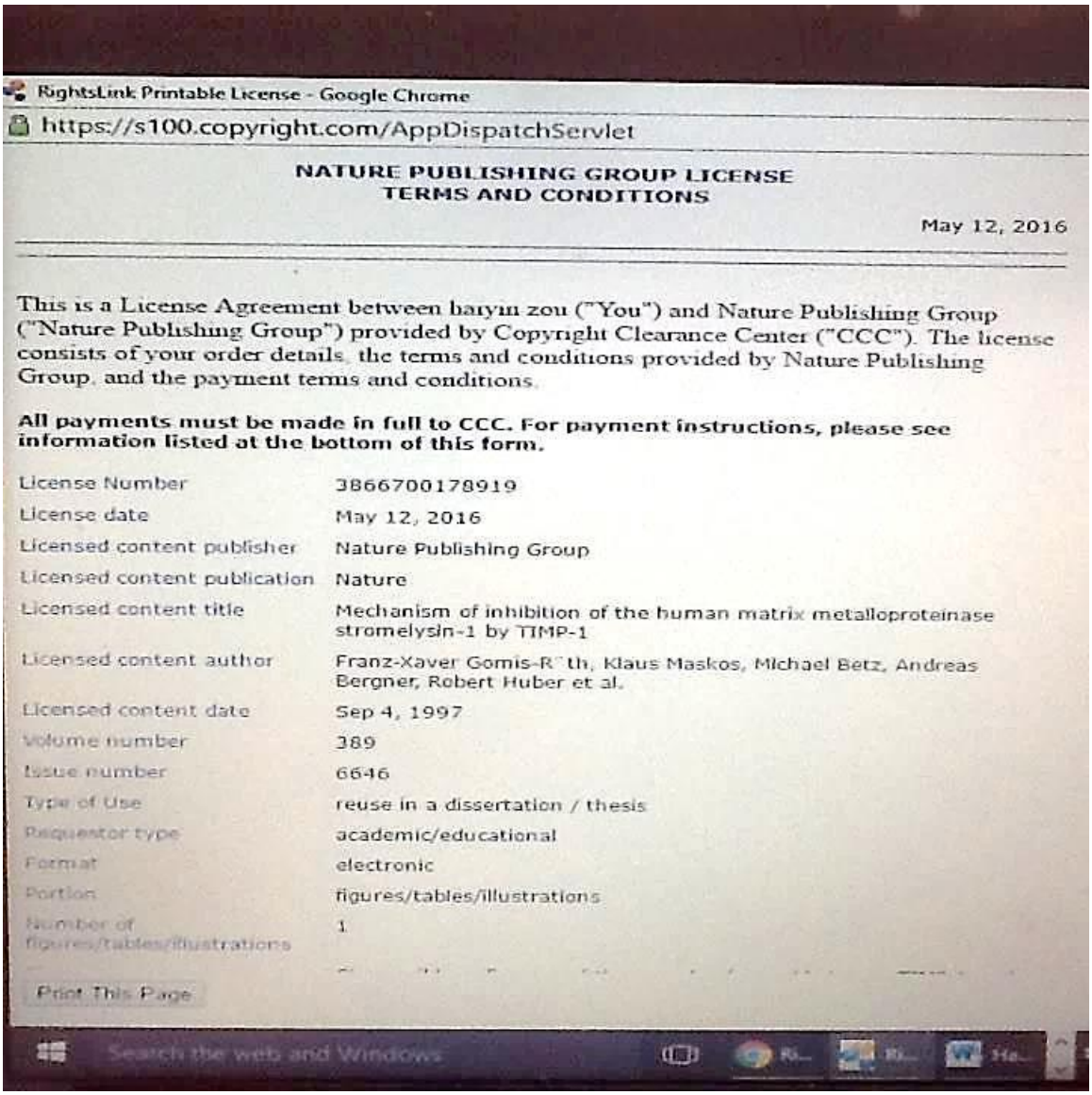

RightsLink Printable License - Google Chrome

https://s100.copyright.com/AppDispatchServlet

NATURE PUBLISHING GROUP LICENSE
TERMS AND CONDITIONS

May 12, 2016

This is a License Agreement between baiyin zou ("You") and Nature Publishing Group ("Nature Publishing Group") provided by Copyright Clearance Center ("CCC"). The license consists of your order details, the terms and conditions provided by Nature Publishing Group, and the payment terms and conditions.

All payments must be made in full to CCC. For payment instructions, please see information listed at the bottom of this form.

License Number	3866700178919
License date	May 12, 2016
Licensed content publisher	Nature Publishing Group
Licensed content publication	Nature
Licensed content title	Mechanism of inhibition of the human matrix metalloproteinase stromelysin-1 by TIMP-1
Licensed content author	Franz-Xaver Gomis-R¨th, Klaus Maskos, Michael Betz, Andreas Bergner, Robert Huber et al.
Licensed content date	Sep 4, 1997
Volume number	389
Issue number	6646
Type of Use	reuse in a dissertation / thesis
Requestor type	academic/educational
Format	electronic
Portion	figures/tables/illustrations
Number of figures/tables/illustrations	1

Print This Page

Search the web and Windows

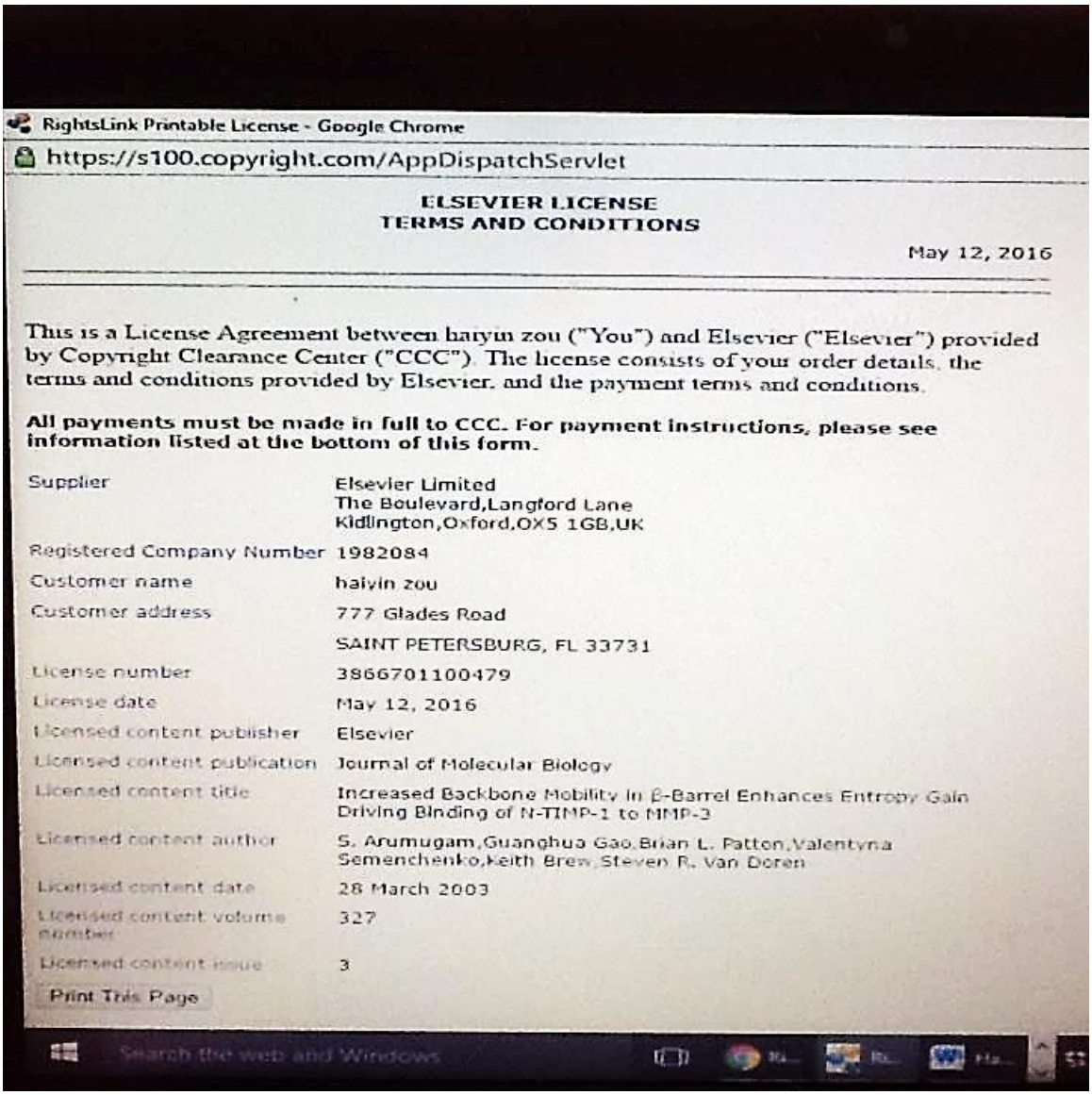

RightsLink Printable License - Google Chrome

https://s100.copyright.com/AppDispatchServlet

ELSEVIER LICENSE
TERMS AND CONDITIONS

May 12, 2016

This is a License Agreement between haiyin zou ("You") and Elsevier ("Elsevier") provided by Copyright Clearance Center ("CCC"). The license consists of your order details, the terms and conditions provided by Elsevier, and the payment terms and conditions.

All payments must be made in full to CCC. For payment instructions, please see information listed at the bottom of this form.

Supplier	Elsevier Limited The Boulevard,Langford Lane Kidlington,Oxford,OX5 1GB,UK
Registered Company Number	1982084
Customer name	haiyin zou
Customer address	777 Glades Road SAINT PETERSBURG, FL 33731
License number	3866701100479
License date	May 12, 2016
Licensed content publisher	Elsevier
Licensed content publication	Journal of Molecular Biology
Licensed content title	Increased Backbone Mobility in β-Barrel Enhances Entropy Gain Driving Binding of N-TIMP-1 to MMP-3
Licensed content author	S. Arumugam,Guanghua Gao,Brian L. Patton,Valentyna Semenchenko,Keith Brew,Steven R. Van Doren
Licensed content date	28 March 2003
Licensed content volume number	327
Licensed content issue	3

Print This Page

Search the web and Windows

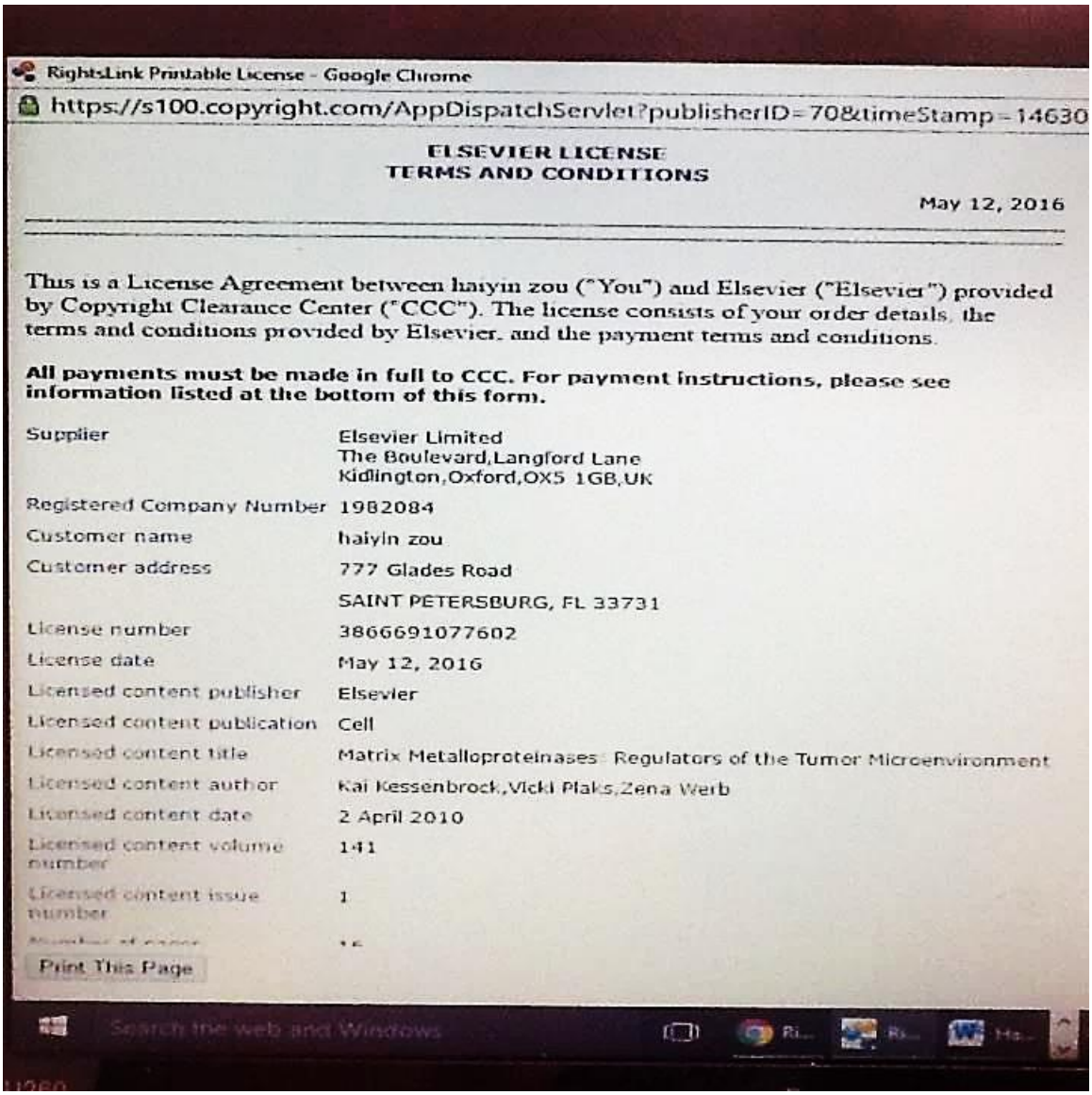
RightsLink Printable License - Google Chrome
https://s100.copyright.com/AppDispatchServlet?publisherID=70&timeStamp=14630
ELSEVIER LICENSE
TERMS AND CONDITIONS
May 12, 2016
This is a License Agreement between haiyin zou ("You") and Elsevier ("Elsevier") provided by Copyright Clearance Center ("CCC"). The license consists of your order details, the terms and conditions provided by Elsevier, and the payment terms and conditions.
All payments must be made in full to CCC. For payment instructions, please see information listed at the bottom of this form.
Supplier
Elsevier Limited
The Boulevard,Langford Lane
Kidlington,Oxford,OX5 1GB,UK
Registered Company Number
1982084
Customer name
haiyin zou
Customer address
777 Glades Road
SAINT PETERSBURG, FL 33731
License number
3866691077602
License date
May 12, 2016
Licensed content publisher
Elsevier
Licensed content publication
Cell
Licensed content title
Matrix Metalloproteinases: Regulators of the Tumor Microenvironment
Licensed content author
Kai Kessenbrock,Vicki Plaks,Zena Werb
Licensed content date
2 April 2010
Licensed content volume number
141
Licensed content issue number
1
Print This Page
Search the web and Windows

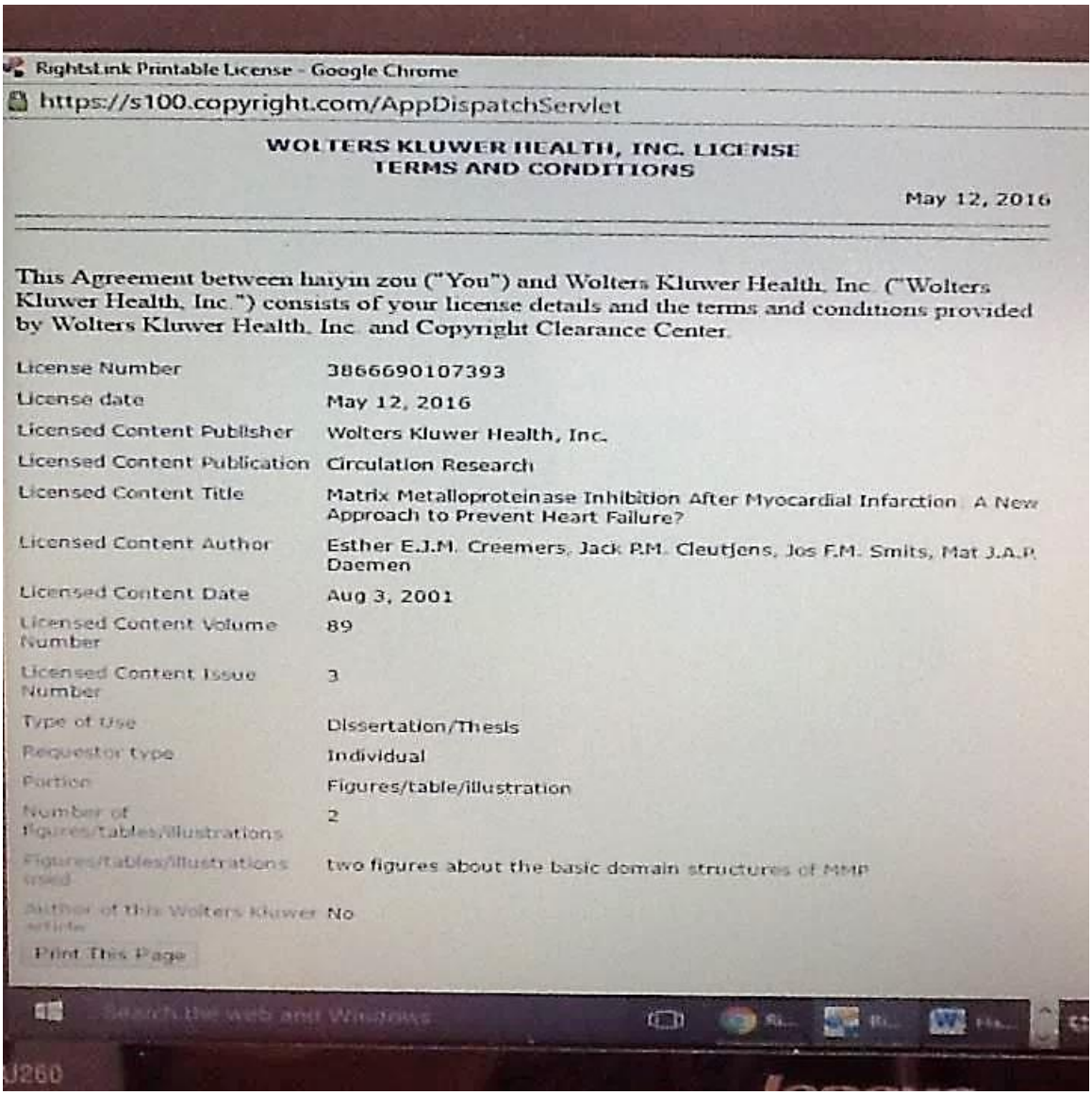

RightsLink Printable License - Google Chrome

https://s100.copyright.com/AppDispatchServlet

WOLTERS KLUWER HEALTH, INC. LICENSE TERMS AND CONDITIONS

May 12, 2016

This Agreement between haiyu zou ("You") and Wolters Kluwer Health, Inc. ("Wolters Kluwer Health, Inc.") consists of your license details and the terms and conditions provided by Wolters Kluwer Health, Inc. and Copyright Clearance Center.

License Number	3866690107393
License date	May 12, 2016
Licensed Content Publisher	Wolters Kluwer Health, Inc.
Licensed Content Publication	Circulation Research
Licensed Content Title	Matrix Metalloproteinase Inhibition After Myocardial Infarction: A New Approach to Prevent Heart Failure?
Licensed Content Author	Esther E.J.M. Creemers, Jack P.M. Cleutjens, Jos F.M. Smits, Mat J.A.P. Daemen
Licensed Content Date	Aug 3, 2001
Licensed Content Volume Number	89
Licensed Content Issue Number	3
Type of Use	Dissertation/Thesis
Requestor type	Individual
Portion	Figures/table/illustration
Number of figures/tables/illustrations	2
Figures/tables/illustrations used	two figures about the basic domain structures of MMP
Author of this Wolters Kluwer article	No

Print This Page

VI BIBLIOGRAPHY

Amour, A., Knight, C. G., Webster, A., Slocombe, P. M., Stephens, P. E., Knäuper, V., … Murphy, G. (2000). The in vitro activity of ADAM-10 is inhibited by TIMP-1 and TIMP-3. *FEBS Lett*., 473, 275–9.

Amour, A., Slocombe, P. M., Webster, A., Butler, M., Knight, C. G., Smith, B. J., … Murphy, G. (1998). TNF-alpha converting enzyme (TACE) is inhibited by TIMP-3. *FEBS Lett*., 435, 39–44.

Arnold, F. H., Wintrode, P. L., Miyazaki, K., & Gershenson, A. (2001). How enzymes adapt: lessons from directed evolution. *Trends Biochem Sci*, 26, 100–06.

Arumugam, S., Gao, G., Patton, B. L., Semenchenko, V., Brew, K., & Van Doren, S. R. (2003). Increased Backbone Mobility in β-Barrel Enhances Entropy Gain Driving Binding of N-TIMP-1 to MMP-3. *J*. *Mol*. *Biol*., 327(3), 719–734.

Arza, B., De Maeyer, M., Felez, J., Collen, D., & Lijnen, H. R. (2001). Critical role of glutamic acid 202 in the enzymatic activity of stromelysin-1 (MMP-3). *Eur*. *J*. *Biochem*., 268, 826-31

Arumugam, S., & Van Doren, S. R. (2003). Global orientation of bound MMP-3 and N-TIMP-1 in solution via residual dipolar couplings. *Biochemistry*, 42(26), 7950–8.

Baker, A. H., Edwards, D. R., & Murphy, G. (2002). Metalloproteinase inhibitors: biological actions and therapeutic opportunities. *J*. *Cell Sci*, 115(Pt 19), 3719–27.

Baker, B.M., & Murphy, K.P. (1998). Prediction of binding energetics from structure using empirical parameterization. *Methods Enzymol*., 295, 294-314

Barasch, J., Yang, J., Qiao, J., Tempst, P., Erdjument-Bromage, H., Leung, W., & Oliver, J. A. (1999). Tissue inhibitor of metalloproteinase-2 stimulates mesenchymal growth and regulates epithelial branching during morphogenesis of the rat metanephros. *J*. *Clin Invest*, 103(9), 1299–307.

Batra, J., Robinson, J., Soares, A. S., Fields, A. P., Radisky, D. C., & Radisky, E. S. (2012). Matrix metalloproteinase-10 (MMP-10) interaction with tissue inhibitors of metalloproteinases TIMP-1 and TIMP-2: binding studies and crystal structure. *J*. *Biol*. *Chem*, 287(19), 15935–46.

Bauer, E. A., Stricklin, G. P., Jeffrey, J. J., & Eisen, A. Z. (1975). Collagenase production by human skin fibroblasts. *Biochem*. *Biophys*. *Res*. *Commun*., 64(1), 232–40.

Bertaux, B., Hornebeck, W., Eisen, A. Z., & Dubertret, L. (1991). Growth stimulation of human keratinocytes by tissue inhibitor of metalloproteinases. *J*. *Invest*. *Dermatol*., 97(4), 679–85.

Bigg, H. F., Morrison, C. J., Butler, G. S., Bogoyevitch, M. A., Wang, Z., Soloway, P.

D., & Overall, C. M. (2001). Tissue inhibitor of metalloproteinases-4 inhibits but does not support the activation of gelatinase A via efficient inhibition of membrane type 1-matrix metalloproteinase. *Cancer Res.*, 61(9), 3610–8.

Bogan, A. A., & Thorn, K. S. (1998). Anatomy of hot spots in protein interfaces. *J. Mol. Biol.*, 280(1), 1–9.

Brew, K., Dinakarpandian, D., & Nagase, H. (2000). Tissue inhibitors of metalloproteinases: evolution, structure and function. *Biochim. Biophys. Acta*, 1477(1-2), 267–83.

Brew, K., & Nagase, H. (2010). The tissue inhibitors of metalloproteinases (TIMPs): an ancient family with structural and functional diversity. *Biochim. Biophys. Acta*, 1803(1), 55–71.

Burrage, P. S., Mix, K. S., & Brinckerhoff, C. E. (2006). Matrix metalloproteinases: role in arthritis. *Front. Biosci*, 11, 529–43.

Campoy, A.V., and Freire, E. (2005). ITC in the post-genomic era….? Priceless. *Biophys. Chem*. 115, 115-124.

Chaires, J. B. (2008). Calorimetry and thermodynamics in drug design. *Annu. Rev. Biophys.*, 37, 135–51.

Chen, L., Rydel, T.J., Gu, F., Dunaway, C.M., Pikul, S., Dunham, K.M., and Barnett, B.L. (1999) Crystalstructure of the stromelysin catalytic domain at 2.0 A resolution: inhibitor-induced conformational changes. *J. Mol. Biol.*, 293, 545-547.

Chesler, L., Golde, D. W., Bersch, N., & Johnson, M. D. (1995). Metalloproteinase inhibition and erythroid potentiation are independent activities of tissue inhibitor of metalloproteinases-1. *Blood*, 86(12), 4506–15.

Coussens, L. M., Fingleton, B., & Matrisian, L. M. (2002). Matrix metalloproteinase inhibitors and cancer: trials and tribulations. *Science*, 295(5564), 2387–92.

Creemers EE1, Cleutjens JP, Smits JF, Daemen MJ. (2001). Matrix metalloproteinase inhibition after myocardial infarction: a new approach to prevent heart failure? *Circ Res.*, 89:201-10.

D'Armiento, J., Dalal, S. S., Okada, Y., Berg, R. A., & Chada, K. (1992). Collagenase expression in the lungs of transgenic mice causes pulmonary emphysema. *Cell*, *71*(6), 955–61.

Delaisse, J. M., Eeckhout, Y., & Vaes, G. (1988). Bone-resorbing agents affect the production and distribution of procollagenase as well as the activity of collagenase in bone tissue. *Endocrinology*, *123*(1), 264–76.

Dunn, B.(2001) Quantitative amino acid analysis. *Protein Sci.*, Chapter 3:Unit 3.2.

Eftink, M.R., Anusiem, A.C., and Biltonen, R.L. (1983) Enthalpy-entropy compensation and heat capacity changes for protein-ligand interactions: general thermodynamic models and data for the binding of nucleotides to ribonuclease A. *Biochemistry*, 22, 3884-3896.

Eijsink, V. G. H., Bjørk, A., Gåseidnes, S., Sirevåg, R., Synstad, B., van den Burg, B., & Vriend, G. (2004). Rational engineering of enzyme stability. *J. Biotechnol.*, *113*(1-

3), 105–20.

Falconer RJ & Collins BM. (2011) Survey of the year 2009: applications of isothermal titration calorimetry. *J Mol Recognit.,* 24(1):1-16.

Fernandez-Catalan, C., Bode, W., Huber, R., Turk, D., Calvete, J. J., Lichte, a, … Maskos, K. (1998). Crystal structure of the complex formed by the membrane type 1-matrix metalloproteinase with the tissue inhibitor of metalloproteinases-2, the soluble progelatinase A receptor. *EMBO J.*, *17*(17), 5238–48.

Fisher, G. J., Quan, T., Purohit, T., Shao, Y., Cho, M. K., He, T., … Voorhees, J. J. (2009). Collagen fragmentation promotes oxidative stress and elevates matrix metalloproteinase-1 in fibroblasts in aged human skin. *Am. J. Pathol.*, *174*(1), 101–14.

Fisher, J. F., & Mobashery, S. (2006). Recent advances in MMP inhibitor design. *Cancer Metastasis Rev.*, *25*(1), 115–36.

Gálvez, B. G., Matías-Román, S., Albar, J. P., Sánchez-Madrid, F., & Arroyo, A. G. (2001). Membrane type 1-matrix metalloproteinase is activated during migration of human endothelial cells and modulates endothelial motility and matrix remodeling. *J. Biol. Chem.*, *276*(40), 37491–500.

Gearing, A. J., Beckett, P., Christodoulou, M., Churchill, M., Clements, J., Davidson, A. H., … Gordon, J. L. (1994). Processing of tumour necrosis factor-alpha precursor by metalloproteinases. *Nature*, *370*(6490), 555–7.

Giver, L., Gershenson, A., Freskgard, P. O., & Arnold, F. H. (1998). Directed evolution of a thermostable esterase. *Proc. Natl. Acad. Sci. U. S. A.*, *95*(22), 12809–13.

Gomis-Rüth, F. X., Maskos, K., Betz, M., Bergner, A., Huber, R., Suzuki, K., … Bode, W. (1997). Mechanism of inhibition of the human matrix metalloproteinase stromelysin-1 by TIMP-1. *Nature*, *389*(6646), 77–81.

Grossman, M., Tworowski, D., Dym, O., Lee, M.-H., Levy, Y., Murphy, G., & Sagi, I. (2010). The intrinsic protein flexibility of endogenous protease inhibitor TIMP-1 controls its binding interface and affects its function. *Biochemistry*, *49*(29), 6184–92.

Hamze, A. B., Wei, S., Bahudhanapati, H., Kota, S., Acharya, K. R., & Brew, K. (2007). Constraining specificity in the N-domain of tissue inhibitor of metalloproteinases-1; gelatinase-selective inhibitors. *Protein Sci.*, *16*(9), 1905–13.

Harada, T., Arii, S., Mise, M., Imamura, T., Higashitsuji, H., Furutani, M., … Imamura, M. (1998). Membrane-type matrix metalloproteinase-1(MT1-MTP) gene is overexpressed in highly invasive hepatocellular carcinomas. *J. Hepatol., 28*(2), 231–9.

Huang, W., Meng, Q., Suzuki, K., Brew, K., & Nagase, H. (1997). PROTEIN CHEMISTRY AND STRUCTURE : Mutational Study of the Amino-terminal Domain of Human Tissue Inhibitor of Inhibitory Region for Matrix Metalloproteinases. *J. Biol. Chem.,* 272, 22086-22091

Hu, J., Van den steen, P.E., Sang, Q.-X. a, & Opdenakker, G. (2007). Matrix metalloproteinase inhibitors as therapy for inflammatory and vascular diseases. *Nat*

Rev Drug Discov., 6, 480-98

Iyer, S., Wei, S., Brew, K., & Acharya, K. R. (2007). Crystal structure of the catalytic domain of matrix metalloproteinase-1 in complex with the inhibitory domain of tissue inhibitor of metalloproteinase-1. *J*. *Biol*. *Chem*., *282*(1), 364–71.

Johannes,T., & Zhao, H. (2006). Directed evolution of enzymes and biosynthetic pathways. *Microbiology*, 9:261–267

Jacobsen, J., Visse, R., Sørensen, H. P., Enghild, J. J., Brew, K., Wewer, U. M., & Nagase, H. (2008). Catalytic properties of ADAM12 and its domain deletion mutants. *Biochemistry*, *47*(2), 537–47.

Jones, S., & Thornton, J. M. (1996). Principles of protein-protein interactions. *Proc*. *Natl*. *Acad*. *Sci*. *U*. *S*. *A*., *93*(1), 13–20.

Kang, K.-H., Park, S.-Y., Rho, S. B., & Lee, J.-H. (2008). Tissue inhibitor of metalloproteinases-3 interacts with angiotensin II type 2 receptor and additively inhibits angiogenesis. *Cardiovasc*. *Res*., *79*(1), 150–60.

Kar, S., Subbaram, S., Carrico, P. M., & Melendez, J. A. (2010). Redox-control of matrix metalloproteinase-1: a critical link between free radicals, matrix remodeling and degenerative disease. *Respir*. *Physiol*. *Neurobiol*., *174*(3), 299–306.

Kawasaki, Y., & Freire, E. (2011). Finding a better path to drug selectivity. *Drug Discov*. *Today, 16*(21-22), 985–90.

Kessenbrock K, Plaks V, Werb Z.(2010). Matrix metalloproteinases: regulators of the tumor microenvironment. *Cell*, 141(1):52-67

Kim, H. E., Dalal, S. S., Young, E., Legato, M. J., Weisfeldt, M. L., & D'Armiento, J. (2000). Disruption of the myocardial extracellular matrix leads to cardiac dysfunction. *J*. *Clin*. *Invest*., *106*(7), 857–66.

Kumar, S., Ma, B., Tsai, C., Sinha, N., and Nussinov, R (2000) Folding and binding cascades: dynamic landscapes and population shifts. *Protein Sci*. , 9, 10-19.

Ladbury, J. E. (2010). Calorimetry as a tool for understanding biomolecular interactions and an aid to drug design. *Biochem*. *Soc*. *Trans*., *38*(4), 888–93.

Lee, M.-H., Rapti, M., & Murphy, G. (2003). Unveiling the surface epitopes that render tissue inhibitor of metalloproteinase-1 inactive against membrane type 1-matrix metalloproteinase. *J*. *Biol*. *Chem*., *278*(41), 40224–30.

Lee, M.-H., Rapti, M., Knaüper, V., & Murphy, G. (2004). Threonine 98, the pivotal residue of tissue inhibitor of metalloproteinases (TIMP)-1 in metalloproteinase recognition. *J*. *Biol*. *Chem*. 279, 17562-17569.

Lemaître, V., & D'Armiento, J. (2006). Matrix metalloproteinases in development and disease. *Birth Defects Res*. *C*. *Embryo Today*, *78*(1), 1–10.

Li, J., Brick, P., O'Hare, M. C., Skarzynski, T., Lloyd, L. F., Curry, V. A., … Cawston, T. E. (1995). Structure of full-length porcine synovial collagenase reveals a C-terminal domain containing a calcium-linked, four-bladed beta-propeller. *Structure*, *3*(6), 541–9.

Li, Z., Clarke, M. P., Barker, M. D., & McKie, N. (2005). TIMP3 mutation in Sorsby's

fundus dystrophy: molecular insights. *Expert Rev*. *Mol*. *Med*., *7*(24), 1–15.

Liu, X.-W., Taube, M. E., Jung, K.-K., Dong, Z., Lee, Y. J., Roshy, S., … Kim, H.-R. C. (2005). Tissue inhibitor of metalloproteinase-1 protects human breast epithelial cells from extrinsic cell death: a potential oncogenic activity of tissue inhibitor of metalloproteinase-1. *Cancer Res*., *65*(3), 898–906.

Lovejoy B, Cleasby A, Hassell AM, Luther MA, Weigl D, McGeehan G, Lambert MH, Jordan SR. (1994). Structural analysis of the catalytic domain of human fibroblast collagenase. *Ann N Y Acad Sci*.,732:375-8

Lu, Y., Berry, S. M., & Pfister, T. D. (2001). Engineering novel metalloproteins: design of metal-binding sites into native protein scaffolds. *Chem*. *Rev*., *101*(10), 3047–80.

Lu, Y., Yeung, N., Sieracki, N., & Marshall, N. M. (2009). Design of functional metalloproteins. *Nature*, *460*(7257), 855–62.

Manka, S. W., Carafoli, F., Visse, R., Bihan, D., Raynal, N., Farndale, R. W., … Nagase, H. (2012). Structural insights into triple-helical collagen cleavage by matrix metalloproteinase 1. *Proc*. *Natl*. *Acad*. *Sci*. *U*. *S*. *A*., *109*(31), 12461–6.

Martin, A., Kather, I., & Schmid, F. X. (2002). Origins of the high stability of an in vitro-selected cold-shock protein. *J*. *Mol*. *Biol*., *318*(5), 1341–9.

Maskos, K., Lang, R., Tschesche, H., & Bode, W. (2007). Flexibility and variability of TIMP binding: X-ray structure of the complex between collagenase-3/MMP-13 and TIMP-2. *J*. *Mol*. *Biol*. *366*(4), 1222–31.

Meng Q, Malinovskii V, Huang W, Hu Y, Chung L, Nagase H, Bode W, Maskos K, Brew K (1999). Residue 2 of TIMP-1 is a major determinant of affinity and specificity for matrix metalloproteinases but effects of substitutions do not correlate with those of the corresponding P1' residue of substrate. *J*. *Biol*. *Chem*. 274(15):10184-9

Mercer, B. A., Kolesnikova, N., Sonett, J., & D'Armiento, J. (2004). Extracellular regulated kinase/mitogen activated protein kinase is up-regulated in pulmonary emphysema and mediates matrix metalloproteinase-1 induction by cigarette smoke. *J*. *Biol*. *Chem*., *279*(17), 17690–6.

Mills, J. H., Khare, S. D., Bolduc, J. M., Forouhar, F., Mulligan, V. K., Lew, S., … Baker, D. (2013). Computational design of an unnatural amino acid dependent metalloprotein with atomic level accuracy. *J*. *Am*. *Chem*. *Soc*., *135*(36), 13393–9.

Mitra, P., Shultis, D., & Zhang, Y. (2013). EvoDesign: De novo protein design based on structural and evolutionary profiles. *Nucleic Acids Res*., *41*, 273–80.

Miyazaki, K., Wintrode, P. L., Grayling, R. A., Rubingh, D. N., & Arnold, F. H. (2000). Directed evolution study of temperature adaptation in a psychrophilic enzyme. *J*. *Mol*. *Biol*., *297*(4), 1015–26.

Morgunova, E., Tuuttila, A., Bergmann, U., & Tryggvason, K. (2002). Structural insight into the complex formation of latent matrix metalloproteinase 2 with tissue inhibitor of metalloproteinase 2. *Proc*. *Natl*. *Acad*. *Sci*. *U*. *S*. *A*., *99*(11), 7414–9.

Murphy, G., & Nagase, H. (2008). Progress in matrix metalloproteinase research. *Mol*.

Aspects Med., *29*(5), 290–308.

Murphy, G., & Willenbrock, F. (1995). Tissue inhibitors of matrix metalloendopeptidases. *Methods Enzymol*., *248*, 496–510.

Muskett, F. W., Frenkiel, T. A., Feeney, J., Freedman, R. B., Carr, M. D., & Williamson, R. A. (1998). High resolution structure of the N-terminal domain of tissue inhibitor of metalloproteinases-2 and characterization of its interaction site with matrix metalloproteinase-3. *J*. *Biol*. *Chem*., *273*(34), 21736–43.

Nagase, H., & Brew, K. (2002). Engineering of tissue inhibitor of metalloproteinases mutants as potential therapeutics. *Arthritis Res*., *4 Suppl 3*, S51–61.

Nagase, H., Meng, Q. I., Malinovskii, V., Huang, W. E. N., Chung, L., Bode, W., Brew, K. (1999). Engineering of Selective TIMPs. *Ann*. *N*. *Y*. *Acad*. *Sci*., 878, 1-11

Nanda, V., Rosenblatt, M. M., Osyczka, A., Kono, H., Getahun, Z., Dutton, P. L., … Degrado, W. F. (2005). De novo design of a redox-active minimal rubredoxin mimic. *J*. *Am*. *Chem*. *Soc*.,, *127*(16), 5804–5.

Ogata, Y., Itoh, Y., & Nagase, H. (1995). Steps involved in activation of the pro-matrix metalloproteinase 9 (progelatinase B)-tissue inhibitor of metalloproteinases-1 complex by 4-aminophenylmercuric acetate and proteinases. *J*. *Biol*. *Chem*., *270*(31), 18506–11.

Okada, A., Tomasetto, C., Lutz, Y., Bellocq, J. P., Rio, M. C., & Basset, P. (1997). Expression of matrix metalloproteinases during rat skin wound healing: evidence that membrane type-1 matrix metalloproteinase is a stromal activator of pro-gelatinase A. *J*. *Cell Biol*., *137*(1), 67–77.

Pavlaki M. & Zucker S. (2003) Matrix metalloproteinase inhibitors (MMPIs): the beginning of phase I or the termination of phase III clinical trials. *Cancer Metastasis Rev*., 22(2-3):177-203.

Pettersen EF, Goddard TD, Huang CC, Couch GS, Greenblatt DM, Meng EC, and Ferrin TE. (2004) UCSF Chimera-a visualization system for exploratory research and analysis. J Comput Chem. 25, 1605-1612.

Pierce, M. M., Raman, C. S., & Nall, B. T. (1999). Isothermal titration calorimetry of protein-protein interactions. *Methods, 19*(2), 213–21.

Polette, M., Nawrocki, B., Gilles, C., Sato, H., Seiki, M., Tournier, J. M., & Birembaut, P. (1996). MT-MMP expression and localisation in human lung and breast cancers. *Virchows Arch*., *428*(1), 29–35.

Prabhi, N. V, & Sharp, K. A. (2005). Heat capacity in proteins. *Annu*. *Rev*. *Phys*. *Chem*., *56*, 521–48.

Qi, J. H., Ebrahem, Q., Moore, N., Murphy, G., Claesson-Welsh, L., Bond, M., … Anand-Apte, B. (2003). A novel function for tissue inhibitor of metalloproteinases-3 (TIMP3): inhibition of angiogenesis by blockage of VEGF binding to VEGF receptor-2. *Nat*. *Med*., *9*(4), 407–15. 6

Rao JS, Gondi C, Chetty C, Chittivelu S, Joseph PA, Lakka SS.(2005). Inhibition of invasion, angiogenesis, tumor growth, and metastasis by adenovirus-mediated

transfer of antisense uPAR and MMP-9 in non-small cell lung cancer cells. *Mol Cancer Ther*. , 4(9):1399-408

Roybal, C. N., Marmorstein, L. Y., Vander Jagt, D. L., & Abcouwer, S. F. (2005). Aberrant accumulation of fibulin-3 in the endoplasmic reticulum leads to activation of the unfolded protein response and VEGF expression. *Invest*. *Ophthalmol*. *Vis*. *Sci*.,, *46*(11), 3973–9.

Sarver, R. W., Peevers, J., Cody, W. L., Ciske, F. L., Dyer, J., Emerson, S. D., … Mochalkin, I. (2007). Binding thermodynamics of substituted diaminopyrimidine renin inhibitors. *Anal*. *Biochem*., *360*(1), 30–40.

Sato, H., Takino, T., Okada, Y., Cao, J., Shinagawa, A., Yamamoto, E., & Seiki, M. (1994). A matrix metalloproteinase expressed on the surface of invasive tumour cells. *Nature*, *370*(6484), 61–5.

Schönbeck, U., Mach, F., & Libby, P. (1998). Generation of biologically active IL-1 beta by matrix metalloproteinases: a novel caspase-1-independent pathway of IL-1 beta processing. *J*. *Immunol*., *161*(7), 3340–6.

Schonbrun J, Dill KA.(2003). Fast protein folding kinetics. *Proc Natl Acad Sci U*.*S*.*A*. 100(22):12678-82

Seiki, M. (1999). Membrane-type matrix metalloproteinases. *APMIS : Acta*. *Pathol*. *Microbiol*.*Immunol* .*Scand*., *107*(1), 137–43.

Seo, D.-W., Li, H., Qu, C.-K., Oh, J., Kim, Y.-S., Diaz, T., … Stetler-Stevenson, W. G. (2006). Shp-1 mediates the antiproliferative activity of tissue inhibitor of metalloproteinase-2 in human microvascular endothelial cells. *J*. *Biol*. *Chem*., *281*(6), 3711–21.

Sheinerman, F. B., Norel, R., & Honig, B. (2000). Electrostatic aspects of protein-protein interactions. *Curr*. *Opin*. *Struct*. *Biol*., *10*(2), 153–9.

Smith, M. R., Kung, H., Durum, S. K., Colburn, N. H., & Sun, Y. (1997). TIMP-3 induces cell death by stabilizing TNF-alpha receptors on the surface of human colon carcinoma cells. *Cytokine*, *9*(10), 770–80.

Spiller, B., Gershenson, A., Arnold, F. H., & Stevens, R. C. (1999). A structural view of evolutionary divergence. *Proc*. *Natl*. *Acad*. *Sci*. *U*. *S*. *A*., *96*(22), 12305–10.

Spolar RS, Livingstone JR, & Record MT Jr. (1992) Use of liquid hydrocarbon and amide transfer data to estimate contributions to thermodynamic functions of protein folding from the removal of nonpolar and polar surface from water. *Biochemistry*. 31(16):3947-55.

Stetler-Stevenson, W. G., Krutzsch, H. C., & Liotta, L. A. (1989). Tissue inhibitor of metalloproteinase (TIMP-2). A new member of the metalloproteinase inhibitor family. *J*. *Biol*. *Chem*., *264*(29), 17374–8.

Stone, E. M., Lotery, A. J., Munier, F. L., Héon, E., Piguet, B., Guymer, R. H., … Schorderet, D. F. (1999). A single EFEMP1 mutation associated with both Malattia Leventinese and Doyne honeycomb retinal dystrophy. *Nat*. *Genet*., *22*(2), 199–202.

Stracke, J. O., Hutton, M., Stewart, M., Pendás, A. M., Smith, B., López-Otin, C., …

Knäuper, V. (2000). Biochemical characterization of the catalytic domain of human matrix metalloproteinase 19. Evidence for a role as a potent basement membrane degrading enzyme. *J. Biol. Chem.*, *275*(20), 14809–16.

Touw, D. S., Nordman, C. E., Stuckey, J. A., & Pecoraro, V. L. (2007). Identifying important structural characteristics of arsenic resistance proteins by using designed three-stranded coiled coils. *Proc. Natl. Acad. Sci. U. S. A.*, *104*(29), 11969–74.

Turner, N. J. (2009). Directed evolution drives the next generation of biocatalysts. *Nat. Chem. Biol.*, *5*(8), 567–73.

Visse R, Nagase H.(2003). Matrix metalloproteinases and tissue inhibitors of metalloproteinases: structure, function, and biochemistry. *Circ Res.,* 92(8):827-39.

Weber, B. H., Vogt, G., Pruett, R. C., Stöhr, H., & Felbor, U. (1994). Mutations in the tissue inhibitor of metalloproteinases-3 (TIMP3) in patients with Sorsby's fundus dystrophy. *Nat. Genet.,* *8*(4), 352–6.

Wei, S., Chen, Y., Chung, L., Nagase, H., & Brew, K. (2003). Protein engineering of the tissue inhibitor of metalloproteinase 1 (TIMP-1) inhibitory domain. In search of selective matrix metalloproteinase inhibitors. *J. Biol. Chem.*, *278*(11), 9831–4.

Williamson, R. A., Martorell, G., Carr, M. D., Murphy, G., Docherty, A. J., Freedman, R. B., & Feeney, J. (1994). Solution structure of the active domain of tissue inhibitor of metalloproteinases-2. A new member of the OB fold protein family. *Biochemistry*, *33*(39), 11745–59.

Wintrode, P. L., & Arnold, F. H. (2000). Temperature adaptation of enzymes: lessons from laboratory evolution. *Adv. Protein Chem., 55*, 161–225.

Wisniewska, M., Goettig, P., Maskos, K., Belouski, E., Winters, D., Hecht, R., … Bode, W. (2008). Structural determinants of the ADAM inhibition by TIMP-3: crystal structure of the TACE-N-TIMP-3 complex. *J. Mol. Biol.*, *381*(5), 1307–19.

Woessner, J. F. (1991). Matrix metalloproteinases and their inhibitors in connective tissue remodeling. *FASEB J.*, *5*(8), 2145–54.

Wu, B., Arumugam, S., Gao, G., Lee, G. I., Semenchenko, V., Huang, W., … Van Doren, S. R. (2000). NMR structure of tissue inhibitor of metalloproteinases-1 implicates localized induced fit in recognition of matrix metalloproteinases. *J. Mol. Biol.*, *295*(2), 257–68.

Wu, Y., Wei, S., Van Doren, S. R., & Brew, K. (2011). Entropy increases from different sources support the high-affinity binding of the N-terminal inhibitory domains of tissue inhibitors of metalloproteinases (N-TIMPs) to the catalytic domains of matrix metalloproteinases (MMPs) -1 and-3. *J. Biol. Chem.*, 286, 16891-16899

Yoshizaki, T., Sato, H., Maruyama, Y., Murono, S., Furukawa, M., Park, C. S., & Seiki, M. (1997). Increased expression of membrane type 1-matrix metalloproteinase in head and neck carcinoma. *Cancer*, *79*(1), 139–44.

Zhao, H., & Arnold, F. H. (1999). Directed evolution converts subtilisin E into a functional equivalent of thermitase. *Protein Eng.*, *12*(1), 47–53.